2023-09-13

Waste to an Asset, H2S to Hydrogen: A DFT Study

Baratifar, Sam

UNIVERSITY OF CALGARY

Waste to an Asset, H_2S to Hydrogen: A DFT Study

by

Sam Baratifar

A THESIS

SUBMITTED TO THE FACULTY OF GRADUATE STUDIES

IN PARTIAL FULFILMENT OF THE REQUIREMENTS FOR THE

DEGREE OF MASTER OF SCIENCE

GRADUATE PROGRAM IN CHEMISTRY

CALGARY, ALBERTA

SEPTEMBER, 2023

Abstract

Electrolysis of hydrogen sulfide (H_2S) offers a green and zero-emission process for producing hydrogen and for treating the harmful H_2S from oil and gas industries. However, the development of such technology requires an efficient and stable catalyst. Herein, we investigate the mechanism of electrochemical H_2S oxidation reaction (H_2SOR) over various metal oxides and metal sulfides using Density Functional Theory (DFT) calculations. We demonstrate why RuO_2 has been widely reported as an active H_2SOR catalyst. We also show that metal oxides are susceptible to sulfur poisoning, which makes their long-term commercial operation challenging. By including surface coverage analysis for S-intermediates, we identify TiO_2 as a promising and durable catalyst for H_2SOR with 0.49 V calculated overpotential. We also investigated the H_2SOR activity of pristine and doped metal sulfides. We show that even doping metal sulfides reduces the overpotential needed to drive the H_2SOR and facilitates hydrogen production. This research paves the way for the creation of more effective catalysts by providing a computational understanding of H_2S electrolysis over various catalysts.

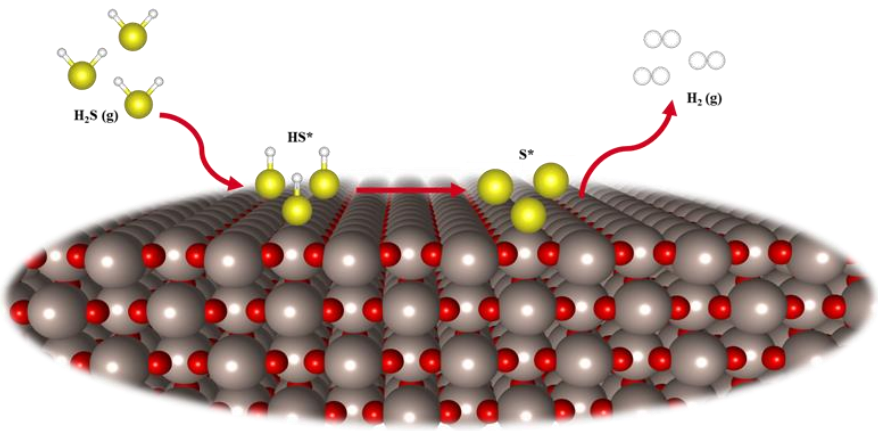

Preface

This thesis is an original, unpublished, independent work by the author, S. Baratifar.

Acknowledgement

Dear Professor Dolgos,

I am writing to express my heartfelt gratitude for your invaluable guidance and support throughout the process of completing my thesis. Your expertise and encouragement have been instrumental in helping me achieve my academic goals.

Your dedication and commitment to mentoring me have been an inspiration, and I could not have completed this program without your guidance, help, and time. Your valuable insights, constructive feedback, and advice have helped me to navigate the challenges of this academic journey and have contributed significantly to the quality of my work.

I am also grateful for the time and effort that you have invested in reviewing and editing my thesis and for your unwavering support and belief in my abilities. Your guidance has enabled me to grow both professionally and personally, and I am proud to have had you as my thesis adviser.

My Dear Parents and Sister,

Undoubtedly, your endless support from overseas has been the most paramount reason that I could successfully finish my master's degree here in Canada. I will not forget the kindness you have always given me during this period, and I will always be thankful for your kind words.

My dear colleagues and friends,

I would like to thank Hirbod, Amir Azar, Amir Mostaghimi, Pouya, Pezhvak, Lian, Tiago, Narges, Hatef, Bryan, Brooke, and Alistair for their support during this time. We have made so many good memories together, and this will definitely continue in the future as well.

Dear Canada First Research Excellence Fund (CFREF) Representatives,

I want to express my deepest gratitude for providing me with the resources and funding required to complete my master's degree.

Table of Contents

Table of Figures

Chapter 1. Introduction

1.1. Background

During the past few years, there has been a great deal of attention on transitioning from fossil fuels to clean energy sources. Fossil fuels have been the primary source of energy for many years, but their negative impact on the environment is undeniable. One of the most significant impacts of fossil fuels is air pollution. Burning fossil fuels releases pollutants such as carbon dioxide, sulfur dioxide, nitrogen oxides, and particulate matter into the atmosphere.[1,2] These pollutants contribute to the formation of smog and acid rain, which have serious health consequences, especially for vulnerable populations such as children, the elderly, and those with respiratory illnesses. In addition, carbon dioxide is a greenhouse gas that contributes to climate change, which has far-reaching consequences for the environment, including rising sea levels, more frequent and severe natural disasters, and the loss of biodiversity.[3]

Fossil fuels also have a detrimental impact on water and soil quality. The extraction and transportation of fossil fuels can lead to oil spills, which pollute water sources and harm aquatic life. The use of coal in power plants produces toxic waste that is often stored in large pits or ponds, posing a risk to nearby communities and ecosystems. The mining of coal and other minerals used in energy production can also lead to habitat destruction, land subsidence, and soil erosion, which can have long-term impacts on the environment.[4]

In addition, the burning of fossil fuels also contributes to climate change, which has serious implications for the environment and human health. Climate change can lead to rising temperatures, more frequent and severe droughts and heat waves, and changes in precipitation

patterns. These changes can lead to food and water scarcity, which can have significant impacts on public health and social stability. Climate change also threatens biodiversity, as many species are unable to adapt to the rapid changes in their environment.[5]

Given the negative impacts of fossil fuels on the environment, it is critical that we think of an alternative, cleaner, and more sustainable energy sources. Renewable energy sources such as solar, wind, and hydropower can provide energy without releasing harmful pollutants into the atmosphere. In addition, energy efficiency measures such as improving insulation in buildings and using more efficient appliances can reduce the amount of energy we need to use, which can also help to reduce our reliance on fossil fuels. By taking action to transition to cleaner energy sources and reduce our energy consumption, we can help to mitigate the negative impacts of fossil fuels on the environment and build a more sustainable future.[6]

Electrocatalysis is a vital component of clean energy technology, enabling more efficient and selective electrochemical reactions that are essential for a sustainable future. By utilizing catalysts to facilitate the conversion of energy from one form to another, electrocatalysis can enhance the performance and sustainability of renewable energy systems such as fuel cells, electrolyzers, and batteries.[7–9] These electrochemical reactions are essential in the production of clean fuels such as hydrogen, which can be used in fuel cells to generate electricity without emitting harmful pollutants, thus reducing greenhouse gas emissions.[10] Furthermore, electrocatalysis can be used to produce value-added chemicals from renewable feedstocks, replacing traditional fossil fuel-based methods.[11] This technology also plays a crucial role in carbon capture and utilization, where electrochemical processes are used to convert carbon dioxide into useful products such as methane, methanol, or formic acid.[12,13] The development of advanced electrocatalysts is crucial to overcoming the current limitations of electrochemical systems and

further improving their efficiency and selectivity. Researchers are working on the development of new materials, such as transition metal alloys, metal-organic frameworks, and molecular catalysts, to achieve enhanced electrocatalytic performance.[14–16] In conclusion, electrocatalysis is a promising technology that has enormous potential to support a sustainable energy future and mitigate climate change by reducing greenhouse gas emissions and supporting the development of clean energy technologies.

Currently, there are quite a few electrochemical reactions that will lead to the production of hydrogen as a by-product. Water electrolysis (WOR)[17], partial methane oxidation[18], carbon dioxide reduction reaction (CO_2RR)[19], and hydrogen sulfide oxidation reaction (H_2SOR)[20] are among the green ways of hydrogen production and are considered sustainable hydrogen production processes. All these electrochemical reactions need active and selective catalysts, enhanced electrodes, and proper electrolytes to function efficiently and to be considered affordable hydrogen production processes. The catalyst material is one of the most important parts of an electrochemical system. This material needs to be selective, active, and stable at the same time to drive hydrogen production with the least energy consumption possible.

1.1.1. Water Electrolysis

Water electrolysis is a process that involves the splitting of water molecules into hydrogen and oxygen gases using an electric current.[17] This process is achieved by passing an electric current through water, which causes the water molecules to break down into their constituent elements. The hydrogen and oxygen gases produced can be used for a variety of applications, including fuel cells, energy storage, and industrial processes.[21]

The process of water electrolysis involves the use of an electrolytic cell, which consists of two electrodes (an anode and a cathode) and an electrolyte solution.[22] The electrodes are typically made of a conductive material such as platinum or graphite, while the electrolyte solution is usually a dilute solution of sulfuric acid or sodium hydroxide.[23]

When an electric current is passed through the electrolytic cell, the water molecules near the anode are oxidized, releasing oxygen gas and positively charged hydrogen ions (protons). The hydrogen ions then migrate towards the cathode, where they are reduced to hydrogen gas by gaining electrons from the cathode.[24] The overall reaction can be represented as follows:[25]

$$2H_2O(l) \rightarrow 2H_2(g) + O_2(g) \quad (1)$$

The efficiency of water electrolysis depends on a number of factors, including the type of electrolyte used, the current density, the catalysts used, and the temperature of the electrolyte solution. Higher current densities and temperatures can increase the rate of hydrogen production but can also lead to increased energy consumption and reduced efficiency.[26]

One of the main applications of water electrolysis is in the production of hydrogen gas for use in fuel cells. Fuel cells are electrochemical devices that convert the chemical energy of hydrogen and oxygen into electrical energy, with water as the only by-product.[27] Hydrogen fuel cells have the potential to be a clean and efficient source of energy for a variety of applications, including transportation, stationary power generation, and portable electronics.[28]

Water electrolysis can also be used in industrial processes, such as the production of chemicals and metals. For example, hydrogen gas produced by electrolysis can be used as a reducing agent in the production of metals such as steel and aluminum.[29] It can also be used in the production of chemicals such as ammonia and methanol.[30]

In recent years, there has been growing interest in the use of water electrolysis as a means of producing hydrogen gas from renewable energy sources. This approach, known as "green hydrogen," involves using renewable energy sources such as solar and wind power to generate the electricity needed for water electrolysis. Green hydrogen has the potential to be a sustainable and carbon-neutral source of energy, as it does not rely on fossil fuels and produces no greenhouse gas emissions.[30]

The main drawback of this reaction, however, is its large energy consumption. Different works on nickel-based, perovskites, and layered double hydroxides (LDHs) have been conducted by different researchers to overcome the overpotential barrier of this reaction.[31–33] No matter the catalyst used there are still drawbacks regarding the minimum required overpotential of around 0.2 V for this reaction. This overpotential is still considered high for hydrogen production purposes as the catalysis community wants to achieve overpotentials less than 0.1 V. This high overpotential requirement comes from the adsorption of oxygen evolution reaction (OER) intermediates is weak on the surface of the catalysts and do not lead to promising activities.[34]

In conclusion, water electrolysis is a process that involves the splitting of water molecules into hydrogen and oxygen gases using an electric current. This process has a wide range of applications, including fuel cells, energy storage, and industrial processes. With the growing interest in renewable energy sources, water electrolysis has the potential to play an important role in the transition to a more sustainable and carbon-neutral energy system. However, the main drawback of this reaction is that it needs high energy requirements in order to yield enough hydrogen for fuel cell applications.

1.2. Problem Statement

As discussed in section 1.1.1, water oxidation reaction needs high overpotentials to yield hydrogen in standard conditions. Consequently, we need to take advantage of H_2SOR for the purpose of producing hydrogen with lower energy consumption. This, however, requires identifying efficient catalysts that tend to lower the energy requirements for this reaction as well as being stable and active towards H_2SOR. Promising catalysts can be identified by two main methods: Computational Catalysis and Experimental Catalysis. In computational catalysis, we use Density Functional Theory (DFT), which will be discussed thoroughly in Chapter 3. DFT allows us to save time and materials in the discovery of catalyst materials. A combination of computational and experimental research is needed to overcome the challenges different catalysts face for various reactions. Computational catalysis helps us to understand the mechanism behind the activity of different catalysts and to identify the limitations in a more atomic-level analysis. In this work, we have used DFT to investigate different catalysts for hydrogen sulfide oxidation reaction. Reasonably, many catalysts have not shown promising results for this reaction based on the previous studies. Thus, we narrowed down our focus to metal oxides and metal sulfides and looked deep into their properties and structure as well as their stability for this reaction.

1.3. Research Objectives

In this work, we use Density Functional Theory (DFT) to investigate the catalytic activity of different metal oxides and metal sulfides for the purpose of hydrogen production from hydrogen sulfide. We hope to understand the elementary steps in the reaction and to develop a general model to computationally evaluate the activity of other catalysts as well. This model also assists future researchers in investigating other catalysts' activities for H_2SOR.

We also elaborate more on the issues that H_2SOR deals with and on how we could overcome these issues. The issues we face in H_2SOR include but are not limited to surface poisoning and low activity. We will give details on different ways to enhance the activities of our investigated catalysts.

1.4. Significance of Study

The following research tries to address the problems associated with hazardous H_2S and to remove this notorious gas from the environment using a carbon-free method. We focus on H_2S electrolysis and hope to find a catalyst that can yield hydrogen and sulfur from this gas. These two elements are among the most useful materials and sources of energy in different industries, like battery manufacturing, agriculture, and transportation.

The practical application of this work can be around using these catalysts in H_2S fuel cells in the future. The driving force of a fuel cell is its' catalyst, and we believe that the investigated catalysts in this work have the potential to be used in H_2S fuel cells. However, the applicability of these catalysts should also be investigated in terms of their kinetics as this study only focuses on the thermodynamic feasibility of these materials.

We have also developed a general, re-usable method that researchers can utilize when investigating the catalytic activity of H_2SOR. This model is helpful because it takes into account the surface poisoning of the catalyst as well.

Chapter 2. Research Background

2.1. Hydrogen as a Source of Energy

Hydrogen is a versatile, clean-burning fuel that has the potential to power a wide range of applications. It is considered an attractive source of energy due to its abundance, zero greenhouse gas emissions when used in fuel cells, and high energy density.

Hydrogen can be produced from a variety of sources, including fossil fuels, water, and biomass. However, the most sustainable method of producing hydrogen is through the use of renewable energy sources such as wind, solar, and hydropower. This process, called electrolysis, involves splitting water into hydrogen and oxygen using an electric current. This method of hydrogen production is known as green hydrogen.

One of the main benefits of hydrogen as a source of energy is that it can be used in fuel cells to generate electricity with only water and heat as byproducts. Fuel cells are electrochemical devices that convert the chemical energy stored in hydrogen into electrical energy. This technology is particularly useful for transportation applications, as it offers a clean alternative to gasoline and diesel-powered vehicles. Hydrogen can also be used in combustion engines, either as a pure fuel or in combination with other fuels. This is particularly useful in industries such as shipping and aviation, where the weight and size of batteries make them impractical for use in large vehicles.

However, there are several challenges associated with the widespread adoption of hydrogen as a source of energy. Firstly, the infrastructure required to produce, store, transport, and distribute hydrogen is still underdeveloped, particularly in comparison to the existing infrastructure for fossil fuels.[35,36] Secondly, while hydrogen is abundant, it is rarely found in its pure form and must be extracted from other compounds, which can be energy-intensive and

expensive.[37] For example, electrolysis requires the development of efficient catalysts that yield hydrogen readily and with the least energy consumption. These catalysts mainly include platinum-based catalysts that are not affordable when used in the long term.

2.2. Hydrogen Production

One of the key benefits of hydrogen is that it can be produced using a variety of methods, each with its own advantages and disadvantages. Some of the most common ways of producing hydrogen are summarized in the following paragraphs.

1. Steam methane reforming (SMR)

Steam methane reforming is currently the most common method of hydrogen production, accounting for around 85% of global hydrogen production. SMR involves reacting natural gas with steam at high temperatures and pressures to produce hydrogen and carbon monoxide. The carbon monoxide is then reacted with more steam to produce additional hydrogen and carbon dioxide.[38] A schematic of this process is shown below.

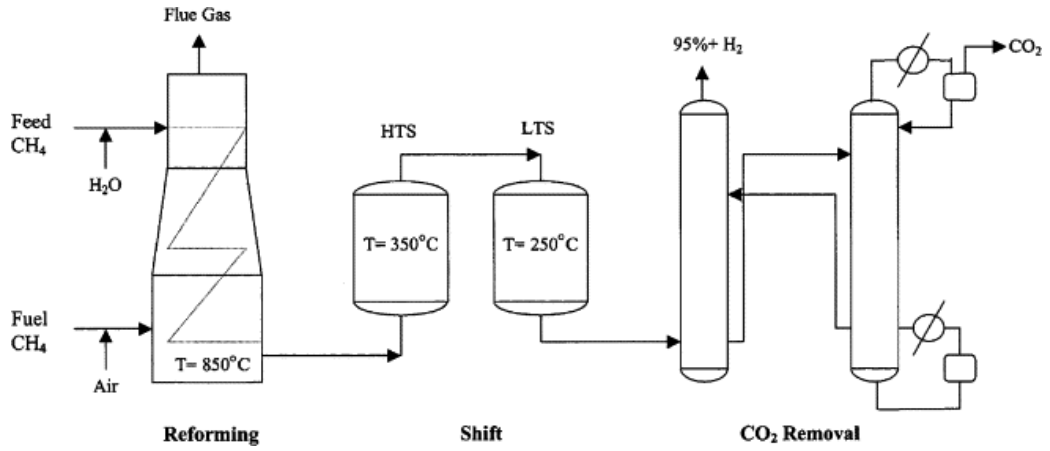

Figure 2.1. Traditional steam methane reforming process for hydrogen production (with permission from Elsevier Ltd)[39]

SMR is a relatively inexpensive method of hydrogen production, but it is also a significant source of greenhouse gas emissions.[40] Carbon dioxide is released during the process, contributing to climate change. As a result, there is increasing interest in finding alternative methods of producing hydrogen that are more environmentally friendly.[41]

2. Electrolysis

Electrolysis is a method of producing hydrogen by using an electrical current to split water or other resources like H_2S into hydrogen. This can be done using a variety of sources of electricity, including renewable sources such as solar and wind power. Electrolysis can be powered using electricity from the grid or using on-site renewable energy sources, making it a potentially carbon-free method of hydrogen production.[42,43]

There are two main types of electrolysis: alkaline electrolysis and proton exchange membrane (PEM) electrolysis. Alkaline electrolysis is the older and more established technology, while PEM electrolysis is a newer and more efficient technology. PEM electrolysis is also more expensive than alkaline electrolysis, but it is better suited for use in small-scale applications such as fuel cells for vehicles.[44,45]

Electrolysis has the advantage of being a potentially carbon-free method of hydrogen production, but the technology is still expensive and not yet widely adopted. However, with continued investment in research and development, the cost of electrolysis is likely to decrease, making it a more attractive option for hydrogen production in the future. This technology requires investigating catalysts and electrode materials that justify the required energy for their price.

3. Biomass gasification

Biomass gasification is a method of producing hydrogen by heating biomass, such as wood chips or agricultural waste, in a low-oxygen environment to produce a gas that contains hydrogen, carbon monoxide, and other gases.[46] The gas is then cleaned and purified to produce hydrogen. Biomass gasification is a renewable method of hydrogen production that can use waste products as feedstock. However, the process can also produce pollutants such as nitrogen oxides and particulate matter. As a result, there is ongoing research into ways to reduce these emissions and improve the efficiency of the process.[47]

4. Photobiological production

Photobiological production is a method of producing hydrogen using algae or other photosynthetic organisms. The process involves exposing the organisms to light and then collecting the hydrogen these organisms produce as a byproduct. Photobiological production is a renewable and potentially carbon-free method of hydrogen production. However, this technology is still in the early stages of development, and there are several challenges to be overcome. For example, the efficiency of the process is currently low, and there are issues with scaling up the technology for large-scale production.[48]

5. Pyrolysis

Pyrolysis is a method of producing hydrogen by heating hydrocarbons, such as methane or propane, in the absence of oxygen to produce hydrogen and other gases. Pyrolysis can be powered using renewable energy sources, making it a potentially carbon-free method of hydrogen production. However, this process can also produce pollutants such as carbon monoxide and particulate matter. As a result, there is ongoing research into ways to reduce these emissions and improve the efficiency of the process.[49,50]

To better differentiate between hydrogen production processes, Natural Resources Canada has introduced color codes for different types of hydrogen types.[30]

Production Process		Feedstock & energy source	Pros and Cons	Examples
GREY	 Produced by steam methane reformation without carbon capture and sequestration (CCS)	**Feedstock:** natural gas, gasified coal	Pros: lowest cost, abundant Cons: highest carbon intensity	Canada produces approximately 3 million tonnes of grey hydrogen per year primarily for industrial use.
BLUE	 Produced from fossil fuels by steam methane reformation, pyrolysis or other processes with carbon capture and sequestration (CCS).	Feedstock: natural gas, coal, crude bitumen	Pros: low-cost, abundant, low CI, pyrolysis offers scale and siting flexibility Cons: SMR pathway siting is constrained by CCUS, feedstock is not renewable	Alberta's Quest project
GREEN	 Produced from water by electrolysis using renewable electricity such as hydroelectricity, wind or solar.	Feedstock: Water Energy source: Renewable electricity	Pros: lowest carbon intensity, scalable Cons: highest cost, opportunity cost - competes with electrification demand	Air Liquide's 20 MW electrolyzer plant in Becancour, Projects developing in BC to support hydrogen fueling network.
NUCLEAR	 Produced from water by electrolysis or high temperatures from nuclear energy	**Feedstock:** Water **Energy source:** Uranium / nuclear electricity	**Pros:** low carbon intensity **Cons:** limited availability and siting constraints	Feasibility study planned in Bruce County.

Figure 2.2. Hydrogen feedstock and production processes [30]

2.3. Hydrogen Storage

Hydrogen is a promising alternative energy source due to its high energy density, abundance, and environmental benefits. However, the storage of hydrogen poses a significant challenge, as it is a gas at room temperature and atmospheric pressure and has a low density.[51] Therefore, several

methods have been developed for storing hydrogen, each with its own advantages and disadvantages.

1. Compressed Hydrogen Storage: Compressed hydrogen storage is one of the most common methods for storing hydrogen. The hydrogen gas is compressed into high-pressure tanks of up to 10,000 psi and stored in tanks made of lightweight and strong materials such as carbon fiber or metal alloys. Compressed hydrogen storage has several advantages, including its simplicity, cost-effectiveness, and direct usability in fuel cells or other applications without further processing.[52]

However, there are also some drawbacks to compressed hydrogen storage. The high-pressure tanks required for this method can be heavy and expensive, which limits their use in some applications. There are also safety concerns associated with high-pressure storage, as the tanks can rupture or leak if damaged or not correctly maintained. Additionally, compressed hydrogen has a relatively low energy density compared to other fuels, which means that a large volume of storage is required to provide a sufficient amount of energy.[51,53]

2. Liquid Hydrogen Storage: Hydrogen can also be stored in a liquid state, which increases its energy density and reduces its volume. Liquid hydrogen is stored in specially designed cryogenic tanks that are insulated to prevent heat from entering the tank and causing the hydrogen to boil off. Liquid hydrogen storage has several advantages, including its higher energy density than compressed hydrogen, which means that a smaller volume of storage is required to provide the same amount of energy. Liquid hydrogen can also be used directly in fuel cells or other applications without further processing.[54]

However, there are also some limitations to liquid hydrogen storage. The cryogenic tanks required for this method are expensive and can be challenging to maintain. Liquid hydrogen also requires specialized handling and transportation, as it must be kept at very low temperatures (-253°C or -423°F) to remain in a liquid state. This means that the infrastructure required for liquid hydrogen storage and transport is more complex than for compressed hydrogen.[55]

3. Metal Hydride Storage: Another method for storing hydrogen is to use metal hydrides, which are materials that can absorb and release hydrogen gas. The metal hydride is loaded with hydrogen gas, and then the hydrogen can be released by heating the material or exposing it to a vacuum. Metal hydrides have several advantages, including their ability to store hydrogen at lower pressures and at room temperature, which makes them safer and more convenient to use than compressed or liquid hydrogen. Metal hydrides can also be recharged by simply adding more hydrogen to the material.[56]

However, metal hydride storage has some hindrances as well. Metal hydrides are relatively heavy and can be expensive, which limits their use in some applications. They can also have slow hydrogen uptake and release rates, which can limit their performance in some applications. Additionally, some metal hydrides can be sensitive to air and moisture, which can degrade their performance over time.[57]

4. Chemical Storage: Hydrogen can also be stored chemically by combining it with other substances to form chemical compounds that release hydrogen when heated or exposed to a catalyst. For example, hydrogen can be stored as ammonia or methanol, which can then be used as fuel for fuel cells or other applications. Chemical storage has several advantages, including its ability to store hydrogen at low pressures and at room temperature, which makes it more convenient and safer to use than compressed or liquid hydrogen. These

materials include but are not limited to nanomaterials, carbon-based materials, metal organic frameworks (MOFs), etc.[58–60]

However, there are some drawbacks to chemical storage. Chemical storage requires additional processing to release the stored hydrogen, which can increase costs and reduce overall efficiency. In addition, these storage materials are usually intricate to synthesize, and this leads to expensive costs of manufacturing.[61]

2.4. Hydrogen Sulfide (H_2S), An Involuntary Gas

Hydrogen sulfide (H_2S) is a colorless, flammable, and toxic gas with a characteristic rotten egg smell. It is a naturally occurring compound and is also produced by various industrial processes.[62,63] In this section, we will discuss the advantages, disadvantages, sources, and other safety aspects of hydrogen sulfide.

Advantages:

- Energy production: Hydrogen sulfide can be used as a source of energy. Some microorganisms, known as sulfate-reducing bacteria, can metabolize H_2S to generate energy for their growth and survival. This process is called anaerobic respiration and is an essential part of the sulfur cycle in nature.[64] Hydrogen sulfide can also be used to produce hydrogen, an essential source of energy that is anticipated to deliver a major part of the world energy demand by 2050.[30,65]
- Claus process: The Claus process, developed by Carl Friedrich Claus in the late 19th century, is an essential industrial technique used to recover sulfur from hydrogen sulfide (H_2S) gas, commonly generated in oil refineries and natural gas processing facilities. This method involves burning hydrogen sulfide gas in the presence of air to produce sulfur

dioxide (SO_2). Subsequently, sulfur dioxide is transformed into elemental sulfur through a series of catalytic reactions across multiple stages. The central reaction in this process is the Claus reaction, which yields elemental sulfur and contributes to cleaner air by reducing sulfur emissions. This recovered sulfur can then be further processed and purified for various industrial applications, such as sulfuric acid or fertilizer production. The Claus process plays a crucial role in both environmental compliance and industrial sulfur recovery.[66] The steam-form hydrogen in this process can be used in the Haber-Bosch process that is used to produce ammonia.

- Medical applications: H_2S has been found to have potential therapeutic applications. It acts as a signaling molecule in the human body, playing a role in various physiological processes, such as vasodilation, inflammation, and cellular protection. Research is ongoing to develop H_2S-releasing drugs for treating conditions like hypertension, heart failure, and neurodegenerative diseases.[67]
- Environmental applications: H_2S can be used for environmental remediation, such as the removal of heavy metals from contaminated water. It reacts with metal ions to form insoluble metal sulfides, which can be easily separated from the water. This process is known as sulfide precipitation and is employed in wastewater treatment plants.[68]

Disadvantages:

- Toxicity: Hydrogen sulfide is highly toxic to humans and animals. Exposure to low concentrations can cause irritation of the eyes, nose, and throat, while higher concentrations can lead to more severe symptoms like headache, dizziness, and nausea. Prolonged exposure to high levels of H_2S can be fatal, as it inhibits cellular respiration and leads to respiratory failure.[20,69]

- Flammability: H_2S is a flammable gas, and its mixtures with air can be explosive. This poses a significant risk in industrial settings, where accidental leaks or releases of H_2S can lead to fires or explosions.[70]
- Corrosiveness: Hydrogen sulfide is corrosive to various metals, such as iron, steel, and copper. It can cause the formation of metal sulfides, which can weaken the structural integrity of pipes, tanks, and other equipment. This can lead to equipment failure and increased maintenance costs in industries that handle H_2S.[71]
- Odor nuisance: The characteristic rotten egg smell of H_2S can be detected by humans at very low concentrations, making it an odor nuisance. This can negatively impact the quality of life of people living near industrial facilities that emit H_2S.[72,73]

Sources:

- Natural sources: Hydrogen sulfide is produced naturally through the decomposition of organic matter in the absence of oxygen. This occurs in environments such as swamps, marshes, and stagnant bodies of water. It is also released during volcanic eruptions and can be found in natural gas deposits.[74]
- Industrial sources: H_2S is generated as a byproduct in various industrial processes, including petroleum refining, natural gas processing, and wastewater treatment. A summary of the industrial sources of H_2S has been mentioned below.
    - Petroleum Refining: H_2S is a common impurity in petroleum and natural gas reserves. During the refining process, H_2S is released from crude oil and natural gas as a by-product. It poses a significant health and safety risk to workers and must be carefully managed and removed to meet regulatory standards.[75]

- Chemical Manufacturing: H_2S is produced in various chemical manufacturing processes like sulfur and different acids productions. It can be a by-product of the production of sulfuric acid, which is used in fertilizers, detergents, and other industrial applications.[76]
- Mining and Metal Processing: Certain metals, such as copper, zinc, and lead, are commonly found in ores as sulfide compounds. During the extraction and refining processes, these sulfide ores are treated with heat or chemicals, releasing H_2S gas. Mining activities, particularly in sulfide-rich deposits, can be significant sources of H_2S emissions.[77]
- Pulp and Paper Industry: In the pulp and paper industry, sulfurous compounds are produced during the pulping process. When sulfur-containing wood chips are treated with chemicals to remove lignin and separate the fibres, H_2S gas is generated as a byproduct. Proper ventilation and control measures are necessary to prevent H_2S release into the atmosphere.[72]
- Sewage Treatment: H_2S is formed during the decomposition of organic matter in sewage treatment facilities. Anaerobic bacteria break down sulfates present in wastewater, producing H_2S as a metabolic byproduct. Effective treatment and odour control systems are crucial to mitigate the release of H_2S from sewage treatment plants.[78]

- Biological sources: Some microorganisms, such as sulfate-reducing bacteria, produce H_2S as a metabolic byproduct. These bacteria are commonly found in the human gut, where they contribute to the production of intestinal gas.[79]

Detection and Monitoring:

- Monitoring H_2S levels is crucial for ensuring the safety of workers and the public in areas where the gas is present. Various detection methods are available, including:
    - Colorimetric detector tubes: These tubes contain a chemical reagent that changes color when exposed to H_2S. The length of the color change corresponds to the concentration of the gas, providing a quick and simple method for measuring H_2S levels.[80]
    - Electrochemical sensors: These sensors use an electrochemical reaction to detect the presence of H_2S. They provide continuous monitoring and can be integrated into portable or fixed gas detection systems.[81]
    - Spectroscopic methods: Techniques such as Fourier-transform infrared (FTIR) spectroscopy and ultraviolet (UV) absorption spectroscopy can be used to detect and quantify H_2S in the air. These methods offer high sensitivity and selectivity but can be more complex and expensive than other detection methods.[82]

In conclusion, hydrogen sulfide is a compound with both advantages and disadvantages. While it has potential applications in energy production, medicine, and environmental remediation, it also poses significant risks due to its toxicity, flammability, and corrosiveness. Proper detection, monitoring, and safety measures are essential for managing the hazards associated with H_2S and protecting workers, the public, and the environment. Electrolysis can help us to convert this notorious gas to very useful materials like sulfur and hydrogen.

2.5. Partial Conversion and Electrochemical Conversion of H_2S to H_2

Catalyst researchers have done a few investigations on both thermal and electrochemical conversion of H_2S to H_2 in the past few years. Both processes possess advantages and disadvantages that will be discussed in the next paragraphs.

Anani et al.[83] have used a combination of graphite, nickel, porous nickel-chromium alloy, and titanium, as well as a Nafion membrane as a cell separator for electrochemical production of hydrogen and sulfur from hydrogen sulfide at a temperature of 80℃. It is found that the anode's activity gets passivated by sulfur deposition as well as the oxidation of sulfide or different polysulfides. They found that the required overpotential can be increased from an initial value of -0.4V to 1.8V during the experiment. This is due to the passivation of the anode by sulfur intermediates.

Chen et al.[62] investigated alkaline carbon nanotubes (CNTs) for H_2S oxidation at 30℃ in the presence of oxygen and humidity. The carbon nanotubes were synthesized by incipient wetness impregnation. They found that the outside voids of the CNTs account for the higher (3.9 times higher than the saturation capacity of a commercial desulfurizer) sulfur saturation of CNT catalysts. This indicated that the catalytic activity of the CNTs is strongly germane to the structure of the CNTs. Scanning electron microscopy and transmission electron microscopy showed that almost all the external voids of CNTs have been occupied by sulfur intermediates. TEM images

further showed that most of the agglomerated sulfur prefers to get accumulated on the external surface of the CNTs rather than the internal tube. A schematic of their work has been shown below.

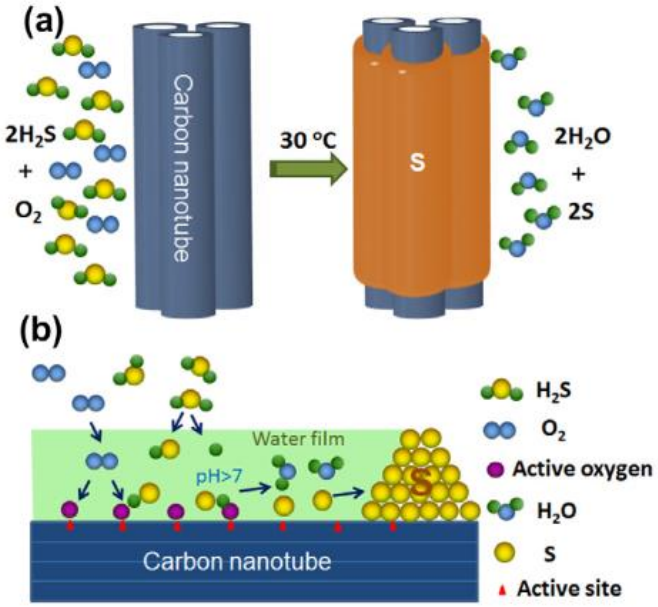

Figure 2.3. A schematic of H_2S oxidation over the alkaline CNTs (a) and reaction step (b) (reprinted from Alkaline carbon nanotubes as effective catalysts for H_2S oxidation. Carbon N Y. 2011 Oct) [62]

Chin and Howard [84] have investigated the contribution of H_2S on the anodic oxidation of hydrogen on Pt over the temperature range of 25°C-170°C. In this work, they used phosphoric acid as electrolyte. The Cyclic Voltammetry (CV) was used to verify the purity of the phosphoric acid electrolyte as well as the adsorption rate of H_2S on the platinum electrode. They found that the anodic oxidation rate decreases significantly due to the H_2S adsorption on platinum. As they increased the experimental temperature, H_2S poisoning was found to decrease. This phenomenon

was further verified by the formation of a layer of elemental sulfur on the anode site hindering the activity of the catalysts.

Zheng et al.[85] did their work on the selective oxidation of H_2S on porous CeO_2 nanocrystals. They came to the fact that the crystal facets of CeO_2 are the primary contributors to the catalytic activity, base properties, and defect sites of the CeO_2. Among the investigated nanocrystals, the specific {110} and {100} facets of CeO_2 nanorods demonstrated the highest activity. The researchers found that the high concentrations of surface oxygens on these facets explain the highest activity among the other investigated structures. They defined the H_2S conversion (X_{H_2S}) according to the following equation:

$$X_{H_2S} = \frac{[H_2S]_{in} - [H_2S]_{out}}{[H_2S]_{in}} \quad (2)$$

In this work, DFT calculations also show an increase in the H_2S adsorption is dependent on the large number of oxygen vacancies on the nanorod CeO_2's {100) and {110} facets.

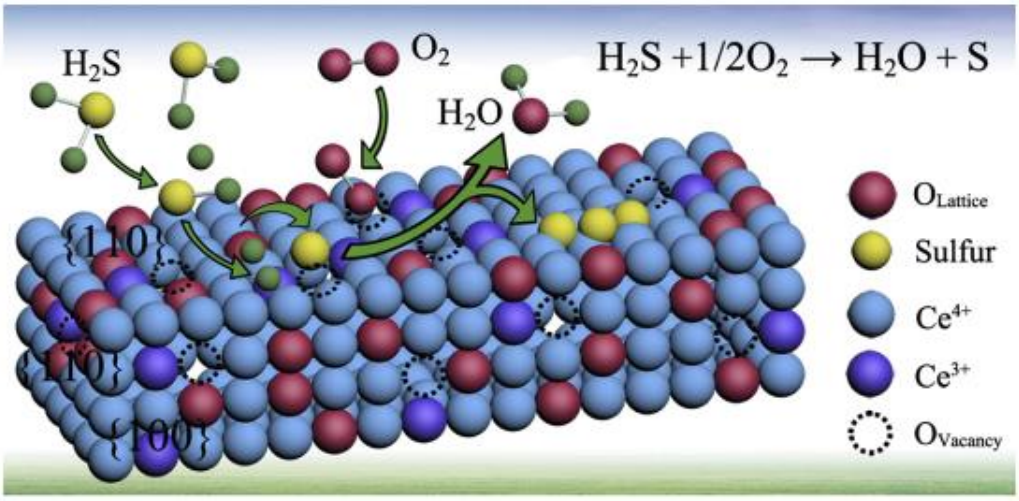

Figure 2.4. A schematic of H_2SOR on the {100} and {110} facets of CeO_2 nanorods (reprinted from Insight into the effect of morphology on catalytic performance of porous CeO_2 nanocrystals for H_2S selective oxidation. Appl Catal B. 2019 Sep 5) [85]

Liu et al.[86] have looked into the H_2S selective oxidation via cobalt nanoparticles surrounded by different layers of nitrogen-doped (N-doped) graphitic carbon. The catalytic performance of Co@NC catalysts initially increases and then decreases with increasing Co content. Co@NC-4, with a suitable Co content, shows an optimal H_2S conversion ratio of nearly 100% with a weight hourly space velocity of 18000 mL $g^{-1}h^{-1}$ at 190°C for 28 hours. This high performance is attributed to optimal mesopore size and abundant pyridinic N. The Co@NC-4 has more defects than other samples, providing space for more adsorption of H_2S molecules. In contrast, the NC sample without Co has converted nearly 95% of H_2S at 250°C. Theoretical calculations indicate that N-doped graphene can regulate the electron density around the Co NPs, promoting the adsorption of H_2S. The researchers believe that the unique electronic and geometrical configurations improve the activity and stability of the process.

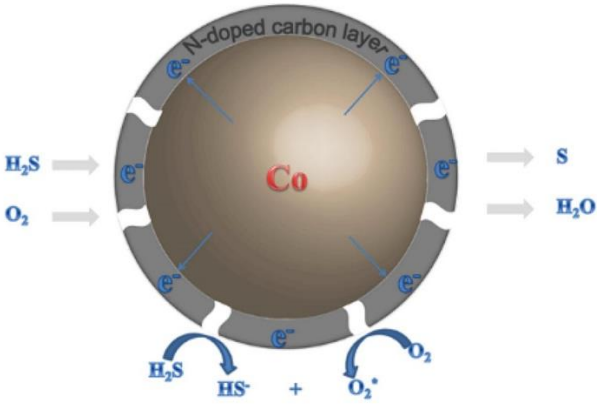

Figure 2.5. Co nanoparticle encapsulated by nitrogen-doped carbon layer for selective H_2S oxidation (reprinted from Rational designed Co@N-doped carbon catalyst for high-efficient H_2S selective oxidation by regulating electronic structures. Chemical Engineering Journal. 2020 Dec 1) [86]

Tasdemir et al.[87] aimed to enhance the catalytic activity of titanium oxide catalyst for selective catalytic oxidation of H_2S to elemental sulfur by adding iron, chromium, and zirconium. Equimolar catalysts of Ti-Fe, Ti-Cr, and Ti-Zr were synthesized using the complexation method and were tested at different O_2/H_2S ratios and temperatures ranging from 200-300°C. The Ti-Fe catalyst with Fe_2TiO_5 crystalline phase and Ti-Cr catalyst with mainly Cr_2O_3 crystalline phase showed complete conversion of H_2S and high sulfur selectivity at 250°C. However, the Ti-Zr catalyst with a relatively high surface and small pore diameter was unable to prevent sulfur deposition on the surface and lost catalytic activity at the same temperature. The Ti-Fe catalyst had a high activity with 100% conversion and sulfur selectivity during the experimental run, even at a lower oxidation temperature of 200°C. The study showed that incorporating iron into the Ti-Fe catalyst structure improved the catalyst's redox ability. The Fe_2TiO_5 mixed metal oxide in the Ti-Fe catalyst was the active phase responsible for the successful conversion of H_2S and high sulfur selectivity in the selective oxidation of H_2S to elemental sulfur.

Zhang et al.[88] synthesized a series of iron oxide supported on alumina-intercalated clay catalysts (referred to as Fe/Al-Lap) with porous structures and high specific surface area. The Fe/Al-Lap catalysts exhibited high catalytic activity in the temperature range of 120-200°C due to the interaction between iron oxide and alumina, which effectively improved the redox property of Fe^{3+}. Additionally, the strong acidity of the catalysts and good dispersion of iron oxide also benefited the oxidation reaction. Among them, the 7%Fe/Al-Lap catalyst showed the best catalytic activity and high stability at 180°C. Furthermore, excessive oxygen was not required in the selective oxidation reaction. Finally, they showed that the catalytic mechanism followed a redox mechanism, while the catalyst deactivation was mainly due to sulfur condensation and the formation of $Fe_2(SO_4)_3$ species on the surface which leads to surface poisoning.

Two interesting studies by Kumar and Nagaiah[89,90] were conducted for H_2SOR using NiCu-MoS_2 and $CoFeS_2$ catalysts, respectively, for pure hydrogen production purposes. In these two studies, they compared the required overpotential with the minimum required overpotential for oxygen evolution reaction (OER). In the first study, the NiCu-MoS_2 catalysts were synthesized by a single-step hydrothermal reaction resulting in flower-like NiCu-MoS_2. The H_2SOR electrocatalytic activity was measured in an H_2S-saturated 1 M NaOH electrolyte. NiCu-MoS_2 demonstrated the minimum required onset potential compared to MoS_2, Cu-MoS_2, or Ni-MoS_2, i.e. 0.21 V_{RHE}. This overpotential is way lower than the minimum required overpotential in the oxygen evolution reaction (1.23 V_{RHE}) for producing the same amount of hydrogen. Their study also shows that this catalyst exhibits high durability for 150 hours and a faradaic efficiency of around 98.1%. In the second study, they looked into the catalytic activities of nanorod-embedded wheat grain CoFeS2 (Co=3: Fe=1) for H_2SOR. They witnessed a steep increase in the activity around 0.23 V_{RHE}, which they referred to as the onset potential. They also compared this catalyst with FeS_2 and CoS_2 catalysts and showed that the onset potentials for these two electrocatalysts are way higher than the promising $CoFeS_2$ (3: 1) catalyst. The catalyst's stability was also measured by chronoamperometric measurement for 120 hours. The catalyst showed little to no degradation after 120 hours and a faradaic efficiency of about 97.8%. A comparison between the required overpotential for H_2SOR and OER has been schematically shown below by Kumar and Nagaiah.

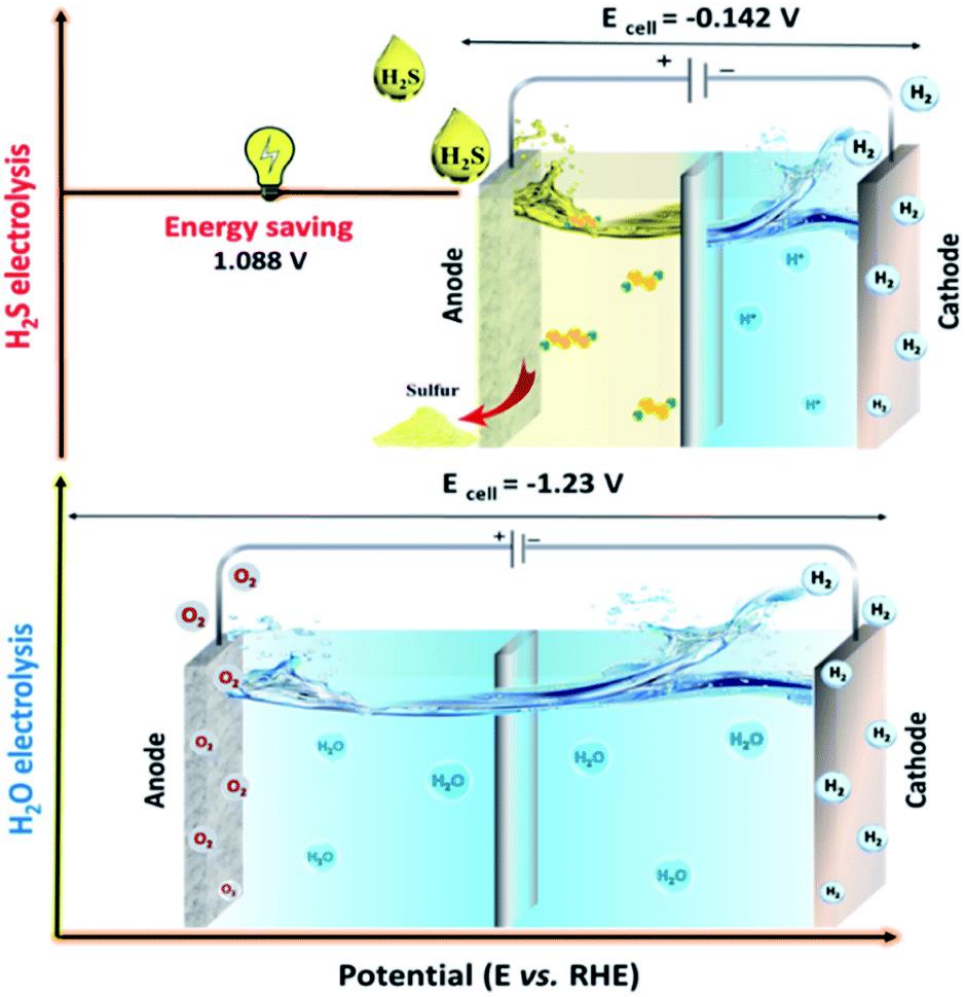

Figure 2.6. A comparison between the cell voltage of H_2SOR and OER (with permission from the royal society of chemistry) [90]

Kraia et al.[91] prepared ceria (CeO_2) supported transition metals (i.e., Co, Ni, Fe, and Cu) for H_2S decomposition in the temperature range of 550-850°C and at atmospheric pressure. They used the wet impregnation method to synthesize 20 wt.% Co-, Ni-, Fe-, and Cu-CeO_2. They found

out that the H_2S conversion rate is directly relevant to the experimental temperature. As the experimental temperature increases, the H_2S conversion increases as well. Among the investigated materials, Co-CeO_2 showed the most promising performance in terms of both stability and activity.

Tolba et al.[92] did a computational study on the effect of doping transition metals on the catalytic activity of TiO_2 (101) surfaces. They doped TiO_2 (101) with Cr^{4+}, V^{4+}, Mn^{4+}, and Nb^{4+}. Their calculation of defect formation energy showed that doping TiO_2 with the before-mentioned transition metals increase both stability and activity of the catalyst toward H_2S splitting to hydrogen and sulfur. Their DFT calculations revealed that doping TiO_2 (101) with V^{4+} decreases the adsorbed-H_2S splitting energy in favour of easier hydrogen production. They believe that the redistribution of charge upon adsorption is the main reason contributing to the improved activity as well as stability of the doped catalysts.

Raybaud et al.[93] investigated the nature of active sites in MoS_2 catalyst when it is in contact with H_2S gas. It is generally believed that the industrial catalysts for hydrodesulfurization are mainly based on transition-metal-sulfide catalysts. The coordinatively unsaturated sites at the edge of these catalysts have the highest activity among the other sites. The researcher came to the conclusion that the H_2S dissociation on the Mo-terminated edges of the MoS_2 catalyst is an exothermic process. These edge sites can show a sulfur coverage of up to 50%.

Lyu et al.[94] found a promising carbon-rich carbon nitride nanocatalyst for H_2S oxidation at room temperature. They demonstrated that introducing carbon atoms in a carbon nitride matrix can positively lead to the generation of catalytically more active sites due to the change in the electronic system. Carbon introduction can also provide oxygen-containing functional groups on the surface of the nanocatalysts, which results in an H_2S conversion rate of 99% and a S selectivity of up to 95%. However, the experimental temperature needs to be around 200℃. They also used

DFT calculations to find the adsorption energies of different species on the nanocatalysts. The adsorption energies of their species were calculated using the following equation:

$$E_{ads} = E_{ad+sub} - E_{sub} - E_{ad} \quad (3)$$

where E_{ads} is the total adsorption energy (substrate with intermediate), E_{sub} is the slab (substrate) energy, and E_{ad} is the total energy of a single H_2S molecule. DFT calculations also proved that introducing carbon to the system results in higher catalytic activities of H_2S selective oxidation.

Mohamadi and Bashiri[95] studied the kinetics of H_2S conversion to H_2 on Pt (111) surface using kinetic Monte Carlo (kMC) simulation. They measured H_2 desorption intensity at various temperatures to find the highest yield at the lowest temperature. The researchers found out that H_2SOR is completed after 5μs with a percent yield of around 98% at 227℃.

Xu et al.[96] worked on the catalytic composition of H_2S into H_2 and S using microwave radiation. They synthesized MeS-based (Me = Ni and Co) microwave catalyst. Using the mechanical mixing method, NiS and CoS nanoparticles were added to $Al_2O_3/BaMn_{0.2}Cu_{0.8}O_3$ resulting in final products of $NiS/\gamma\text{-}Al_2O_3/BaMn_{0.2}Cu_{0.8}O_3$ and $CoS/\gamma\text{-}Al_2O_3/BaMn_{0.2}Cu_{0.8}O_3$, respectively. They found that mid-temperature microwave radiation can break the chemical equilibrium of the H_2S decomposition reaction. The H_2S conversion to H_2 was seen to be 80.33% for $CoS/\gamma\text{-}Al_2O_3/BaMn_{0.2}Cu_{0.8}O_3$ at 788℃ and 44.98% for $NiS/\gamma\text{-}Al_2O_3/BaMn_{0.2}Cu_{0.8}O_3$ at 650℃.

An experimental and computational study was done by Zhang et al.[20] on the catalytic activity of the graphene-encapsulated metal catalyst for H_2SOR. Through the template-assisted synthesis method, the researchers successfully prepared CoNi nanoparticles under a reducing atmosphere. These nanoparticles were then encapsulated by graphene shells by a chemical vapor deposition (CVD) method at 600℃ and then were doped by one nitrogen atom. Using cyclic

voltammetry (CV) experiments, Zhang et al. compared their CoNi@NGs with other precious materials, including IrO_2 or 40% Pt/C. CoNi@NGs showed superior activity compared to the mentioned precious materials. Electrochemical Impedance Spectroscopy (EIS) was also done, and CoNi@NGs showed the least resistance to the reaction. Experimental durability measurements were also done, and the catalyst did not show any degradation after 500 hours of reaction. DFT calculations were also performed to account for the promising activity of CoNi@NGs towards H_2SOR. In general, the binding strength of the reaction intermediates on the surface can play an important role in the final activity of the catalyst. In the case of H_2SOR, they found that a catalyst showing Gibbs free energy of adsorbed S (ΔG_{S^*}) of around 0 would be considered a promising catalyst. Pure graphene or CoNi nanoparticles have either very strong or very weak adsorption energies, which is not favored in H_2SOR. Projected density of states (PDOS) analysis also showed that the electronic modification by the encapsulating graphene and the doped nitrogen is the contributing result to this superior activity.

2.6. Summary of Past Research

Thermal and electrochemical oxidation of H_2S has been attracted attention during the past few years since it provides a carbon-free method for converting this hazardous gas to different useful elements like hydrogen, oxygen, and sulfur. Although different catalysts have been used for this purpose, they are associated with either intricate synthesis or high required overpotentials starting from 0.22 V. Thermal oxidation of H_2S still suffers from high temperature requirements which limits the practical application of this approach. Conclusively, the most suitable catalysts for electrochemical oxidation of H_2S include Co- and Ni-doped metal sulfides and metal oxides that can yield hydrogen with low temperature requirements but suffer from intricate designs.

Chapter 3. Methodology

3.1. Examples of Density Functional Theory (DFT) in Real Life

Prior to defining what Density Functional Theory (DFT) is, there are real-world cases of DFT applications that we can look at. An example of the literature is first provided to better identify the possible applications of DFT and what can be achieved.

3.1.1. Ammonia Synthesis by Heterogeneous Catalysis

One chemical process of paramount importance is the catalytic synthesis of ammonia (NH_3). The Haber-Bosch process is an industrial method for producing ammonia by combining nitrogen (N_2) and hydrogen (H_2) gas under high pressure and temperature conditions in the presence of an iron-based catalyst[1]. Invented by Fritz Haber in 1909 and industrialized by Carl Bosch in 1913, this process has become the primary method for ammonia production, driving the global fertilizer industry and contributing significantly to worldwide food production.

The Haber-Bosch process operates at high pressure (150-350 atm) and temperature (350-550°C) to thermodynamically favor ammonia formation. Nitrogen and hydrogen gases are typically mixed in a 1:3 molar ratio, then introduced to the reactor containing an iron-based catalyst, which lowers the activation energy required for the reaction to occur. The catalysts are primarily composed of iron, with promoters such as potassium, calcium, or aluminum oxide, enhancing their performance.[97]

The overall reaction for ammonia synthesis is exothermic, represented by the following equation (Eq. 4).[98]

$$N_2(g) + 3H_2(g) \rightleftharpoons 2NH_3(g)\ \Delta H° = -92.4\ kJ/mol \quad (4)$$

Some noteworthy alternatives include electrochemical, photochemical, and biological methods. Electrochemical synthesis utilizes electric current to drive the reaction, and when combined with renewable energy sources, it has the potential to significantly reduce the environmental impact of ammonia production.[99] Photochemical synthesis uses light to facilitate the ammonia formation process, while biological methods, such as microbial nitrogen fixation, leverage natural processes to produce ammonia under ambient conditions.

As for electrochemical reactions, different metal catalysts like iron (Fe) and ruthenium (Ru) have been used to get this reaction to proceed. Fe and Ru nanoparticles have shown high catalytic activities for this reaction.[100] However, the reason behind the overall surface reactivity of these catalysts is still unknown. This issue brings up a fundamental question: Is there a connection between the shape and size of nanoparticles and their activity? The answer to this question can potentially be used to further investigate catalysts that could be more promising for ammonia synthesis. Hellman et al. used DFT to unravel the answer to this question.[99] They found that the ammonia synthesis net reaction goes through 12 distinct steps on a catalyst. The rate of reaction for each of these steps depends on the local coordination of metal atoms that are involved in the reaction. They found that the most paramount step in ammonia synthesis is N_2 bond breaking, as it is the most energy-intensive step.

3.2. Density Functional Theory (DFT)

3.2.1. The Born-Oppenheimer Approximation and The Schrödinger Equation

We will start with the idea of describing the properties of some well-defined collection of atoms. Energy and the change in their energies due to their movement is one of the important aspects of

these atoms. An atom's nuclei and rotating electrons define where an atom is. Since the atomic nuclei are 1800 times heavier than the electrons, we could acknowledge that electrons respond to their surroundings way more rapidly. Thus, we can imagine different scenarios happening inside an atom. In the first scenario, we find the lowest energy state for a given set of electrons rotating around the nuclei; we refer to this state as the ground state of electrons. This mathematical separation of electrons and nuclei is called the Born-Oppenheimer approximation.[100]

The Born-Oppenheimer approximation (BOA) is a fundamental concept in quantum chemistry and molecular physics. It allows for the simplification of molecular wave functions and the separation of nuclear and electronic motion in molecules, which greatly reduces the computational complexity of quantum mechanical calculations. The approximation is based on the observation that nuclei are much heavier than electrons and, therefore, move much more slowly.[101]

In a molecule, the motion of electrons and nuclei are coupled, as electrons are attracted to the positively charged nuclei and repelled by other electrons. This coupling results in a complex, multi-dimensional potential energy surface (PES) that governs the behavior of the system. Solving the Schrödinger equation for this coupled system is a daunting task, even for relatively small molecules.[102]

The BOA simplifies this problem by assuming that the motion of the electrons can be treated independently of the motion of the nuclei. This is justified by the large mass difference between electrons and nuclei; it is assumed that the electrons can adjust instantaneously to any change in the position of the nuclei.[103,104] This allows one to separate the molecular wave function into an electronic wave function and a nuclear wave function. The electronic wave function depends only on the positions of the electrons and the fixed positions of the nuclei, while the nuclear wave function depends on the positions of the nuclei.[103]

The BOA leads to two separate equations: the electronic Schrödinger equation and the nuclear Schrödinger equation. The electronic Schrödinger equation is solved first for a fixed nuclear configuration, yielding the electronic wave function and the electronic energy. The nuclear Schrödinger equation is then solved using the electronic energy as an effective potential energy surface for the motion of the nuclei.[105]

However, the BOA is not always valid, and there are cases where it breaks down. For instance, when dealing with light elements like hydrogen or with light molecules like graphene, the mass difference between the electrons and nuclei is not as large, and the approximation becomes less accurate. Additionally, in some processes involving electronically excited states, such as photochemical reactions and non-adiabatic transitions, the BOA may fail due to a strong coupling between electronic and nuclear motion.[106,107]

The simplest, time-independent, non-relativistic Schrödinger equation is $H\Psi=E\Psi$. In this equation, H corresponds to the Hamiltonian operator, and Ψ is a set of electronic wave functions (i.e., solutions). Each of these solutions, Ψ_n, has a corresponding eigenvalue, E_n, which is a real number. This number satisfies the equation. However, this form of the Schrödinger equation will be converted to a more complex form when we want to describe the interactions between multiple electrons and multiple nuclei. A more detailed description of the Schrödinger equation is:

$$[-\frac{\hbar^2}{2m}\sum_{i=1}^{N}\nabla_{\mathrm{r}}^2+\sum_{i=1}^{N}V(r_i)+\sum_{i=1}^{N}\sum_{j<i}U(r_i,r_j)]\Psi=E\Psi \quad (5)$$

Where m is the electron mass, and Ψ is the electronic wave function. The three summations in this formula correspond to the kinetic energy of each electron, the interaction energy between each electron and the collection of atomic nuclei, and the interaction energy between different electrons, respectively.[100]

Despite the fact that the electron wave function relies on the coordinates of all electrons, it can be simplified by approximating it as a product of individual electron wave functions, denoted as $\Psi = \Psi_1(r)\Psi_2(r)...\Psi_N(r)$. This simplified form, known as a Hartree product, has been backed up by practical reasons. It's important to note that the number of electrons (N) is significantly larger than the number of nuclei (M) due to each atom having one nucleus and numerous electrons. For instance, if we consider a single CO_2 molecule, the full wave function would be a 66-dimensional function (3 dimensions for each of the 22 electrons). However, if we were studying a nanocluster consisting of 100 Pt atoms, the full wave function would require over 23,000 dimensions. These numbers illustrate why solving the Schrödinger equation for real-world materials has been a challenging task that has occupied brilliant minds for a considerable portion of a century.[100]

The situation becomes even more challenging when we examine the Hamiltonian, *H*. The term in the Hamiltonian that accounts for electron-electron interactions is particularly crucial in terms of solving the equation. The form of this contribution implies that the individual electron wave function, $\Psi(r)$, we defined earlier, cannot be determined without simultaneously considering the wave functions associated with all the other electrons. In other words, the Schrödinger equation represents a many-body problem. While solving the Schrödinger equation can be considered the fundamental problem of quantum mechanics, it's important to recognize that the wave function for a specific set of coordinates cannot be directly observed. The observable quantity, in principle, is the probability that the N electrons are located at a particular set of coordinates, $r_1,..., r_N$. This probability is given by $\Psi^*(r_1,..., r_N)\,\Psi\,(r_1,..., r_N)$, where the asterisk denotes a complex conjugate.[100]

Additionally, it is worth noting that in experiments, we generally do not distinguish between individual electrons in the material as electron 1, electron 2, and so on. Furthermore, even if we wanted to assign such labels, it would be difficult to do so. This means that the physically

relevant quantity is actually the probability that a set of N electrons, regardless of their order, have coordinates r_1,..., r_N. A closely related quantity is the electron density at a specific position in space, n(r). This can be expressed in terms of the individual electron wave functions:

$$n(r) = 2\sum_i \Psi_i^*(r)\Psi_i(r) \quad (6)$$

Here, the summation is performed over all the individual electron wave functions occupied by electrons. Thus, the term within the summation represents the probability of an electron in the individual wave function $\Psi_i(r)$ being located at position r. The factor of 2 arises from the spin of electrons, and the Pauli exclusion principle dictates that each individual electron wave function can be occupied by two electrons with different spins. This is a purely quantum mechanical phenomenon without a classical physics counterpart. The key point of this discussion is that the electron density, n(r), which depends on only three coordinates, contains a significant amount of observable information from the full wave function solution to the Schrödinger equation, which depends on 3N coordinates.[100]

3.2.2. The Arrival of Density Functional Theory

The central idea behind DFT is to describe the electronic structure of a system in terms of electron density rather than the wavefunctions of individual electrons. According to the Hohenberg-Kohn theorems, the ground-state properties of a many-electron system can be uniquely determined by its electron density.[108] This means that instead of solving the complex many-body Schrödinger equation, which is computationally expensive and often impractical, DFT enables the calculation of the electron density using a more tractable approach. In DFT, the total energy of a system is expressed as a functional of the electron density.[109] This functional is typically split into two terms:

the kinetic energy of the electrons and the electron-electron interaction energy. The functional is usually approximated using exchange-correlation functionals, which account for the effects of electron exchange and correlation.[109] Exchange interaction captures the quantum mechanical effect that arises when two electrons simultaneously sway their positions, and correlation effect arises from the repulsion between electrons due to their Coulombic interactions. The correlation term accounts for the fact that the behavior of an electron is influenced by the positions and motions of all other electrons in the system.[100,110]

The Kohn-Sham equations are the fundamental equations of DFT. These equations introduce a set of fictitious non-interacting electrons, called Kohn-Sham orbitals, that reproduce the same electron density as the actual interacting electrons. Solving the Kohn-Sham equations involves finding the self-consistent electron density that minimizes the total energy of the system.[100]

DFT has significantly advanced our understanding of catalysis and has become an essential tool for theoretical and computational chemistry. However, it is important to note that DFT calculations rely on certain approximations and assumptions, such as the exchange-correlation functional used, which can introduce errors.[100] Researchers continuously strive to develop more accurate and efficient functionals to overcome these limitations and expand the applicability of DFT.

3.3. *k*-Points in DFT

In density functional theory (DFT), k-points refer to the sampling points in reciprocal space used to discretize the Brillouin zone of a crystalline material. The Brillouin zone is a mathematical construct in solid-state physics that represents the allowed electronic states in a periodic crystal

lattice. In DFT calculations, the Brillouin zone is typically divided into a finite number of *k*-points, and the electronic energy of the material are evaluated at these specific *k*-points.[100] This allows us to determine the electronic properties of different materials.

Sampling the Brillouin zone with *k*-points is necessary because solving the Kohn-Sham equations, which form the basis of DFT, is computationally demanding for the entire Brillouin zone. By using a finite set of *k*-points, DFT calculations become more tractable, allowing for the efficient treatment of electronic structures in materials. The choice of *k*-points is crucial as it affects the accuracy and convergence of the DFT calculations. Generally, a denser k-point sampling provides a more accurate description of the electronic structure, but it also increases the computational cost. Therefore, a compromise is often made to balance accuracy and computational efficiency.[111]

3.4. DFT Structure Models

In computational chemistry, a proper catalyst model should be carefully designed and defined to better represent the real-world catalyst structure. In this research, the atomic simulation environment (ASE) package was used to construct all the catalyst models.[112] This package allows us to readily prepare our desired model as well as to dope various elements into our structure to positively manipulate the catalyst properties. The DFT models used in this research are shown below. A proper model must be periodic to present the most real experimental structure.[113,114] We use small models in DFT calculation to save computational time and resources. An important assumption in the periodic system is that the designed small model has been extended from two directions (*x* and *y*) to better represent a real catalyst surface. Designing a periodic system is important as it affects the final energies of a DFT system. If a DFT system is large, the electronic

relaxations will not get converged to the final energy we expect, and the calculations will remain half-completed. This is mainly because of limited computational resources.

We have investigated the catalytic activity of metal oxides (IrO_2, RuO_2, TiO_2, and MoO_2), metal sulfides (WS_2, TiS_2, MoS_2, and VS_2), and transition-metal-doped metal sulfides (Co-MoS_2, Ni-VS_2, etc.). For the undoped metal sulfides, we have investigated the catalytic activity on both the basal plane and edge. For metal oxides, we use a two-by-two four-layer (110) slab as the DFT model. For both undoped and doped metal sulfides, we use a three-by-three monolayer (001) slab. The reason for this decision comes from the experimental results, the literature, and the most stable facet.[3,93,115,116] We use DFT calculations to find the formation energy of each facet and choose the most stable facet for our calculations.

In designing the model, we also define a vacuum layer between the atomic layers of the structure. This vacuum should be large enough to prevent the interactions of our surface with the upper layer. We have considered a vacuum size of 18Å since this is considered large enough by the catalysis community and can prevent the unwanted interactions between the catalyst surface and its' upper layer in the *z* direction.[117–119] This is an important consideration in DFT calculation as unwanted interactions can result in catalyst layer reconstruction or incorrect final energies. A schematic of an appropriate vacuum size has been shown in Figure 3.1.

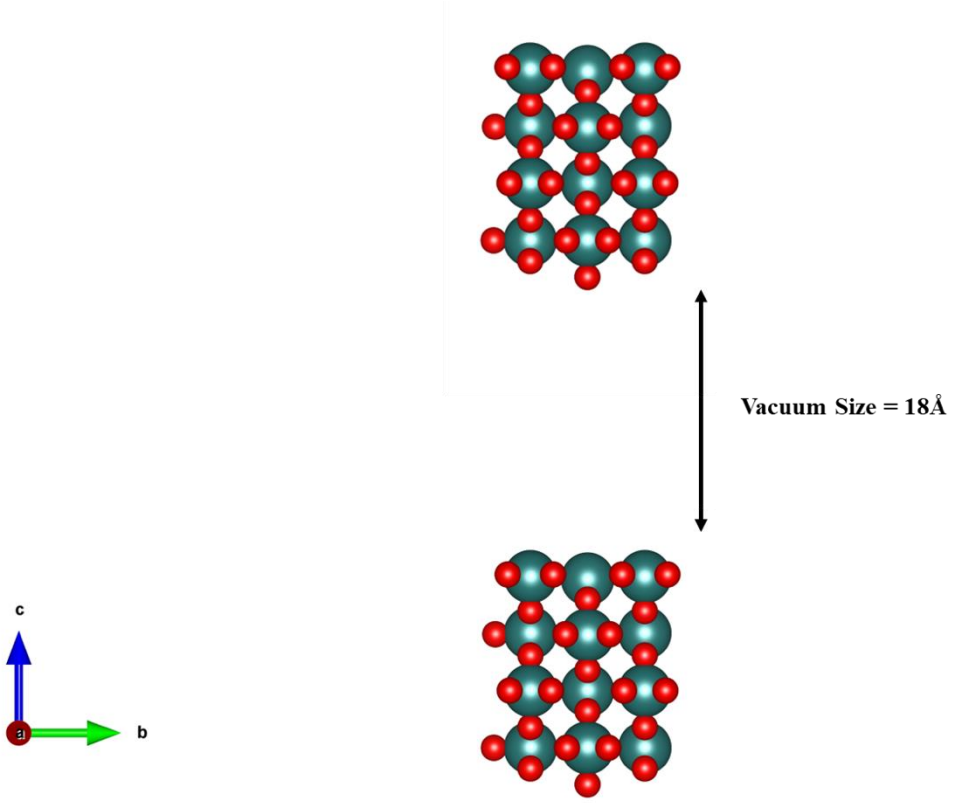

Figure 3.1. The vacuum between two models to prevent the unwanted electronic interaction between two slabs.

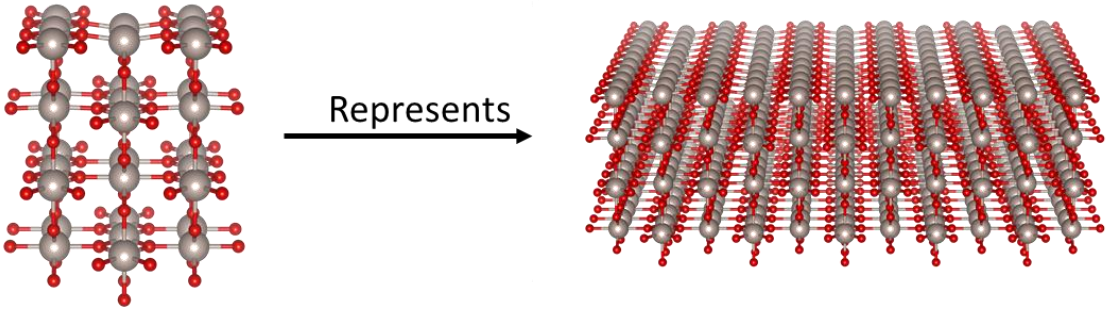

Figure 3.2. Periodicity representation of Iridium Oxide (IrO_2); the atoms in red are Oxygen, and the atoms in grey are Iridium

Assigning an incorrect DFT model will result in inaccurate prediction of the energies and final activities. These delegations are affected by different scenarios. A schematic of these considerations has been shown below by Christopher.[120]

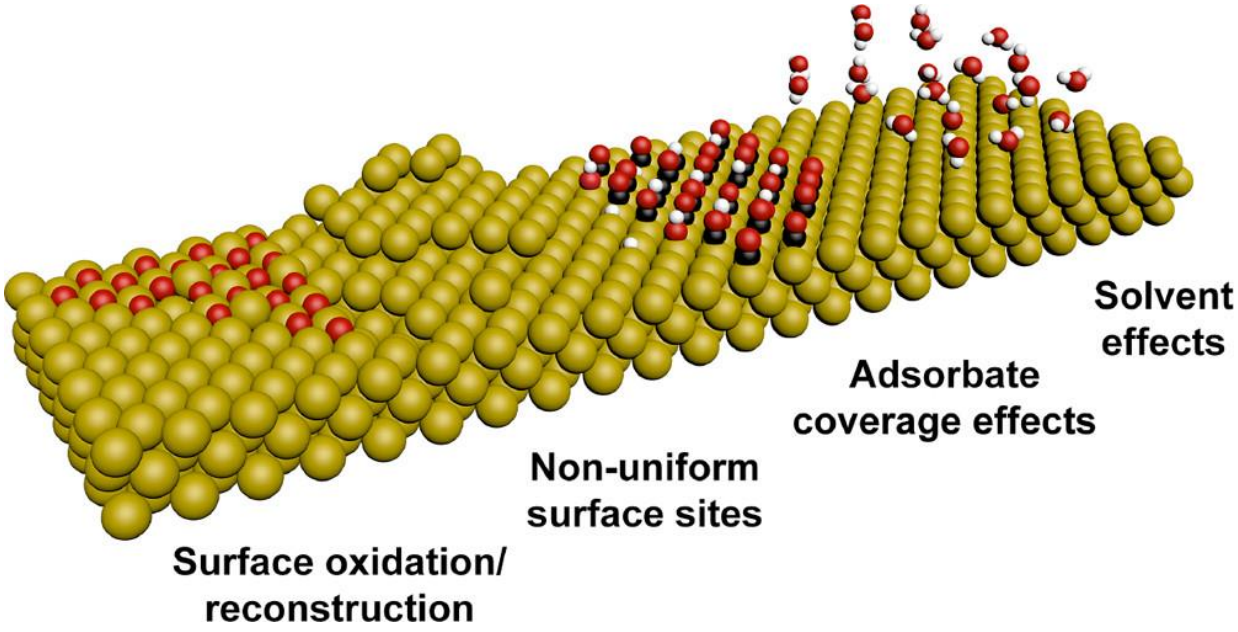

Figure 3.3. Factors need to be carefully considered while designing a catalyst model (reprinted from Surface-Mediated Processes for Energy Production and Conversion: Critical Considerations in Model System Design for DFT Calculations. Vol. 3, ACS Energy Letters. American Chemical Society; 2018. p. 3015–6.) [120]

The first consideration in taking a DFT model for the calculations is the solvent effect. Many catalytic processes happen in solutions where a liquid is present in the system. This will affect the chemical reaction since the solvent can change the properties of the catalyst and will interact with the adsorbates. A study by Yeh and Janik[117] shows how important it is to consider the solvent effect in DFT calculations. They investigated the Oxygen Reduction Reaction (ORR) activity of Pt (111) with and without solvent effect. They also looked into the density of the solution and how this can change the final energies. They found the Gibbs free energies of the intermediates and drew the corresponding Gibbs free energy diagram. Figure 3.4 shows this difference. The dark and blue lines demonstrate the Gibbs free energies at 0.8V and 1.2V, respectively.

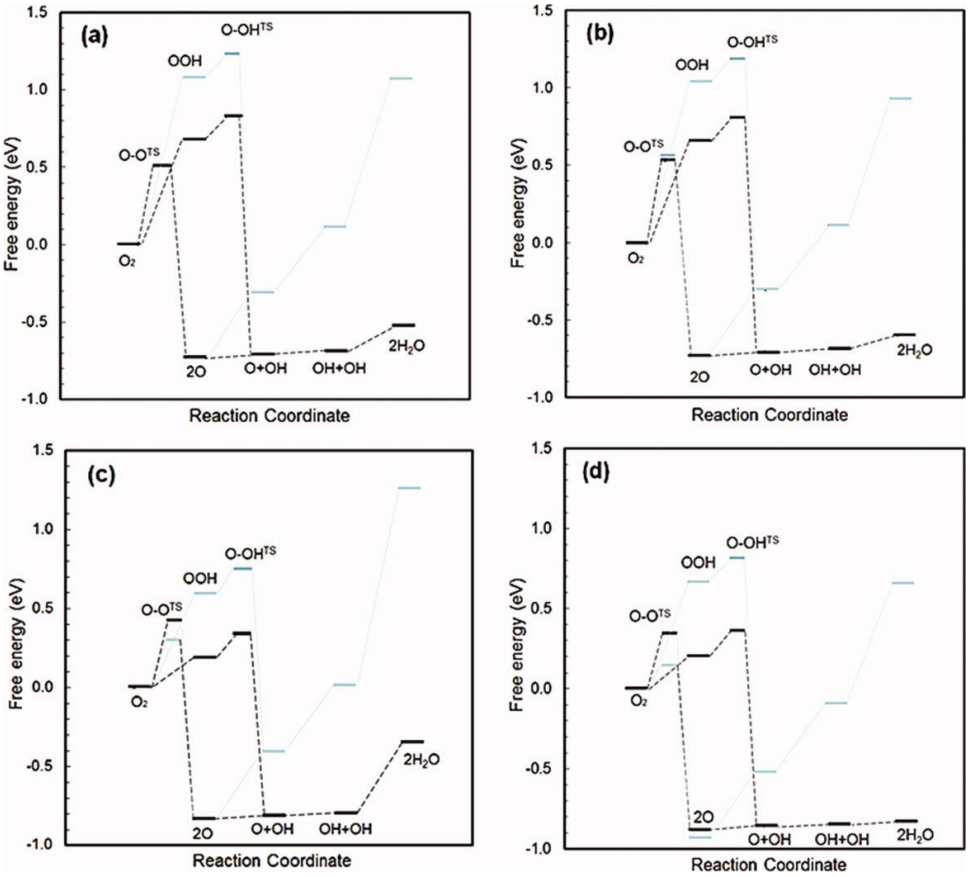

Figure 3.4. Gibbs free energy diagram for the ORR over the Pt (111) surface from a) the linear free energy model, b) the electric field model, c) the solvated model at $\rho = 1.0$ g.mL^{-1}, and d) the solvated model at $\rho = 0.86$ g.mL^{-1} (Rprinted from Density functional theory-based electrochemical models for the oxygen reduction reaction: Comparison of modeling approaches for electric field and solvent effects. J Comput Chem. 2011 Dec;32(16):3399–408.) [117]

This diagram shows that the energy levels can drastically change when the system is exposed to a solution. The researchers found that including water molecules as the solvent facilitates the OOH* reduction to OH* and consequently lowers the required overpotential.[121]

The second consideration in the DFT structure model is the surface reconstruction of the catalyst. Surface reconstruction usually happens under oxidizing environment. In this phenomenon, the composition of the catalyst changes. This change in composition can influence

the catalytic activity during the time. In DFT, we must carefully investigate this issue by adding or deducting specific elements or molecules from the surface to achieve the best DFT model.

Two review papers by Zeng et al. and Luo et al. have focused on some of the surface reconstructions in the water splitting reaction (OER).[122,123] They found that there are different reconstruction strategies in a system, and each of these contributes to the activity in a different means. These issues can be solved through a variety of methods, like introducing water to the system or defect engineering. A schematic table of various reconstruction strategies has been shown below.[123]

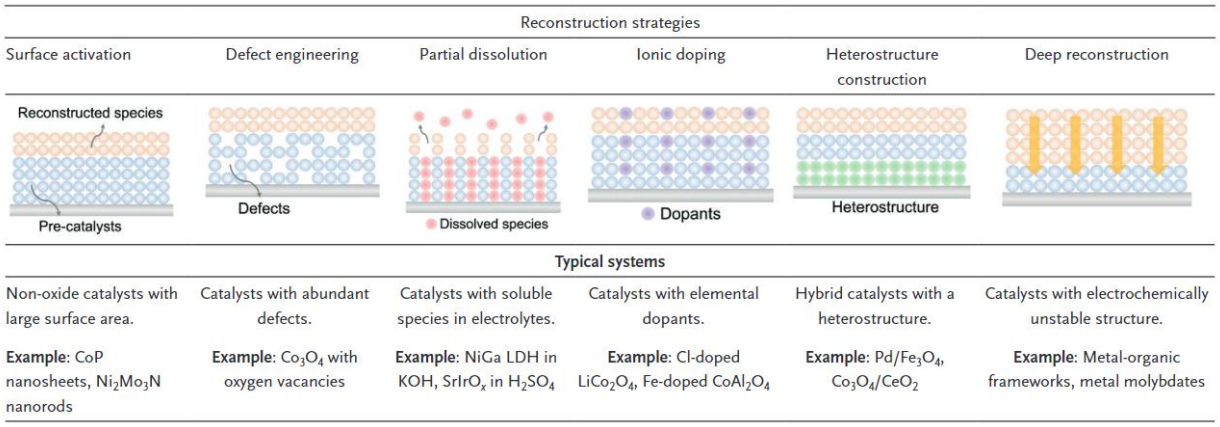

Figure 3.5. Different reconstruction strategies in water splitting reaction (reprinted from Surface Reconstruction of Water Splitting Electrocatalysts. Vol. 12, Advanced Energy Materials. John Wiley and Sons Inc; 2022.) [123]

The third important consideration, and the one we have looked into in this research, is the surface coverage effect by the reaction intermediates. This phenomenon happens when the interactions between the reaction intermediates and the catalyst's surface are very strong. This phenomenon has also been referred to as surface poisoning. We elaborate more on this topic in Chapter 4.

3.5. Reaction Intermediates

Every chemical reaction goes through a series of elementary steps before the production of end-products and reaching the end. These elementary steps (pathways) should be thoughtfully investigated because some of these steps determine the rate of the reaction and will influence how efficiently a product can be obtained. Most of these elementary steps include so-called reaction intermediates that are considered short-lived, high-energy, and extremely reactive molecules that, when generated in a chemical reaction, will turn into more stable molecules. H_2S oxidation reaction goes through the following elementary steps, found by Mohamadi and Bashiri in Eq. 1-5:[95]

$$H_2S_{(g)} + * \rightarrow H_2S*, \quad (7)$$

$$H_2S* + * \rightarrow HS* + (H^+ + e^-)*, \quad (8)$$

$$HS* + * \rightarrow S* + (H^+ + e^-)*, \quad (9)$$

$$(H^+ + e^-)* + (H^+ + e^-)* \rightarrow H_{2(g)} + 2*, \quad (10)$$

$$S* + S* \rightarrow 1/4S_{8(s)} + 2*, \quad (11)$$

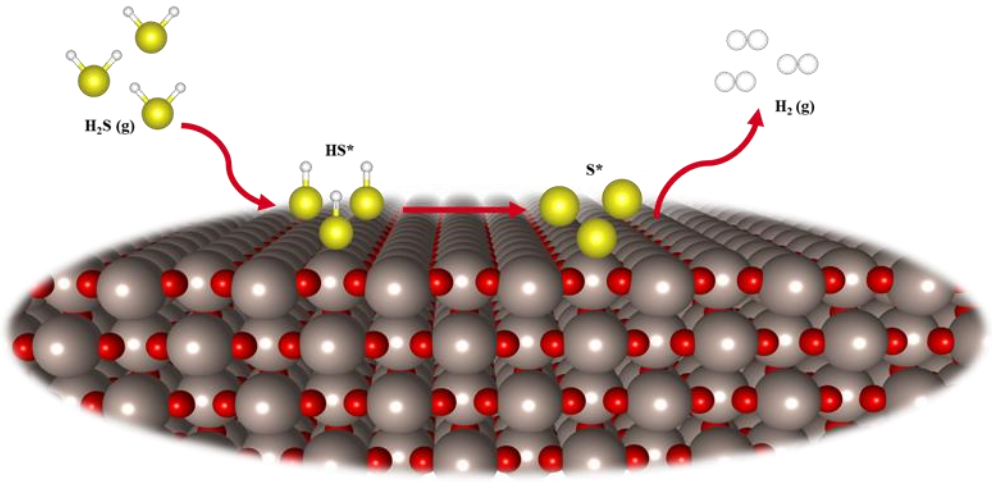

Figure 3.6. A schematic of H_2S electrolysis to sulfur and hydrogen

Each intermediate contributes differently to the final activity of the catalyst because they have different adsorption energies. These adsorption energies, when considered altogether in a Gibbs free energy diagram, can result in uphill or downhill trends that change the catalytic activity. As an example, the famous OER has three intermediates (HOO*, HO*, and O*). A work by Massaro et al. shows that the adsorption of HO* on the surface is stronger than the adsorption of O* or HOO*. Thus, the adsorption of HO* on the surface is considered the rate-limiting step.[124]

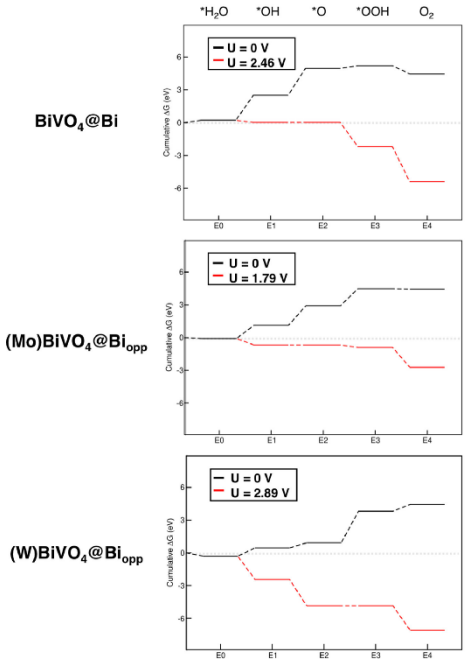

Figure 3.7. Different adsorption energies of OER intermediates on the surface of doped Bismuth Vanadate catalyst (reprinted from Oxygen Evolution Reaction at the Mo/W-Doped Bismuth Vanadate Surface: Assessing the Dopant Role by DFT Calculations. *Molecular Catalysis* 2022, *517*.) [124]

3.6. Computational Hydrogen Electrode (CHE)

The computational hydrogen electrode (CHE) is a theoretical concept introduced to assess the thermodynamics of electrochemical reactions involving hydrogen. It is particularly relevant in the context of electrocatalysis, where it serves as a reference state for comparing the energy of adsorbed species on catalyst surfaces. This concept simplifies the analysis of electrochemical reactions by providing a unified reference scale for comparing the energetics of various processes involving hydrogen.[125]

The CHE concept is based on the standard hydrogen electrode (SHE), which is a widely used experimental reference electrode that consists of a platinum electrode in contact with a

solution of 1 M $HClO_4$ and hydrogen gas at a partial pressure of 1 atm (1.01325 bar). The potential of the SHE is defined as 0 V, conventionally.

In computational studies, the CHE provides a means of determining the free energy of adsorbed hydrogen atoms on a catalyst surface relative to the free energy of a proton and an electron in a solution. This is achieved by calculating the energy difference between the adsorbed hydrogen and the reference hydrogen state (e.g., the gas phase H_2 molecule). The free energy change associated with the reference reaction ($2H^+ + 2e^- \rightarrow H_2$) is then used to relate the energy of adsorbed hydrogen to the thermodynamic scale of the SHE.[125]

The CHE approach has been widely adopted in computational studies of electrocatalytic reactions, particularly for the hydrogen evolution reaction (HER) and the oxygen reduction reaction (ORR). By using the CHE as a reference, researchers can systematically compare the performance of different catalyst materials and identify trends in activity as a function of adsorption energies.[125,126]

The CHE concept has also been extended to reactions involving other adsorbates, such as CO and O_2, by relating their adsorption energies to the free energy of the corresponding elementary reaction steps.[127] This approach, known as the "generalized CHE," provides a unified framework for understanding the trends in electrocatalytic activity across different reactions and materials.

3.7. Computational Details and Parameters

Vienna Ab-initio Simulation Package (VASP) code was used to perform to carry out the electronic structure calculations.[128] Atomic Simulation Environment (ASE) was used to simulate the model.[129] The Perdew-Burke-Ernzerhof (PBE) exchange-correlation functional of the Generalized Gradient Approximation (GGA) is used to describe the exchange-correlation effects.

This approximation enhances the local density approximation (LDA) by considering the relationship between exchange-correlation energy and the gradient of the electron density. By incorporating this gradient dependence, GGA functionals are able to account for non-local effects and offer improved accuracy in characterizing molecular and solid-state systems.[130] We have used PBE functional because it is one of the most accurate functional to estimate the electronic interaction between different molecules and metal surfaces.[131] Projected augmented wave (PAW) pseudopotentials with a cut-off energy of 500 eV were used. The Monkhorst-Pack meshes (*k*-points) of (4 × 4 × 1) was determined for all metal oxide calculations, (3 × 3 × 1) for all metal sulfide surface calculations, and (1 × 3 × 1) for all metal sulfide edge calculations. Energy and force convergence criteria were set to 10^{-7} eV and 0.005 eV/Å, respectively. A four-layer slab model was used for the simulation of the oxides. A monolayer three by three structure was used for all the metal sulfides. The bottom two layers of metal oxides were constrained, and the two upper layers, along with the intermediates were allowed to relax. No constraints were used for mono-layer metal sulfides. The computational hydrogen electrode (CHE) introduced by Nørskov et al. was adapted, which exploits that the free energy of a coupled proton-electron is equivalent to the energy of H_2 in the gas phase at standard conditions.[132]

3.8. ZPE and Entropy Contributions

In DFT, zero-point energy (ZPE) refers to the energy associated with the zero-point vibrations of atoms in a crystal lattice. It is a quantum mechanical effect arising from the Heisenberg uncertainty principle, which states that even at absolute zero temperature (0 K), particles still possess a minimum amount of energy due to their inherent vibrational motion. To include ZPE in DFT

calculations, one approach is to employ the quasi-harmonic approximation (QHA). The QHA treats the lattice vibrations as harmonic oscillators and considers the anharmonicity of the lattice potential energy. The phonon frequencies and vibrational modes of the crystal lattice are calculated using methods such as density functional perturbation theory (DFPT) or the frozen phonon approach. These vibrational frequencies are then used to evaluate the ZPE correction to the total energy.[133]

Entropy is a measure of the system's disorder or randomness. In DFT, entropy contributions are considered in the calculation of thermodynamic properties, such as free energy, reaction energies, and phase stability. The entropy can be decomposed into different components, including vibrational entropy and configurational entropy. Vibrational entropy is associated with lattice vibrations and is calculated by considering the phonon frequencies obtained from DFT calculations. The phonon density of states is used to determine the vibrational contributions to entropy. Configurational entropy accounts for the different arrangements or configurations of atoms or molecules in a system. It is often estimated using statistical mechanics approaches, such as the quasi-harmonic approximation or the Debye model.[100]

3.9. Gibbs Free Energy Diagram

Once we have all the energy values, we can start drawing the Gibbs free energy diagram based on each intermediate's Gibbs free energy. We use the following equations (Eq. 12-14) to find the Gibbs free energy of each intermediate. The final values from these equations with electron-proton transfer contributions will be used to draw the Gibbs free energy diagram for each catalyst.

$$\Delta G_{H_2S^*} = (E_{H_2S^*} + ZPE_{H_2S^*} - TS_{H_2S^*}) - E_{slab} - (E_{H_2S(g)} + ZPE_{H_2S(g)} - TS_{H_2S(g)}) \quad (12)$$

$$\Delta G_{HS^*} = (E_{HS^*} + ZPE_{HS^*} - TS_{HS^*}) + 0.5^*(E_{H_2} + ZPE_{H_2} - TS_{H_2}) - E_{slab} - (E_{H_2S(g)} + ZPE_{H_2S(g)} - TS_{H_2S(g)}) \quad (13)$$

$$\Delta G_{S^*} = (E_{S^*} + ZPE_{S^*} - TS_{S^*}) + 1^*(E_{H_2} + ZPE_{H_2} - TS_{H_2}) - E_{slab} - (E_{H_2S(g)} + ZPE_{H_2S(g)} - TS_{H_2S(g)}) \quad (14)$$

In these equations, E is defined as the energy and E_{slab} is defined as the surface energy without any intermediates.

3.10. Limiting Potential (U_L) and Overpotential (η)

Limiting potential (U_L) in electrochemistry refers to the potential (voltage) at which the rate of an electrochemical reaction becomes limited by the rate of mass transport of the reactants or products to or from the electrode surface. At the limiting potential, the reaction rate is no longer controlled by the electrode kinetics but by the diffusion of the species involved in the reaction.

In other words, the limiting potential is the voltage at which the concentration of the reactants at the electrode surface becomes so low (or the concentration of the products becomes so high) that the reaction rate is limited by the diffusion process. This potential is important in the study of electrochemical systems, as it helps to determine the maximum current that can be achieved for a given reaction and the efficiency of the system. It is also useful in understanding the behavior of electrochemical cells under different conditions, such as varying concentrations, temperatures, and electrode materials.[134,135]

In DFT, the limiting potential is the most straightforward standard for an electrocatalyst's activity. Limiting potential is the potential at which all the steps of the reaction are downhill in the Gibbs free energy diagram at U = 0 V.[136]

Overpotential (η) in electrochemistry refers to the difference between the actual potential (voltage) required to drive an electrochemical reaction (i.e., the limiting potential) and its thermodynamically predicted potential (equilibrium potential). It is a measure of the extra energy needed to overcome various factors that slow down the reaction, such as activation energy, concentration gradients, and resistive losses in the electrode and electrolyte.

In other words, overpotential is the additional voltage applied to an electrochemical cell beyond the equilibrium potential to achieve a desired reaction rate. It is often expressed in volts (V) and can be positive or negative, depending on whether the reaction is an oxidation or reduction process. Overpotential is an important parameter in the design and optimization of electrochemical systems, such as batteries, fuel cells, and electrolyzers.[134,135]

In DFT, the overpotential refers to the highest energy difference between two consecutive steps in the Gibbs free energy diagram at the working potential (aka equilibrium potential). For H_2SOR, the working potential is U = 0.14 V.[125]

3.11. Surface Coverage Analysis

In most of the systems, the catalytic reaction happens on the surface of the catalyst. As we discussed in Chapter 2, a catalyst surface is exposed to different intermediates existing in a chemical reaction. These intermediates can poison the catalyst surface resulting in catalyst degradation. In a few cases, this poisoning will contribute positively to a catalyst activity, counterintuitively. In this section, we will discuss both cases and why this is an important consideration in the H_2S oxidation reaction.

A study by Chang et al. was performed to investigate the dependence of 2-eletron oxygen reduction reaction on the oxidized Pt surface. Coverage analysis and DFT calculation were done,

and researchers found out that the activity improves once they reach an optimum level of surface oxidation (Pd_3@3V-O*/HO*). This structure has three oxygen intermediates in three vacancies of the surface and one free HO intermediate. This means that once the surface is oxidized with different oxygen or hydroxy molecules, the intermediate adsorption energy gets augmented, and the required overpotential for H_2O_2 production becomes lower.[137]

Verga et al. used DFT calculations to study the coverage effect on the adsorption of oxygen atoms on Pt nanoparticles. The researchers constrained the movement of Pt atoms in the nanocluster to save computational resources. They found out that the higher oxygen coverage leads to the weaker binding of following oxygen atoms on the surface and leads to lower required overpotential for fuel cell applications.[138]

Two different studies by Pillay et al. and Dou et al. were carried out to investigate the negative effect of catalyst poisoning on the activity. Pillay et al. showed that although the presence of Co improves the adsorption of the intermediates on the Pt catalyst, the following oxidized Co-S molecules will hinder the reaction and lead to higher required overpotentials.[139] Dou et al. investigated the effect of H_2S and HCl on the activities of Ni and Fe catalysts for steam reforming. They found out that both HCl and H_2S can poison the surface of both Ni and Fe catalysts by chemisorption.[140]

In this work, we have performed surface coverage analysis by adding different intermediates on the surface of our metal oxide catalysts. First, we add one intermediate (S or HS) to the surface, and then we relax our model structure. Second, we take the previously relaxed structure, and we add the second intermediate (S if we started with S; HS if we started with HS). Again, we do DFT calculations to relax our model structure. We continue putting the consecutive intermediates until the surface is fully covered by these intermediates. In all the investigated metal oxides, we could

see that the Gibbs free energy gets reduced, indicating a more stable surface for the reaction. This means that the surfaces all of metal oxides tend to adsorb H_2SOR intermediates strongly, which can affect the catalyst performance and durability in long-term applications.

3.12. DFT Strengths and Weaknesses

Conclusively, DFT comes with a combination of pros and cons. It is a powerful computational technique that helps catalysts researchers to save a lot of time and resources by determining the most promising structures and materials for the trial-and-error phase. The structure models in DFT are easy to manipulate with. The results from DFT calculations can complement the experimental analysis by providing a mechanistic understanding of the catalytic reaction.

On the other hand, as mentioned before, DFT is not completely accurate and always comes with roughly 5% inaccuracy. With DFT, we usually cannot take different experimental conditions, such as the effect of temperature, the electrolyte used, and the pressure into consideration. In addition, DFT cannot fully predict the electronic energies for complex model structures consisting of more than 200 heavy elements.[141,142]

Chapter 4. Results and Discussion

4.1. Catalytic Activities of Metal Oxides

4.1.1. Gibbs Free Energy Diagram Before Surface Poisoning

To model the H_2S electrochemical oxidation reaction, we follow the mechanism introduced in Eq. 15-18.

$$H_2S_{(g)} + * \rightarrow H_2S*, \quad (15)$$

$$H_2S* \rightarrow HS* + (H^+ + e^-), \quad (16)$$

$$HS* \rightarrow S* + (H^+ + e^-), \quad (17)$$

$$S* \rightarrow 1/4S_{8(s)} + *, \quad (18)$$

The first step is a non-electrochemical step that involves the adsorption of the H_2S molecule on the surface. The second step is an electrochemical oxidation step, which forms the first intermediate of the reaction, i.e., HS*. Further electrochemical oxidation of HS* results in forming S*. Up to this step, both protons have been extracted from H_2S and have been released into the solution. This is the step where two protons and two electrons combine and form hydrogen. Therefore, the hydrogen production step is the second to last step. The last step in the free energy diagram is the phase transition in which the adsorbed S* species will transition to the most thermodynamically favored phase of solid sulfur (S_8).[20] Since our focus in this study is on understanding the trends in the activity of different oxides in extracting hydrogen from H_2S, we skip simulating the phase transition for the last step.[132] Sulfur production occurs through consecutive steps of polysulfurization that have been investigated in the report by Zhang et al.[20] It

is also known that the accumulated sulfur atoms on the surface lead to catalyst poisoning that hinders the activity of the catalyst.[143]

All different possible active sites (coordinatively under-saturated site (CUS), bridge, and hollow) on the surface were studied (Figure 4.1) and the most stable ones (Table 4.1) are used to construct the free energy diagrams.

Figure 4.2(a) displays the free energy diagram for the four rutile oxides studied herein at the working potential, U = 0.14 V. At this potential, the chemical potential of the electrochemical steps is shifted down by -*ne*U, where *n* is the number of transferred electrons. Using this method, we can calculate the theoretical overpotential for the H_2SOR reaction, which is the largest difference between each subsequent electrochemical step at U = 0.14 V. This analysis indicates that the examined oxides except IrO_2 and RuO_2 are highly active for H_2SOR with the calculated overpotentials of 0 V. For IrO_2 and RuO_2, the calculated overpotentials are 0.27 V and 0.17 V, respectively, which are associated with the step $HS^* \rightarrow S^* + (H^+ + e^-)$. We note that most of the studied oxides have negative adsorption energies for S-intermediates, with MoO_2 being the worst, implying a high risk of sulfur poisoning during the electrochemical cycle. RuO_2-based catalyst is the most efficient catalyst for H_2SOR with low required overpotential and moderate adsorption energies for S-intermediates, which agrees with the experimental observation.[144]

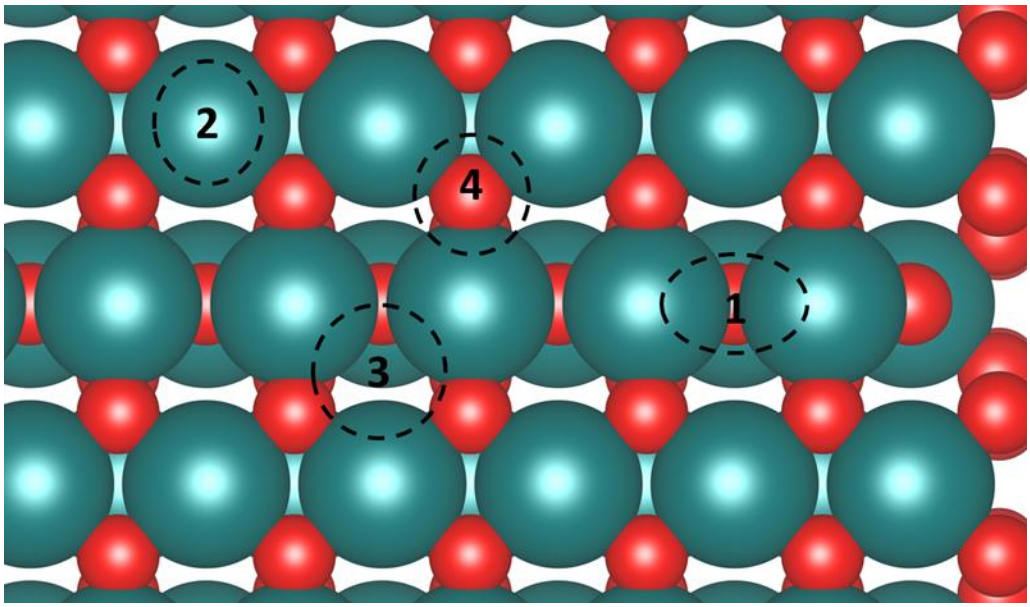

Figure 4.1. Different active sites investigated for metal oxide catalysts; Active sites number 1, 2, 3, and 4 correspond to the numbers in table 4.1. 1 is referred to as a bridge site and 2 is referred to as a coordinatively under-saturated site (CUS). 3 and 4 are other possible active sites. This figure is the top view of RuO_2.

Catalyst	*IrO_2*	*RuO_2*	*TiO_2*	*MoO_2*
Active Site				
H_2S - 1*	0.2	**-0.63**	0.34	-0.5
H_2S - 2*	0	-0.09	-0.14	-1.27
H_2S - 3*	**-1.6**	-0.54	-0.7	-0.6
H_2S - 4*	-0.6	-0.11	**-0.23**	**-1.43**
HS - 1*	-0.11	-0.53	0.38	-2.03
HS - 2*	0.29	0.3	-0.23	-0.42
HS - 3*	**-2.16**	**-0.99**	**-1.48**	**-2.92**

HS - 4*	-1.2	-0.59	-1.18	-1.81
S - 1*	-0.05	0.52	0.06	**-3.27**
S - 2*	-0.36	-0.01	-0.7	-1.28
S - 3*	**-1.75**	**-0.68**	**-1.34**	-3.18
S - 4*	0.69	1.15	0.1	-2.01

Table 4.1. Gibbs free energies for H_2SOR intermediates on all active sites on metal oxides (eV)

Figure 4.2(b) shows that HS* and S* adsorption energies linearly correlate on the examined oxide surfaces, which is similar to the observed trend for HO* and O* intermediates in oxygen evolution reaction.[145,146] This scaling relation shows that all oxides bind S-intermediates strongly, ranging from -3 eV to -1eV for HS* as an example. For all the examined oxides, the last step, which is the phase transition of adsorbed S* to polysulfide, is uphill. This step is not electrochemical and increasing the applied electrode potential does not reduce the thermodynamic barrier for phase transition. As a result, the high adsorption energies for S-intermediates poison the active sites and may prevent further oxidation of H_2S.

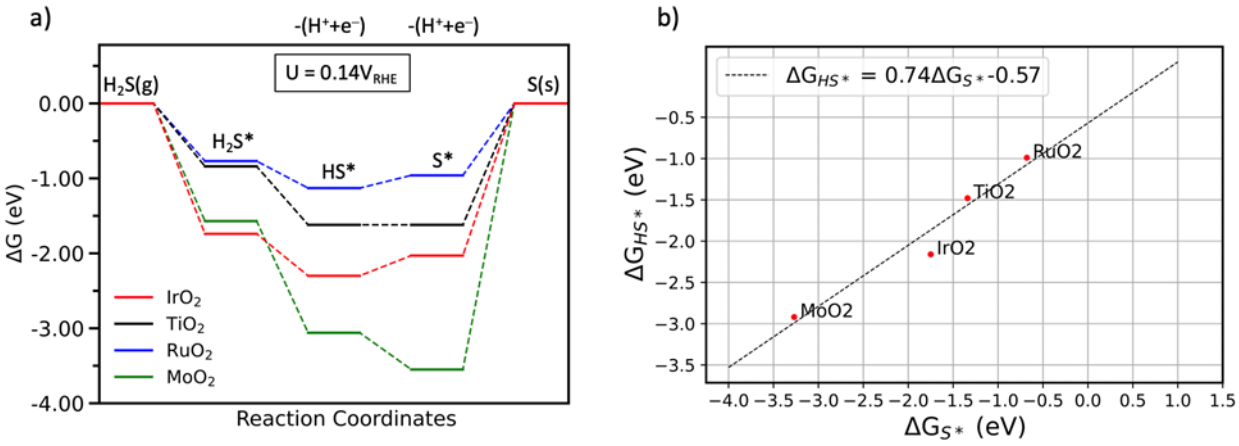

Figure 4.2. (a) Free energy diagram for H_2S oxidation reaction over the bare surface of different metal oxides at U = 0.14 V_{RHE}. (b) Scaling relation between free adsorption energies of HS* and S* on different examined oxides.

4.1.2. Surface Coverage Analysis for Metal Oxides

The fact that oxides bind S-intermediates strongly indicates that the long-term operation requires studying the relative stability of intermediates at the surface under reaction conditions. This has proven to be very important for electrochemical reactions such as CO_2 reduction reaction on oxides.[147] To take this into account, we investigate the relative stability of S-intermediates under reaction conditions by including coverage of different monolayer (ML) quantities of HS* and S* intermediates. The most stable coverages for each surface were identified under the standard potential of H_2S electrochemical oxidation (0.14 V_{RHE}) and modelled the H_2S oxidation reaction in the presence of those adsorbed species as spectators. Figure 4.3 displays the relative stabilities of various S-intermediate coverages as a function of electrode potential for all of the four examined oxides in this study. To obtain Figure 4.3, we have used the $\Delta G = G^0 - nU$ formula where G^0 is the calculated Gibbs free energy for each intermediate addition step, n is the number of existing hydrogen molecules for each intermediate addition (for HS* = 0.5, 1, 1.5, and 2; for S* = 1, 2, 3, 4), and U is the applied potential (range = 0 V to 1 V). The following equations (Eq. 19-26) show the linear equations used for this analysis for TiO_2 as an example. The first number is the total

Gibbs free energy calculated from DFT calculations and entropy and ZPE corrections. The coefficient behind the U is the number of hydrogen transfers in the system, and U is the theoretical H_2SOR potential, which is 0.14V.

$$\Delta G_{1S^*} = -1.34-1*U \quad (19)$$

$$\Delta G_{2S^*} = -0.97-2*U \quad (20)$$

$$\Delta G_{3S^*} = -0.78-3*U \quad (21)$$

$$\Delta G_{4S^*} = -0.12-4*U \quad (22)$$

$$\Delta G_{1HS^*} = -1.48-0.5*U \quad (23)$$

$$\Delta G_{2HS^*} = -2.2-1*U \quad (24)$$

$$\Delta G_{3HS^*} = -1.65-1.5*U \quad (25)$$

$$\Delta G_{4HS^*} = -1.04-2*U \quad (26)$$

For each coverage calculation, all possible combinations of adsorption sites were investigated for S* and HS* intermediates, and only the most stable ones were reported in Figure 4.3.

This analysis indicates that high coverages of S* and HS* stabilize the oxide surfaces, which is why they are prone to sulfur poisoning. Besides, for each individual oxide surface, we can identify the most stable surface coverage under the standard redox potential of H_2SOR, which is shown by the black vertical dashed-dotted line in Figures 4.3(a) to 4.3(d). We refer to the one sulfur coverage as 0.25 ML, which corresponds to the presence of only one sulfur on the four available sites at the oxide surface. Therefore, the full surface coverage (4 sulfur atoms on the surface) would be 1 ML. For instance, for RuO_2, the most stable surface at U = 0.14 V_{RHE} is the 1

ML surface (i.e., covered by 4 sulfur atoms). Figure 4.4(a) displays the most stable coverage for each oxide surface at U = 0.14 V.

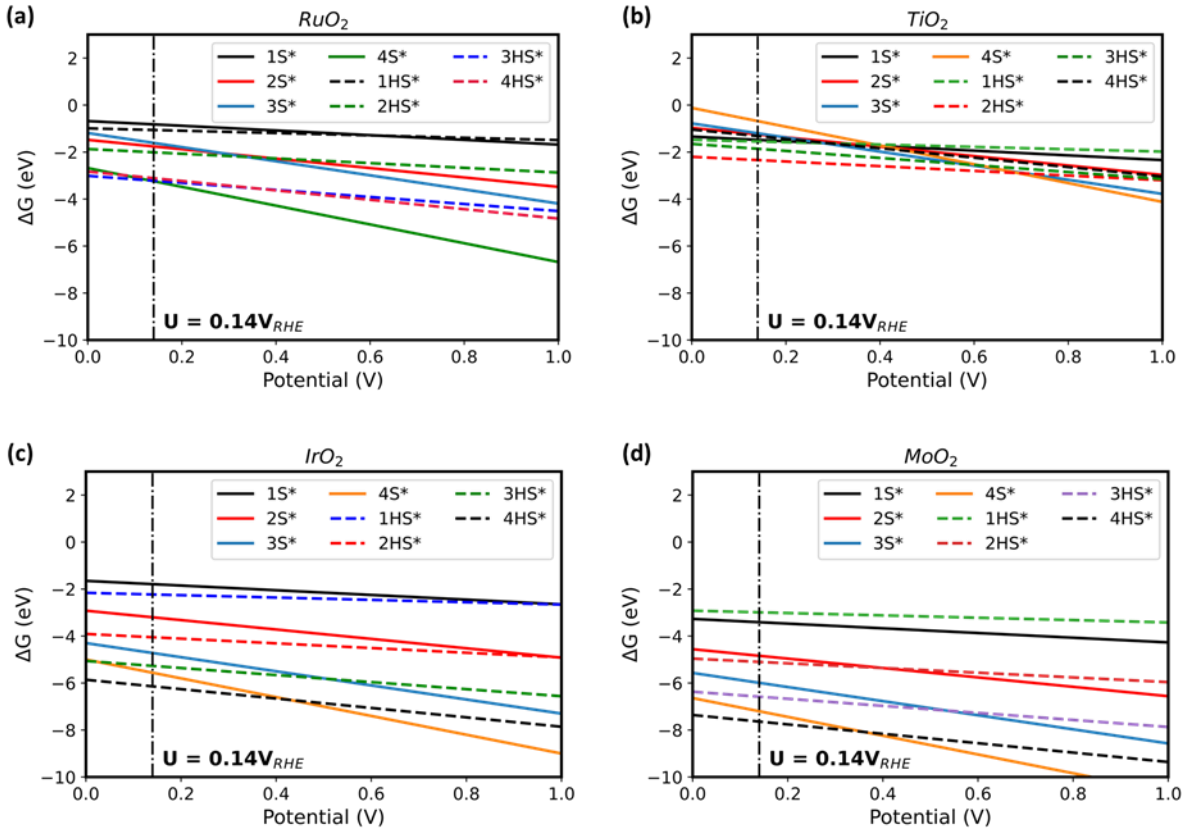

Figure 4.3. Relative stability plots for different S* and HS* coverages on the surface of (a) RuO_2, (b) TiO_2, (c) IrO_2, and (d) MoO_2.

4.1.3. Gibbs Free Energy Diagram After Surface Poisoning

Now that we have determined the equilibrium surface coverage, we will use these surfaces instead of the bare surface to simulate the H_2SOR. The fully covered surface with sulfur atoms is the equilibrium coverage for almost all oxides (Figure. 4.4(a)). Using those surfaces, we calculate the free energy of H_2SOR intermediates and revise our free energy diagram (Figure. 4.4(b)). As can be seen, most of the downhill steps in Fig. 4.2 become uphill, which indicates that the

electronic structure of the oxide surfaces is modified after sulfur poisoning. In the case of TiO_2 and MoO_2, this modification is in favor of the H_2SOR, requiring reasonable overpotentials of 0.49V and 0.68V, respectively, to initiate the reaction (Figure 4.4(c)). Since these overpotentials are associated for the catalysts that are already poisoned by sulfur atoms, we believe that these overpotentials are small enough to be considered promising catalysts for H_2SOR taking into account that TiO_2 and MoO_2 do not require any overpotentials before surface poisoning. An in-depth experimental study would be helpful to investigate the durability of these two catalysts in H_2S-exposed environment. We would like to emphasize that rutile is not the most stable crystal structure for MoO_2, so the likelihood of it becoming a practical catalyst for H_2SOR is low. As a result, we believe TiO_2 will be the most promising catalyst for long-term H_2SOR operation. Other oxide surfaces, such as IrO_2 and RuO_2, which initially showed high activity toward H_2SOR, appear to be losing activity, indicating that long-term operation with these catalysts will become a real issue.

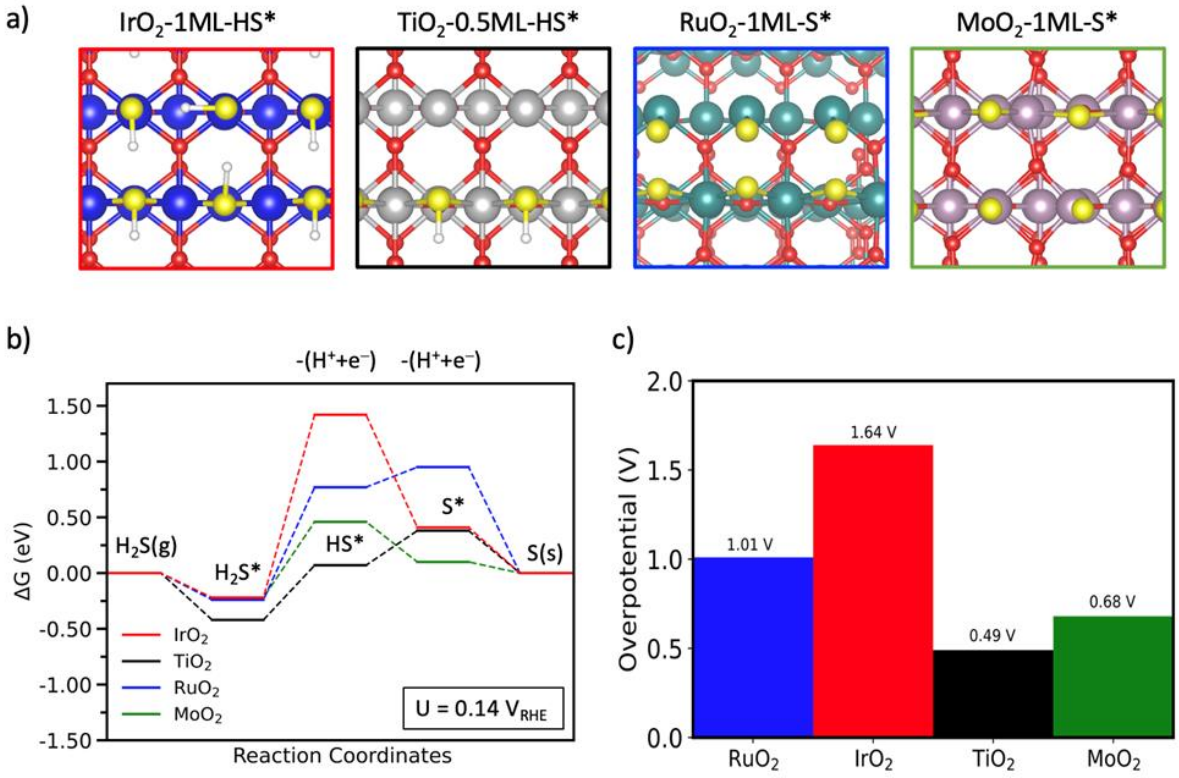

Figure 4.4. (a) Top view of the four rutile oxides studied herein with most stable S-intermediate coverages at U= 0.14 V_{RHE}. (b) Free energy diagram of H_2SOR over different metal oxides covered with S-intermediates shown in (a). (c) Calculated H_2SOR overpotentials.

The revised free energy diagram demonstrates how crucial it is to take into account the coverage of the sulfur species on the catalyst surface. Additionally, we observe that the final thermodynamic step (the desorption of S* as solid sulfur from the catalyst's surface) has a decreasing free energy, suggesting a facile phase transition to solid sulfur at the surface.

In summary, this comprehensive analysis provides valuable insights into the identification of the most promising catalysts for long-term operation of H_2SOR. The examination of free energy diagrams in Figures 4.2(a) and 4.4(b) allows us to draw important conclusions regarding the performance of various catalysts. Comparing the diagrams, it becomes evident that TiO_2 and MoO_2 exhibit superior characteristics compared to RuO_2. While RuO_2 initially demonstrates promising

hydrogen production rates, it becomes less active once it undergoes surface poisoning by sulfur atoms. This phenomenon necessitates higher overpotentials for RuO_2 compared to TiO_2 or MoO_2. Hence, the stability of the catalyst throughout the reaction is a crucial factor to consider. These findings emphasize the significance of the catalyst's stability, highlighting that metal oxides are highly susceptible to sulfur poisoning, which greatly affects their activity. The degree of poisoning restricts their efficiency and longevity as catalysts. Therefore, selecting a catalyst with excellent stability and resistance to sulfur poisoning is paramount in the search for an efficient H_2SOR catalyst.

In light of this, our investigation extended to exploring metal sulfides, particularly MoS_2. Metal sulfides, including MoS_2, possess inherent saturation with sulfur, making them less prone to sulfur poisoning.[93,148] This characteristic makes them attractive candidates for H_2SOR catalysts. To ensure a comprehensive analysis, we considered a range of metal sulfides, including MoS_2, TiS_2, WS_2, and VS_2, studying both their edge and basal planes. In the case of the basal plane, we examined both pristine structures and structures with vacancies doped with single atoms of first-row transition metals. By delving into the specific characteristics of these metal sulfides, we aimed to gain a deeper understanding of their potential as effective catalysts for H_2SOR. This investigation allowed us to assess their stability, activity, and resistance to sulfur poisoning, further expanding the scope of catalyst selection.

4.2. Catalytic Activities of Metal Sulfides

4.2.1. Pristine Metal Sulfides, Basal Plane, and Edge

To model the H_2SOR on sulfides edge and basal plane, we followed the mechanism introduced in Eq. 15-18. Various possible active sites on the basal planes and edge were studied (Figure 4.5 and

4.6, and Tables 4.2 and 4.3). The active sites that give the minimum adsorption energies were selected to construct the free energy diagrams. Figures 4.7(a)-(b) display the H_2SOR on MoS_2 and VS_2 edge and basal plane at the equilibrium potential U = 0.14 V_{RHE}. As can be seen, in both cases the basal plane is very inactive (large overpotentials associated with either the first or second electrochemical oxidation step), but edge sites are reasonably active. In particular, the edge sites in the MoS_2 show no uphill step at U = 0.14 V, indicating that there is no overpotential to drive the H_2SOR at first, but as with pure metal oxides, S-poisoning soon becomes an issue because S* binds too strongly. The edge site of VS_2, on the other hand, requires 0.59 V_{RHE} overpotential to drive the H_2SOR, and sulfur poisoning is not an issue. We do not need to investigate the surface coverage for pure metal sulfides due to the reason that they do not tend to adsorb S* as strong as metal oxides.

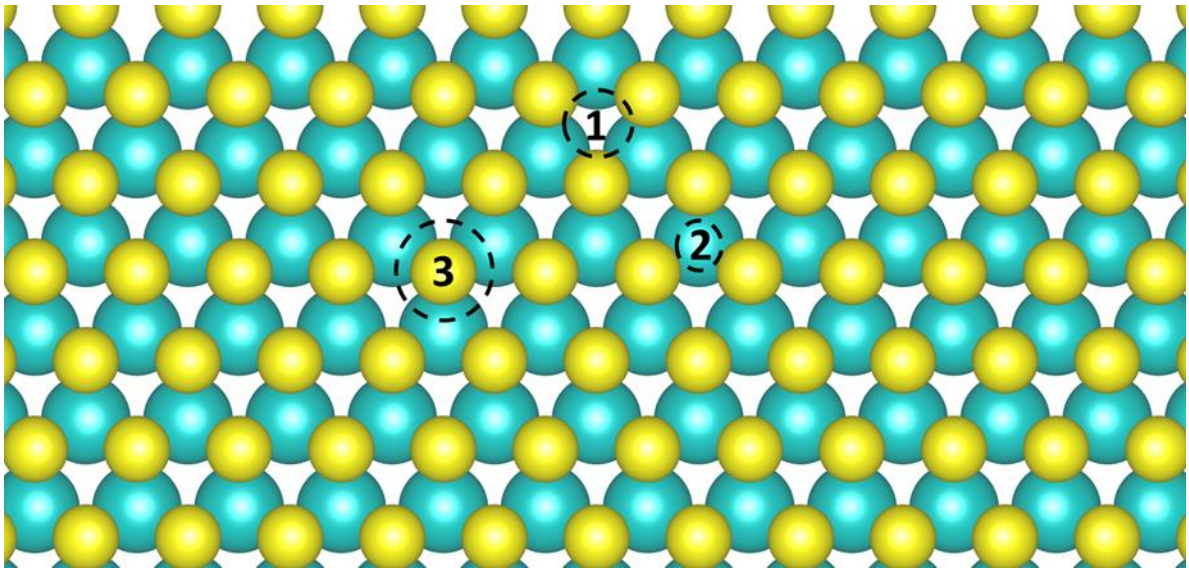

Figure 4.5. below shows different active sites investigated for the basal plane of metal sulfide catalysts; Active sites number 1, 2, and 3 correspond to the numbers in table 4.2. This is the top view of MoS_2.

Catalyst	*TiS_2*	*MoS_2*	*WS_2*	*VS_2*
Active Site				
H_2S - 1*	**-0.16**	**-0.06**	**-0.06**	**-0.39**
H_2S - 2*	-0.14	**-0.06**	-0.06	-0.38
H_2S - 3*	-0.15	0.01	0.01	-0.4
HS - 1*	4.19	**1.49**	**1.52**	**-0.08**
HS - 2*	4.06	1.92	1.72	1.34
HS - 3*	**1.88**	1.78	1.72	1.54
S - 1*	2.29	2.88	2.96	2.58
S - 2*	2.12	4	3.8	1.86
S - 3*	**1.28**	**1.29**	**1.48**	**0.66**

Table 4.2. Gibbs free energies for H_2SOR intermediates on all active sites on the basal plane of undoped metal sulfides (eV)

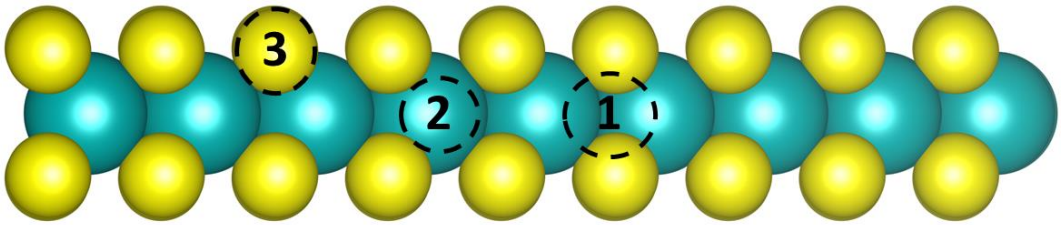

Figure 4.6. Different active sites investigated for the edge of metal sulfide catalysts. Active sites number 1, 2, and 3 correspond to the numbers in table 4.3.

Catalyst	*MoS_2*	*VS_2*
Active Site		
H_2S - 1*	1.09	0.88
H_2S - 2*	-0.06	**-0.34**
H_2S - 3*	**-0.06**	-0.19
HS - 1*	0.36	0.51
HS - 2*	0.36	**0.25**
HS - 3*	**-0.23**	0.51
S - 1*	-0.36	0.6
S - 2*	**-0.36**	0.43
S - 3*	-0.15	**0.4**

Table 4.3. Gibbs free energies for H_2SOR intermediates on all active sites on the edge of MoS_2 and VS_2.

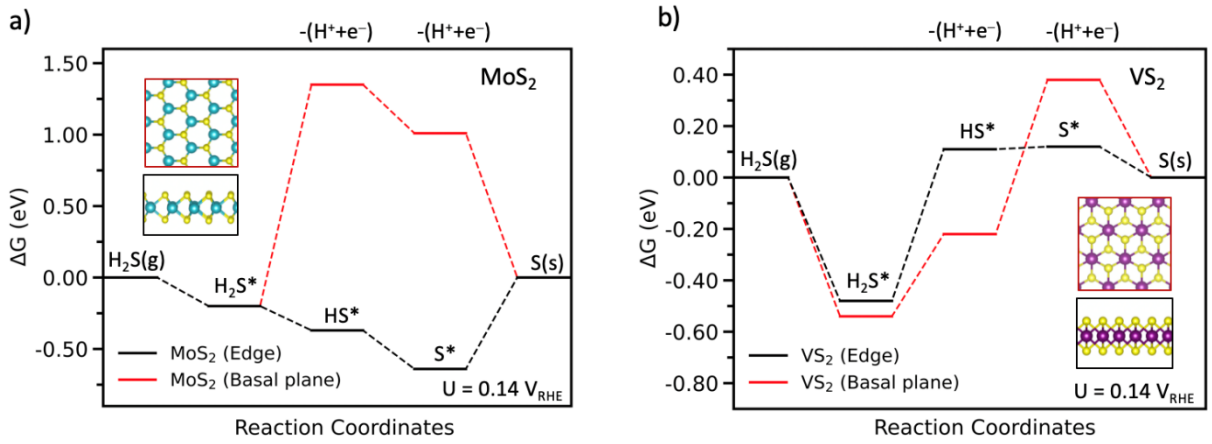

Figure 4.7. Free energy diagram of H_2S oxidation reaction over (a) MoS_2 edge and basal plane sites and (b) VS_2 edge and basal plane sites. The insets show the basal planes and edges of the MoS_2 and VS_2.

4.3. Single transition metal doped into S-vacancy of sulfides basal plane

As discussed above in figures 4.7(a) and 4.7(b), the edge site in MoS_2 and VS_2 are active for H_2SOR but the basal plane has limited activity. Because the edge active sites of MoS_2 and VS_2 account for a small proportion of total active sites, increasing the number of active sites in the basal plane is desirable. Several strategies such as nanostructuring or doping single metal atoms in the basal plane of the 2-dimensional sulfides have been used as common strategies.[148–150] Herein, we investigate various doped transition metals (Co, Cr, Cu, Fe, Mn, Ni, Sc, Ti, V, and Zn) in the S-vacancy of MoS_2 and VS_2. Figure 4.8(a) shows the top and side views of the Cr-doped single S-vacancy of MoS_2 as an example. Every possible active site was investigated for each individual model system, and the most stable one was used to construct the Gibbs free energy diagram.

Transition metal single atoms were found to be the most active sites in all cases (marked with red dashed circles) and were thus used to construct the scaling relationships as well as the free energy diagrams. For doped metal sulfides, there is only one active site (transition metal) for H_2SOR intermediates; therefore, it is not reasonable to investigate the coverage analysis for this individual active site. All other active sites do not favor sulfur adsorption based on the discussion in the previous section. Consequently, investigating the sulfur coverage for these remaining active sites is not helpful for this research.

Figure 4.8(b) shows the scaling relationships between the H_2SOR intermediates for various transition-metal-doped MoS_2. An ideal H_2S catalyst would show similar S* and HS* free adsorption energies and lie on the diagonal black dashed line. As can be seen in this diagram, the free adsorption energies of HS* intermediate are more negative than that of S*, implying most metal-doped MoS_2's tendency to strongly adsorb HS*. This figure shows V and Ti are closer to the diagonal line indicating a low thermodynamic barrier for the oxidation of HS* to S* step. Figure 4.8(c) shows the free energy diagram of H_2SOR on some of the transition-metal-doped MoS_2 catalysts studied herein. The calculated overpotentials for these transition-metal-doped MoS_2 are reported in Figure 4.8(d). These two figures indicate that by doping single atoms of transition metals in the S-vacancies, the adsorption energies of H_2SOR intermediates in the basal plane of MoS_2 can be significantly increased. Doping MoS_2 with Mn single atom would provide a reasonably active H_2SOR catalyst with a calculated overpotential of 0.81 V_{RHE} with no sulfur poisoning. Doping MoS_2 with single atoms of Ti and V, on the other hand, will allow for the electrochemical oxidation of H_2S with negligible overpotentials, 0.17 V_{RHE} and 0.05 V_{RHE} respectively. However, because these dopants strongly adsorb S-intermediates, the final step, which involves the non-electrochemical phase transition, becomes difficult, disrupting the long-

term operation. Free energy diagrams and calculated overpotentials for all the examined transition-metal-doped in MoS_2 can be found in Figure 4.9(a)-(b).

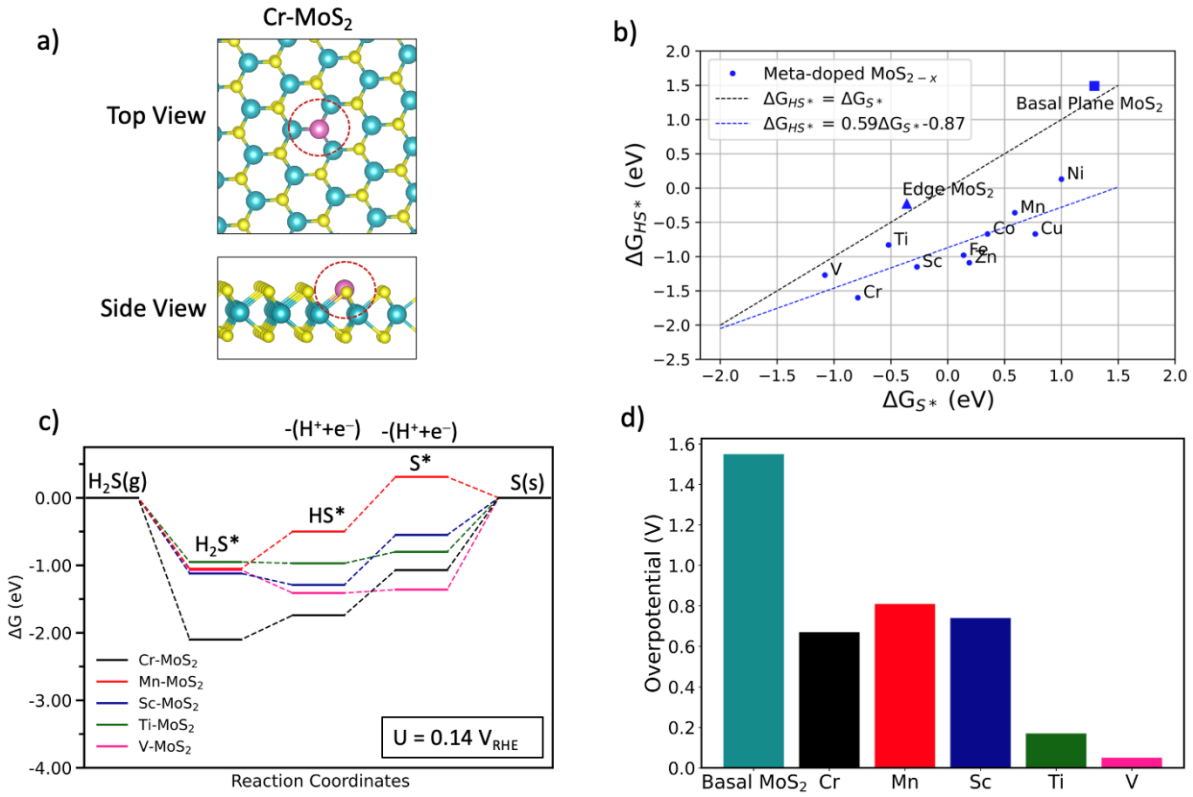

Figure 4.8. (a) Top and side views of Cr-doped MoS_{2-x} catalyst. Red dashed circles mark the active site. Color code; S: yellow, Mo: cyan, Cr: pink. (b) Scaling relationship for transition-metal-doped MoS_2. The black dashed line shows a diagonal line where the free energy of HS* and S* are equal and oxidation of HS* to S* is no longer an uphill step. (c) The free energy diagram for H_2SOR on the most promising transition metal doped MoS_2. (d) The calculated H_2SOR overpotentials corresponding to the transition-metal-doped MoS_2 in (c).

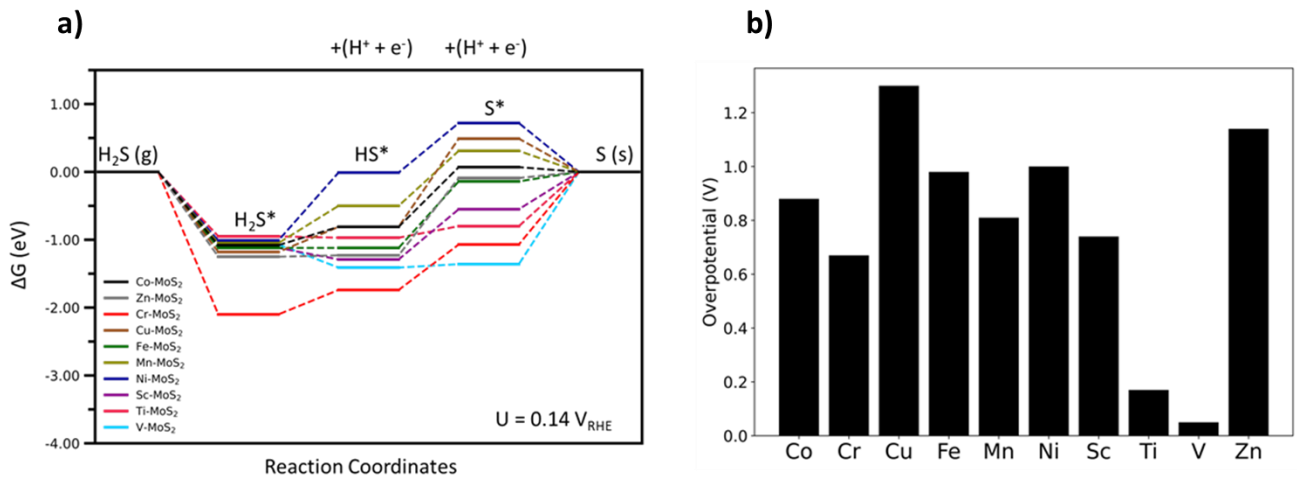

Figure 4.9. Gibbs free energy diagram and required overpotentials for all transition-metal-doped MoS_2

Figure 4.10 shows a similar analysis for the transition-metal-doped single atoms into the S-vacancy of VS_2. Figure 4.10(a) displays the structure of Fe-doped VS_2 as an example. The red dashed circles mark Fe single atom substituted by sulfur which is also the active site for H_2SOR. The scatter plot in Figure 4.10(b) shows the scaling relationships for adsorption free energies of HS* vs. S* intermediates on various examined transition-metal-doped single atoms into the S-vacancy of VS_2. This analysis reveals that the adsorption free energies of HS* and S* intermediates lie neatly on the diagonal line for the majority of the investigated structures, implying that HS* can be easily deprotonated to S*. Figures 4.10(c) and 4.10(d) are the free energy diagram and bar chart summarizing the results for some of the examined transition-metal-doped single atoms into the S-vacancy of VS_2. Free energy diagrams and calculated overpotentials for all the examined transition-metal-doped in VS_2 can be found in Figure 4.11. It is interesting to note that the most uphill electrochemical step for most of the transition-metal-doped VS_2 is the first step, oxidation of H_2S* to S* and further oxidation of HS* to S* is facile. Moreover, similar to the case of transition-metal-doped single atoms into the S-vacancy of MoS_2, doping shifts the adsorption

energies of S-intermediates toward the stronger interaction, which is not favorable to sulfur poisoning.

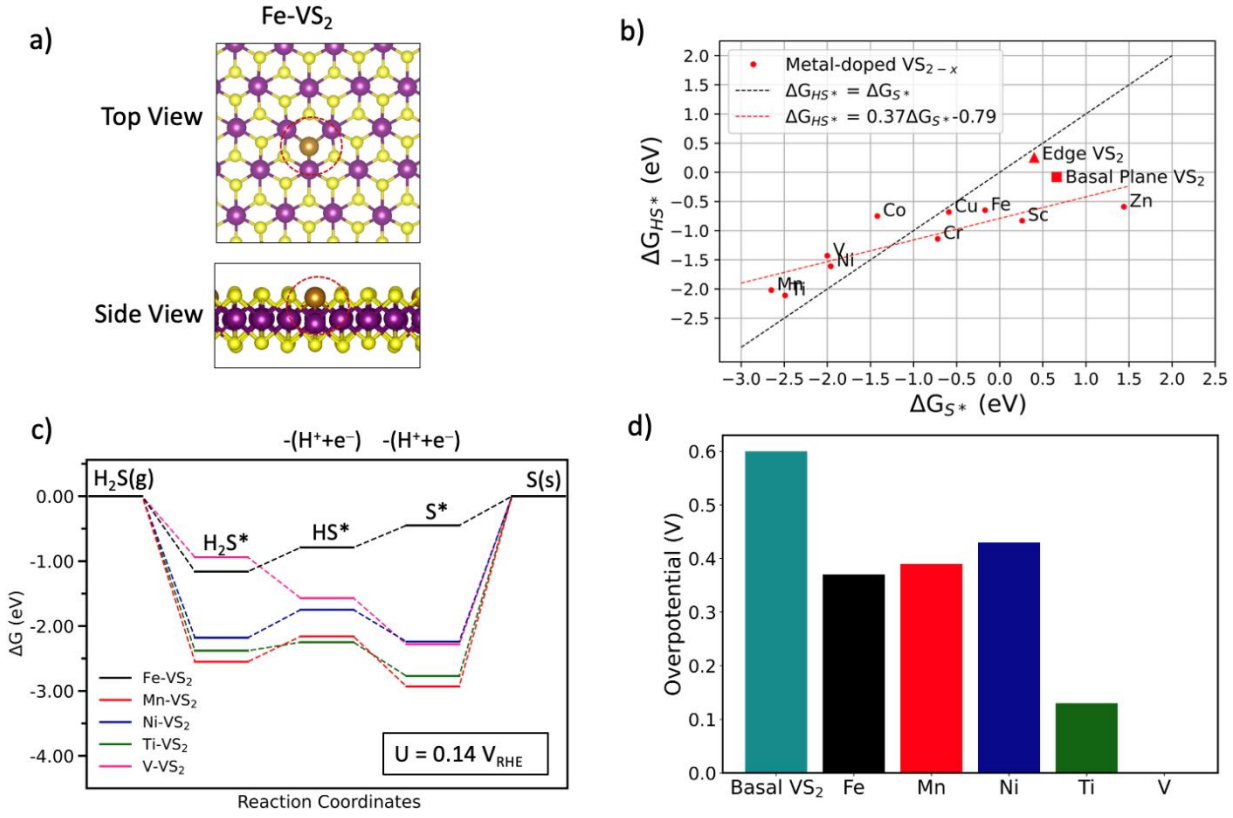

Figure 4.10. (a) Top and side views of Fe-doped VS_{2-x} catalyst. Red dashed circles mark the active site. Color code; S: yellow, V: purple, Fe: orange. (b) Scaling relationship for transition-metal-doped VS_2. Black and red dashed lines show the diagonal and scaling lines, respectively. (c) The free energy diagram for H_2SOR on the most promising transition-metal-doped VS_2. (d) The calculated H_2SOR overpotentials corresponding to the doped transition metal VS_2 in (c).

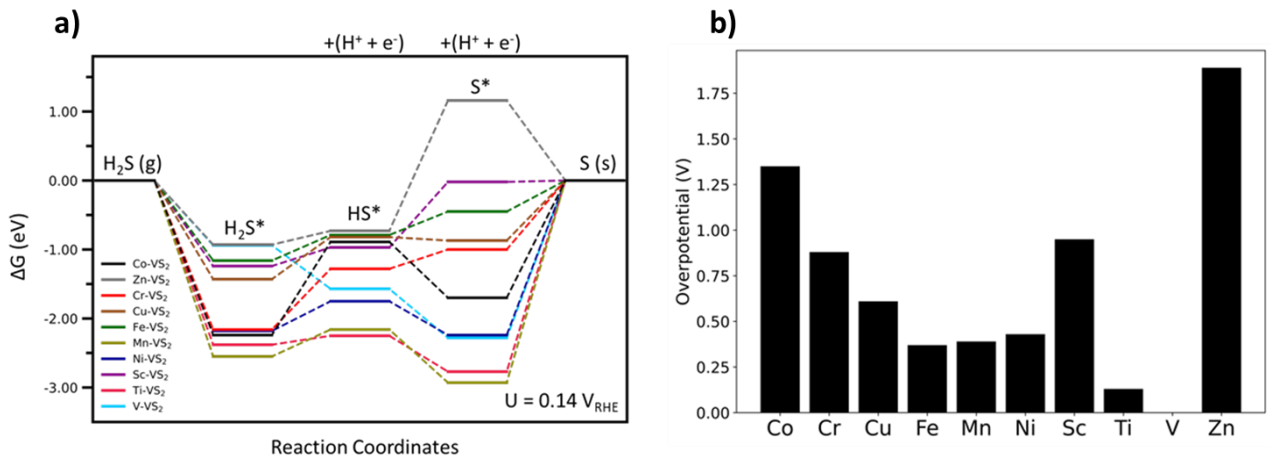

Figure 4.11. Gibbs free energy diagram and required overpotentials for all transition-metal-doped VS_2

These two analyses show that doping inactive metal sulfides with transition metals can improve the activity of the catalyst. Transition metals can modify the electronic structure of the metal sulfides by introducing new free electron pairs and can lead to better H_2SOR activities.[89] Our results are also consistent with the experimental results of H_2SOR on different metal sulfides investigated by Zaman and Chakma. In this work, the applicability of metal sulfides such as MoS_2 and VS_2 has been carefully investigated.[151]

Chapter 5. Conclusions

5.1. Conclusion

The electrochemical H_2S oxidation reaction is a promising method for converting waste H_2S into useful and valuable hydrogen while reducing the anthropogenic impact of H_2S. Herein, we used DFT calculation to study H_2SOR over various metal oxides (RuO_2, IrO_2, TiO_2 and MoO_2) and metal sulfides (MoS_2, VS_2, WS_2, and TiS_2). We showed that all examined metal oxides tend to strongly adsorb the S* and HS* intermediates. The role of S-intermediates in altering the activities of metal oxides was investigated and TiO_2 was found to be the most promising oxide for H_2SOR with an overpotential of 0.49 V. As alternatives to oxides, we also investigated the H_2SOR activity of pristine and doped metal sulfides. On the basal plane of pristine metal sulfides, no H_2SOR activity was observed, but MoS_2 and VS_2 have relatively active edge sites. In order to achieve higher activities in the basal plane, we created S-vacancies and doped MoS_2 and VS_2 with different transition metal single atoms. Our results show that doping transition metal single atoms increases the activities of the MoS_2 and VS_2 basal planes with Ti-VS_{2-x}, V-VS_{2-x}, Ti-MoS_{2-x}, and V-MoS_{2-x} being the most active structures. However, while single-atom doping in the basal plane of MoS_2 and VS_2 appears to result in a lower overpotential to drive the electrochemical H_2SOR, the long-term operation becomes a problem because the active sites are blocked by the S-intermediates, limiting reactivity. This study provides an atomic-scale view and understanding of the challenges associated with H_2SOR catalysis, as well as guidelines for developing more active catalysts.

5.2. Limitations to the Current Study

First, it is paramount to come to the fact that the DFT calculations are not perfectly accurate solutions of the full Schrödinger equation. DFT calculations are only an approximation of the final energies in the Schrödinger equation. Also, the magnitude of this inexactness cannot be estimated. The other limitation to DFT calculation is that although it is useful for a small number of atoms (up to 100), it might not be feasible for calculating the energies of extremely large models where different types of elements have electronic interactions with each other. DFT cannot also take into account the effect of temperature and the electrolyte used correctly, and this might result in incorrect electronic energies.

Second, we believe that there will be other promising catalysts for H_2SOR since we have only investigated the ones that we thought might be considered active for this electrochemical reaction. Doping metal oxides with active materials that help the activity even after the surface poisoning or co-doping metal sulfides with other transition metals that can help to maintain the activity might be some of the ways to improve the activity and stability of H_2SOR catalysts.

Chapter 6. Bibliography

(1) Zhou, Y. N.; Zhu, Y. R.; Chen, X. Y.; Dong, B.; Li, Q. Z.; Chai, Y. M. Carbon–Based Transition Metal Sulfides/Selenides Nanostructures for Electrocatalytic Water Splitting. *Journal of Alloys and Compounds*. Elsevier Ltd January 25, 2021. https://doi.org/10.1016/j.jallcom.2020.156810.

(2) Guo, Y.; Tang, J.; Wang, Z.; Kang, Y. M.; Bando, Y.; Yamauchi, Y. Elaborately Assembled Core-Shell Structured Metal Sulfides as a Bifunctional Catalyst for Highly Efficient Electrochemical Overall Water Splitting. *Nano Energy* **2018**, *47*, 494–502. https://doi.org/10.1016/j.nanoen.2018.03.012.

(3) Audichon, T.; Napporn, T. W.; Canaff, C.; Morais, C.; Comminges, C.; Kokoh, K. B. IrO2 Coated on RuO2 as Efficient and Stable Electroactive Nanocatalysts for Electrochemical Water Splitting. *Journal of Physical Chemistry C* **2016**, *120* (5), 2562–2573. https://doi.org/10.1021/acs.jpcc.5b11868.

(4) Höök, M.; Tang, X. Depletion of Fossil Fuels and Anthropogenic Climate Change-A Review. *Energy Policy* **2013**, *52*, 797–809. https://doi.org/10.1016/j.enpol.2012.10.046.

(5) Oliver, T. H.; Morecroft, M. D. Interactions between Climate Change and Land Use Change on Biodiversity: Attribution Problems, Risks, and Opportunities. *Wiley Interdisciplinary Reviews: Climate Change*. Wiley-Blackwell 2014, pp 317–335. https://doi.org/10.1002/wcc.271.

(6) Qazi, A.; Hussain, F.; Rahim, N. A. B. D.; Hardaker, G.; Alghazzawi, D.; Shaban, K.; Haruna, K. Towards Sustainable Energy: A Systematic Review of Renewable Energy Sources, Technologies, and Public Opinions. *IEEE Access* **2019**, *7*, 63837–63851. https://doi.org/10.1109/ACCESS.2019.2906402.

(7) Zheng, Y.; Jiao, Y.; Qiao, S. Z. Engineering of Carbon-Based Electrocatalysts for Emerging Energy Conversion: From Fundamentality to Functionality. *Advanced Materials* **2015**, *27* (36), 5372–5378. https://doi.org/10.1002/adma.201500821.

(8) Shao, M. Electrocatalysis in Fuel Cells. *Catalysts*. MDPI December 9, 2015, pp 2115–2121. https://doi.org/10.3390/catal5042115.

(9) McCloskey, B. D.; Scheffler, R.; Speidel, A.; Bethune, D. S.; Shelby, R. M.; Luntz, A. C. On the Efficacy of Electrocatalysis in Nonaqueous Li-O2 Batteries. *J Am Chem Soc* **2011**, *133* (45), 18038–18041. https://doi.org/10.1021/ja207229n.

(10) Tran, P. D.; Nguyen, M.; Pramana, S. S.; Bhattacharjee, A.; Chiam, S. Y.; Fize, J.; Field, M. J.; Artero, V.; Wong, L. H.; Loo, J.; Barber, J. Copper Molybdenum Sulfide: A New Efficient Electrocatalyst for Hydrogen Production from Water. *Energy Environ Sci* **2012**, *5* (10), 8912–8916. https://doi.org/10.1039/c2ee22611a.

(11) Tang, C.; Zheng, Y.; Jaroniec, M.; Qiao, S. Z. Electrocatalytic Refinery for Sustainable Production of Fuels and Chemicals. *Angewandte Chemie - International Edition*. John Wiley and Sons Inc September 1, 2021, pp 19572–19590. https://doi.org/10.1002/anie.202101522.

(12) Lee, S. Y.; Jung, H.; Kim, N. K.; Oh, H. S.; Min, B. K.; Hwang, Y. J. Mixed Copper States in Anodized Cu Electrocatalyst for Stable and Selective Ethylene Production from CO_2 Reduction. *J Am Chem Soc* **2018**, *140* (28), 8681–8689. https://doi.org/10.1021/jacs.8b02173.

(13) Ding, P.; Zhao, H.; Li, T.; Luo, Y.; Fan, G.; Chen, G.; Gao, S.; Shi, X.; Lu, S.; Sun, X. Metal-Based Electrocatalytic Conversion of CO_2 to Formic Acid/Formate. *Journal of Materials Chemistry A*. Royal Society of Chemistry November 14, 2020, pp 21947–21960. https://doi.org/10.1039/d0ta08393c.

(14) Kuhl, K. P.; Hatsukade, T.; Cave, E. R.; Abram, D. N.; Kibsgaard, J.; Jaramillo, T. F. Electrocatalytic Conversion of Carbon Dioxide to Methane and Methanol on Transition Metal Surfaces. *J Am Chem Soc* **2014**, *136* (40), 14107–14113. https://doi.org/10.1021/ja505791r.

(15) Blakemore, J. D.; Crabtree, R. H.; Brudvig, G. W. Molecular Catalysts for Water Oxidation. *Chemical Reviews*. American Chemical Society December 9, 2015, pp 12974–13005. https://doi.org/10.1021/acs.chemrev.5b00122.

(16) Liao, P. Q.; Shen, J. Q.; Zhang, J. P. Metal–Organic Frameworks for Electrocatalysis. *Coordination Chemistry Reviews*. Elsevier B.V. October 15, 2018, pp 22–48. https://doi.org/10.1016/j.ccr.2017.09.001.

(17) Ursúa, A.; Gandía, L. M.; Sanchis, P. Hydrogen Production from Water Electrolysis: Current Status and Future Trends. In *Proceedings of the IEEE*; Institute of Electrical and Electronics Engineers Inc., 2012; Vol. 100, pp 410–426. https://doi.org/10.1109/JPROC.2011.2156750.

(18) Amin, A. M.; Croiset, E.; Epling, W. Review of Methane Catalytic Cracking for Hydrogen Production. *International Journal of Hydrogen Energy*. February 2011, pp 2904–2935. https://doi.org/10.1016/j.ijhydene.2010.11.035.

(19) Liu, K. H.; Zhong, H. X.; Li, S. J.; Duan, Y. X.; Shi, M. M.; Zhang, X. B.; Yan, J. M.; Jiang, Q. Advanced Catalysts for Sustainable Hydrogen Generation and Storage via Hydrogen Evolution and Carbon Dioxide/Nitrogen Reduction Reactions. *Progress in Materials Science*. Elsevier Ltd March 1, 2018, pp 64–111. https://doi.org/10.1016/j.pmatsci.2017.09.001.

(20) Zhang, M.; Guan, J.; Tu, Y.; Chen, S.; Wang, Y.; Wang, S.; Yu, L.; Ma, C.; Deng, D.; Bao, X. Highly Efficient H_2 Production from H_2S: Via a Robust Graphene-Encapsulated Metal Catalyst. *Energy and Environmental Science*. Royal Society of Chemistry January 1, 2020, pp 119–126. https://doi.org/10.1039/c9ee03231b.

(21) Feng, Y.; Wang, X.; Huang, J.; Dong, P.; Ji, J.; Li, J.; Cao, L.; Feng, L.; Jin, P.; Wang, C. Decorating CoNi Layered Double Hydroxides Nanosheet Arrays with Fullerene Quantum Dot Anchored on Ni Foam for Efficient Electrocatalytic Water Splitting and Urea Electrolysis. *Chemical Engineering Journal* **2020**, *390*. https://doi.org/10.1016/j.cej.2020.124525.

(22) Zhang, Y. L.; Goh, K.; Zhao, L.; Sui, X. L.; Gong, X. F.; Cai, J. J.; Zhou, Q. Y.; Zhang, H. Da; Li, L.; Kong, F. R.; Gu, D. M.; Wang, Z. B. Advanced Non-Noble Materials in Bifunctional Catalysts for ORR and OER toward Aqueous Metal-Air Batteries. *Nanoscale*. Royal Society of Chemistry November 14, 2020, pp 21534–21559. https://doi.org/10.1039/d0nr05511e.

(23) Galani, S. M.; Mondal, A.; Srivastava, D. N.; Panda, A. B. Development of RuO_2/CeO_2 Heterostructure as an Efficient OER Electrocatalyst for Alkaline Water Splitting. *Int J Hydrogen Energy* **2020**, *45* (37), 18635–18644. https://doi.org/10.1016/j.ijhydene.2019.08.026.

(24) Hu, C.; Zhang, L.; Gong, J. Recent Progress Made in the Mechanism Comprehension and Design of Electrocatalysts for Alkaline Water Splitting. *Energy Environ Sci* **2019**, *12* (9), 2620–2645. https://doi.org/10.1039/c9ee01202h.

(25) Liu, P. F.; Yang, S.; Zhang, B.; Yang, H. G. Defect-Rich Ultrathin Cobalt-Iron Layered Double Hydroxide for Electrochemical Overall Water Splitting. *ACS Appl Mater Interfaces* **2016**, *8* (50), 34474–34481. https://doi.org/10.1021/acsami.6b12803.

(26) Ramireza, P.; Aguilella, V. M.; Manzanaresb, J. A.; Mafgb, S. *Effects of Temperature and Ion Transport on Water Splitting in Bipolar Membranes**; 1992; Vol. 73.

(27) Mekhilef, S.; Saidur, R.; Safari, A. Comparative Study of Different Fuel Cell Technologies. *Renewable and Sustainable Energy Reviews*. Elsevier Ltd 2012, pp 981–989. https://doi.org/10.1016/j.rser.2011.09.020.

(28) Manoharan, Y.; Hosseini, S. E.; Butler, B.; Alzhahrani, H.; Senior, B. T. F.; Ashuri, T.; Krohn, J. Hydrogen Fuel Cell Vehicles; Current Status and Future Prospect. *Applied Sciences (Switzerland)*. MDPI AG June 1, 2019. https://doi.org/10.3390/app9112296.

(29) Rukini, A.; Rhamdhani, M. A.; Brooks, G. A.; Van den Bulck, A. Metals Production and Metal Oxides Reduction Using Hydrogen: A Review. *Journal of Sustainable Metallurgy*. Springer Science and Business Media Deutschland GmbH March 1, 2022. https://doi.org/10.1007/s40831-021-00486-5.

(30) Canada. Natural Resources Canada. *Hydrogen Strategy for Canada: Seizing the Opportunities for Hydrogen : A Call to Action.*

(31) Han, X.; Yu, C.; Yang, J.; Zhao, C.; Huang, H.; Liu, Z.; Ajayan, P. M.; Qiu, J. Mass and Charge Transfer Coenhanced Oxygen Evolution Behaviors in CoFe-Layered Double Hydroxide Assembled on Graphene. *Adv Mater Interfaces* **2016**, *3* (7). https://doi.org/10.1002/admi.201500782.

(32) Guo, Y.; Tong, Y.; Chen, P.; Xu, K.; Zhao, J.; Lin, Y.; Chu, W.; Peng, Z.; Wu, C.; Xie, Y. Engineering the Electronic State of a Perovskite Electrocatalyst for Synergistically Enhanced Oxygen Evolution Reaction. *Advanced Materials* **2015**, *27* (39), 5989–5994. https://doi.org/10.1002/adma.201502024.

(33) Lu, X.; Zhao, C. Electrodeposition of Hierarchically Structured Three-Dimensional Nickel-Iron Electrodes for Efficient Oxygen Evolution at High Current Densities. *Nat Commun* **2015**, *6*. https://doi.org/10.1038/ncomms7616.

(34) Bo, X.; Hocking, R. K.; Zhou, S.; Li, Y.; Chen, X.; Zhuang, J.; Du, Y.; Zhao, C. Capturing the Active Sites of Multimetallic (Oxy)Hydroxides for the Oxygen Evolution Reaction. *Energy Environ Sci* **2020**, *13* (11), 4225–4237. https://doi.org/10.1039/d0ee01609h.

(35) Ishaq, H.; Dincer, I.; Crawford, C. A Review on Hydrogen Production and Utilization: Challenges and Opportunities. *Int J Hydrogen Energy* **2022**, *47* (62), 26238–26264. https://doi.org/10.1016/j.ijhydene.2021.11.149.

(36) Tarkowski, R.; Uliasz-Misiak, B. Towards Underground Hydrogen Storage: A Review of Barriers. *Renewable and Sustainable Energy Reviews*. Elsevier Ltd July 1, 2022. https://doi.org/10.1016/j.rser.2022.112451.

(37) Abdin, Z.; Zafaranloo, A.; Rafiee, A.; Mérida, W.; Lipiński, W.; Khalilpour, K. R. Hydrogen as an Energy Vector. *Renewable and Sustainable Energy Review*s. Elsevier Ltd March 1, 2020. https://doi.org/10.1016/j.rser.2019.109620.

(38) Simpson, A. P.; Lutz, A. E. Exergy Analysis of Hydrogen Production via Steam Methane Reforming. *Int J Hydrogen Energy* **2007**, *32* (18), 4811–4820. https://doi.org/10.1016/j.ijhydene.2007.08.025.

(39) Barelli, L.; Bidini, G.; Gallorini, F.; Servili, S. Hydrogen Production through Sorption-Enhanced Steam Methane Reforming and Membrane Technology: A Review. *Energy*. Elsevier Ltd 2008, pp 554–570. https://doi.org/10.1016/j.energy.2007.10.018.

(40) Sun, P.; Young, B.; Elgowainy, A.; Lu, Z.; Wang, M.; Morelli, B.; Hawkins, T. Criteria Air Pollutants and Greenhouse Gas Emissions from Hydrogen Production in U.S. Steam

Methane Reforming Facilities. *Environ Sci Technol* **2019**, *53* (12), 7103–7113. https://doi.org/10.1021/acs.est.8b06197.

(41) Barelli, L.; Bidini, G.; Gallorini, F.; Servili, S. Hydrogen Production through Sorption-Enhanced Steam Methane Reforming and Membrane Technology: A Review. *Energy*. Elsevier Ltd 2008, pp 554–570. https://doi.org/10.1016/j.energy.2007.10.018.

(42) Zoulias, E.; Varkaraki, E.; Lymberopoulos, N.; Christodoulou, C. N.; Karagiorgis, G. N. *A REVIEW ON WATER ELECTROLYSIS*.

(43) Ayers, K.; Danilovic, N.; Ouimet, R.; Carmo, M.; Pivovar, B.; Bornstein, M. Perspectives on Low-Temperature Electrolysis and Potential for Renewable Hydrogen at Scale. **2019**. https://doi.org/10.1146/annurev-chembioeng.

(44) Zeng, K.; Zhang, D. Recent Progress in Alkaline Water Electrolysis for Hydrogen Production and Applications. *Progress in Energy and Combustion Science*. June 2010, pp 307–326. https://doi.org/10.1016/j.pecs.2009.11.002.

(45) Barbir, F. PEM Electrolysis for Production of Hydrogen from Renewable Energy Sources. *Solar Energy* **2005**, *78* (5), 661–669. https://doi.org/10.1016/j.solener.2004.09.003.

(46) Chang, A. C. C.; Chang, H. F.; Lin, F. J.; Lin, K. H.; Chen, C. H. Biomass Gasification for Hydrogen Production. In *International Journal of Hydrogen Energy*; 2011; Vol. 36, pp 14252–14260. https://doi.org/10.1016/j.ijhydene.2011.05.105.

(47) Shayan, E.; Zare, V.; Mirzaee, I. Hydrogen Production from Biomass Gasification; a Theoretical Comparison of Using Different Gasification Agents. *Energy Convers Manag* **2018**, *159*, 30–41. https://doi.org/10.1016/j.enconman.2017.12.096.

(48) Eroglu, E.; Melis, A. Photobiological Hydrogen Production: Recent Advances and State of the Art. *Bioresour Technol* **2011**, *102* (18), 8403–8413. https://doi.org/10.1016/j.biortech.2011.03.026.

(49) Alvarez, J.; Kumagai, S.; Wu, C.; Yoshioka, T.; Bilbao, J.; Olazar, M.; Williams, P. T. Hydrogen Production from Biomass and Plastic Mixtures by Pyrolysis-Gasification. *Int J Hydrogen Energy* **2014**, *39* (21), 10883–10891. https://doi.org/10.1016/j.ijhydene.2014.04.189.

(50) Schneider, S.; Bajohr, S.; Graf, F.; Kolb, T. State of the Art of Hydrogen Production via Pyrolysis of Natural Gas. *ChemBioEng Reviews*. Wiley-Blackwell October 1, 2020, pp 150–158. https://doi.org/10.1002/cben.202000014.

(51) Schüth, F. Challenges in Hydrogen Storage. *European Physical Journal: Special Topics* **2009**, *176* (1), 155–166. https://doi.org/10.1140/epjst/e2009-01155-x.

(52) Elberry, A. M.; Thakur, J.; Santasalo-Aarnio, A.; Larmi, M. Large-Scale Compressed Hydrogen Storage as Part of Renewable Electricity Storage Systems. *International Journal of Hydrogen Energy*. Elsevier Ltd April 26, 2021, pp 15671–15690. https://doi.org/10.1016/j.ijhydene.2021.02.080.

(53) Felderhoff, M.; Weidenthaler, C.; Von Helmolt, R.; Eberle, U. Hydrogen Storage: The Remaining Scientific and Technological Challenges. *Physical Chemistry Chemical Physics* **2007**, *9* (21), 2643–2653. https://doi.org/10.1039/b701563c.

(54) Züttel, A. Hydrogen Storage Methods. *Naturwissenschaften*. April 2004, pp 157–172. https://doi.org/10.1007/s00114-004-0516-x.

(55) Qiu, Y.; Yang, H.; Tong, L.; Wang, L. Research Progress of Cryogenic Materials for Storage and Transportation of Liquid Hydrogen. *Metals*. MDPI AG July 1, 2021. https://doi.org/10.3390/met11071101.

(56) Schneemann, A.; White, J. L.; Kang, S.; Jeong, S.; Wan, L. F.; Cho, E. S.; Heo, T. W.; Prendergast, D.; Urban, J. J.; Wood, B. C.; Allendorf, M. D.; Stavila, V. Nanostructured Metal Hydrides for Hydrogen Storage. *Chemical Reviews*. American Chemical Society November 28, 2018, pp 10775–10839. https://doi.org/10.1021/acs.chemrev.8b00313.

(57) David, W. I. F. Effective Hydrogen Storage: A Strategic Chemistry Challenge. *Faraday Discussions*. 2011, pp 399–414. https://doi.org/10.1039/c1fd00105a.

(58) David, E. An Overview of Advanced Materials for Hydrogen Storage. In *Journal of Materials Processing Technology*; Elsevier BV, 2005; Vol. 162–163, pp 169–177. https://doi.org/10.1016/j.jmatprotec.2005.02.027.

(59) Jena, P. Materials for Hydrogen Storage: Past, Present, and Future. *Journal of Physical Chemistry Letters*. February 3, 2011, pp 206–211. https://doi.org/10.1021/jz1015372.

(60) Niemann, M. U.; Srinivasan, S. S.; Phani, A. R.; Kumar, A.; Goswami, D. Y.; Stefanakos, E. K. Nanomaterials for Hydrogen Storage Applications: A Review. *J Nanomater* **2008**, *2008* (1). https://doi.org/10.1155/2008/950967.

(61) Yu, X.; Tang, Z.; Sun, D.; Ouyang, L.; Zhu, M. Recent Advances and Remaining Challenges of Nanostructured Materials for Hydrogen Storage Applications. *Progress in Materials Science*. Elsevier Ltd July 1, 2017, pp 1–48. https://doi.org/10.1016/j.pmatsci.2017.03.001.

(62) Chen, Q.; Wang, J.; Liu, X.; Zhao, X.; Qiao, W.; Long, D.; Ling, L. Alkaline Carbon Nanotubes as Effective Catalysts for H_2S Oxidation. *Carbon N Y* **2011**, *49* (12), 3773–3780. https://doi.org/10.1016/j.carbon.2011.05.011.

(63) Zheng, X.; Cai, J.; Cao, Y.; Shen, L.; Zheng, Y.; Liu, F.; Liang, S.; Xiao, Y.; Jiang, L. Construction of Cross-Linked δ-MnO_2 with Ultrathin Structure for the Oxidation of H2S: Structure-Activity Relationship and Kinetics Study. *Appl Catal B* **2021**, *297*. https://doi.org/10.1016/j.apcatb.2021.120402.

(64) Hedderich, R.; Klimmek, O.; Kröger, A.; Dirmeier, R.; Keller, M.; Stetter, K. O. Anaerobic Respiration with Elemental Sulfur and with Disulfides. *FEMS Microbiol Rev* **1998**, *22* (5), 353–381. https://doi.org/10.1111/j.1574-6976.1998.tb00376.x.

(65) Cox, B. G.; Clarke, P. F.; Pruden, B. B. *ECONOMICS OF THERMAL DISSOCIATION OF H,S TO PRODUCE HYDROGEN*; 1998; Vol. 23.

(66) Elsner, M. P.; Menge, M.; Müller, C.; Agar, D. W. The Claus Process: Teaching an Old Dog New Tricks. In *Catalysis Today*; 2003; Vol. 79–80, pp 487–494. https://doi.org/10.1016/S0920-5861(03)00071-3.

(67) Powell, C. R.; Dillon, K. M.; Matson, J. B. A Review of Hydrogen Sulfide (H_2S) Donors: Chemistry and Potential Therapeutic Applications. *Biochemical Pharmacology*. Elsevier Inc. March 1, 2018, pp 110–123. https://doi.org/10.1016/j.bcp.2017.11.014.

(68) Sun, X.; Ji, L.; Huang, W.; Li, Z.; Liao, Y.; Xiao, K.; Zhu, X.; Xu, H.; Feng, J.; Feng, S.; Qu, Z.; Yan, N. Production of H2S with a Novel Short-Process for the Removal of Heavy

Metals in Acidic Effluents from Smelting Flue-Gas Scrubbing Systems. *Environ Sci Technol* **2021**, *55* (6), 3988–3995. https://doi.org/10.1021/acs.est.0c07884.

(69) Burra, K. R. G.; Bassioni, G.; Gupta, A. K. Catalytic Transformation of H_2S for H_2 Production. *Int J Hydrogen Energy* **2018**, *43* (51), 22852–22860. https://doi.org/10.1016/j.ijhydene.2018.10.164.

(70) Mbah, J.; Srinivasan, S.; Krakow, B.; Wolan, J.; Goswami, Y.; Stefanakos, E.; Appathurai, N. Effect of RuO_2-CoS_2 Anode Nanostructured on Performance of H_2S Electrolytic Splitting System. *Int J Hydrogen Energy* **2010**, *35* (19), 10094–10101. https://doi.org/10.1016/j.ijhydene.2010.08.023.

(71) Dong, P.; Zhang, Y.; Zhu, S.; Nie, Z.; Ma, H.; Liu, Q.; Li, J. First-Principles Study on the Adsorption Characteristics of Corrosive Species on Passive Film TiO_2 in a NaCl Solution Containing H_2S and CO_2. *Metals (Basel)* **2022**, *12* (7). https://doi.org/10.3390/met12071160.

(72) Iliuta, I.; Larachi, F. Concept of Bifunctional Redox Iron-Chelate Process for H2S Removal in Pulp and Paper Atmospheric Emissions. *Chem Eng Sci* **2003**, *58* (23–24), 5305–5314. https://doi.org/10.1016/j.ces.2003.09.009.

(73) Wang, B.; Zhang, S.-Y.; Ye, L.-H.; Zhang, X.-F.; Zhang, Y.-F.; Chen, W.-J. *Supporting Information Exploring the Reaction Mechanism of H_2S Decomposition with MS_3 (M = Mo, W) Clusters*.

(74) Robinson, E.; Robbins, R. C. Gaseous Sulfur Pollutants from Urban and Natural Sources. *J Air Pollut Control Assoc* **1970**, *20* (4), 233–235. https://doi.org/10.1080/00022470.1970.10469396.

(75) Marriott, R. A.; Pirzadeh, P.; Marrugo-Hernandez, J. J.; Raval, S. Hydrogen Sulfide Formation in Oil and Gas. *Can J Chem* **2016**, *94* (4), 406–413. https://doi.org/10.1139/cjc-2015-0425.

(76) Bagreev, A.; Bandosz, T. J. H_2S Adsorption/Oxidation on Materials Obtained Using Sulfuric Acid Activation of Sewage Sludge-Derived Fertilizer. *J Colloid Interface Sci* **2002**, *252* (1), 188–194. https://doi.org/10.1006/jcis.2002.8419.

(77) Deng, Q.; Yin, J.; Wu, X.; Zhang, T.; Wang, H.; Liu, M. Research Advances of Prevention and Control of Hydrogen Sulfide in Coal Mines. *Scientific World Journal*. Hindawi Limited 2019. https://doi.org/10.1155/2019/8719260.

(78) Stuetz, R. M.; Fenner, R. A.; Engin, G. *ASSESSMENT OF ODOURS FROM SEWAGE TREATMENT WORKS BY AN ELECTRONIC NOSE, H_2S ANALYSIS AND OLFACTOMETRY*.

(79) Hao, O. J.; Chen, J. M.; Huang, L.; Buglass, R. L. Sulfate-Reducing Bacteria. *Critical Reviews in Environmental Science and Technology*. Taylor and Francis Inc. 1996, pp 155–187. https://doi.org/10.1080/10643389609388489.

(80) Engel, L.; Benito-Altamirano, I.; Tarantik, K. R.; Pannek, C.; Dold, M.; Prades, J. D.; Wöllenstein, J. Printed Sensor Labels for Colorimetric Detection of Ammonia, Formaldehyde and Hydrogen Sulfide from the Ambient Air. *Sens Actuators B Chem* **2021**, *330*. https://doi.org/10.1016/j.snb.2020.129281.

(81) Khan, M. A. H.; Rao, M. V.; Li, Q. Recent Advances in Electrochemical Sensors for Detecting Toxic Gases: NO_2, SO_2 and H_2S. *Sensors (Switzerland)*. MDPI AG February 2, 2019. https://doi.org/10.3390/s19040905.

(82) Wang, Y.; Saad, A. B. M.; Saur, O.; Lavalley, J. C.; Morrow, B. A. *FTIR Study of Adsorption and Reaction of SO_2 and H_2S on Na/SiO_2.*

(83) Anani, A. A.; Mao, Z.; White, R. E.; Srinivasan, S.; Appleby, A. J. Electrochemical Production of Hydrogen and Sulfur by Low-Temperature Decomposition of Hydrogen Sulfide in an Aqueous Alkaline Solution. *J. Electrochem. Soc.* **1990**.

(84) Chin, D.-T.; Howard, P. D. *Hydrogen Sulfide Poisoning of Platinum Anode in Phosphoric Acid Fuel Cell Electrolyte*.

(85) Zheng, X.; Li, Y.; Zhang, L.; Shen, L.; Xiao, Y.; Zhang, Y.; Au, C.; Jiang, L. Insight into the Effect of Morphology on Catalytic Performance of Porous CeO_2 Nanocrystals for H_2S Selective Oxidation. *Appl Catal B* **2019**, *252*, 98–110. https://doi.org/10.1016/j.apcatb.2019.04.014.

(86) Liu, Y.; Song, C.; Wang, Y.; Cao, W.; Lei, Y.; Feng, Q.; Chen, Z.; Liang, S.; Xu, L.; Jiang, L. Rational Designed Co@N-Doped Carbon Catalyst for High-Efficient H_2S Selective Oxidation by Regulating Electronic Structures. *Chemical Engineering Journal* **2020**, *401*. https://doi.org/10.1016/j.cej.2020.126038.

(87) Tasdemir, H. M.; Yasyerli, S.; Yasyerli, N. Selective Catalytic Oxidation of H_2S to Elemental Sulfur over Titanium Based Ti-Fe, Ti-Cr and Ti-Zr Catalysts. *Int J Hydrogen Energy* **2015**, *40* (32), 9989–10001. https://doi.org/10.1016/j.ijhydene.2015.06.056.

(88) Zhang, X.; Dou, G.; Wang, Z.; Li, L.; Wang, Y.; Wang, H.; Hao, Z. Selective Catalytic Oxidation of H_2S over Iron Oxide Supported on Alumina-Intercalated Laponite Clay Catalysts. *J Hazard Mater* **2013**, *260*, 104–111. https://doi.org/10.1016/j.jhazmat.2013.05.008.

(89) Kumar, M.; Nagaiah, T. C. Pure Hydrogen and Sulfur Production from H_2S by an Electrochemical Approach Using a NiCu–MoS_2 Catalyst . *J Mater Chem A Mater* **2022**. https://doi.org/10.1039/d2ta02751h.

(90) Kumar, M.; Nagaiah, T. C. Efficient Production of Hydrogen from H_2S via Electrolysis Using a CoFeS2 Catalyst. *J Mater Chem A Mater* **2022**. https://doi.org/10.1039/d1ta09888h.

(91) Kraia, T.; Kaklidis, N.; Konsolakis, M.; Marnellos, G. E. Hydrogen Production by H_2S Decomposition over Ceria Supported Transition Metal (Co, Ni, Fe and Cu) Catalysts. *Int J Hydrogen Energy* **2019**, *44* (20), 9753–9762. https://doi.org/10.1016/j.ijhydene.2018.12.070.

(92) Tolba, S. A.; Sharafeldin, I.; Allam, N. K. Comparison between Hydrogen Production via H_2S and H_2O Splitting on Transition Metal-Doped TiO_2 (101) Surfaces as Potential Photoelectrodes. *Int J Hydrogen Energy* **2020**, *45* (51), 26758–26769. https://doi.org/10.1016/j.ijhydene.2020.07.077.

(93) Raybaud, P.; Hafner, J.; Kresse, G.; Kasztelan, S.; Toulhoat, H. Ab Initio Study of the H_2-H_2S/MoS_2 Gas-Solid Interface: The Nature of the Catalytically Active Sites. *J Catal* **2000**, *189* (1), 129–146. https://doi.org/10.1006/jcat.1999.2698.

(94) Lyu, S.; Wu, W.; Xiong, R.; Yang, C.; Sa, B.; Zhang, J.; Hou, Y.; Wang, X. *Carbon-Rich Carbon Nitride Nanocatalysts for H_2S Selective Oxidation*.

(95) Mohamadi, S.; Bashiri, H. Kinetic Study of Hydrogen Sulfide Decomposition on Pt(111) Surface. *Int J Chem Kinet* **2020**, *52* (1), 16–22. https://doi.org/10.1002/kin.21325.

(96) Xu, W.; Luo, M.; Peng, R.; Xiang, M.; Hu, X.; Lan, L.; Zhou, J. Highly Effective Microwave Catalytic Direct Decomposition of H_2S into H_2 and S over MeS-Based (Me = Ni,Co) Microwave Catalysts. *Energy Convers Manag* **2017**, *149*, 219–227. https://doi.org/10.1016/j.enconman.2017.07.029.

(97) Liu, H. Ammonia Synthesis Catalyst 100 Years: Practice, Enlightenment and Challenge. *Cuihua Xuebao/Chinese Journal of Catalysis*. Science Press October 20, 2014, pp 1619–1640. https://doi.org/10.1016/S1872-2067(14)60118-2.

(98) Guo, X.; Zhu, Y.; Ma, T. Lowering Reaction Temperature: Electrochemical Ammonia Synthesis by Coupling Various Electrolytes and Catalysts. *Journal of Energy Chemistry*. Elsevier B.V. November 1, 2017, pp 1107–1116. https://doi.org/10.1016/j.jechem.2017.09.012.

(99) Hellman, A.; Baerends, E. J.; Biczysko, M.; Bligaard, T.; Christensen, C. H.; Clary, D. C.; Dahl, S.; Van Harrevelt, R.; Honkala, K.; Jonsson, H.; Kroes, G. J.; Luppi, M.; Manthe, U.; Nørskov, J. K.; Olsen, R. A.; Rossmeisl, J.; Skúlason, E.; Tautermann, C. S.; Varandas, A. J. C.; Vincent, J. K. Predicting Catalysis: Understanding Ammonia Synthesis from First-Principles Calculations. *Journal of Physical Chemistry B* **2006**, *110* (36), 17719–17735. https://doi.org/10.1021/jp056982h.

(100) Sholl, D. S.; Steckel, J. A. *Density Functional Theory : A Practical Introduction*; Wiley, 2009.

(101) Flick, J.; Ruggenthaler, M.; Appel, H.; Rubio, A. Atoms and Molecules in Cavities, from Weak to Strong Coupling in Quantum-Electrodynamics (QED) Chemistry. *Proc Natl Acad Sci U S A* **2017**, *114* (12), 3026–3034. https://doi.org/10.1073/pnas.1615509114.

(102) Gidopoulos, N. I.; Gross, E. K. U. Electronic Non-Adiabatic States: Towards a Density Functional Theory beyond the Born-Oppenheimer Approximation. *Philosophical*

Transactions of the Royal Society A: Mathematical, Physical and Engineering Sciences **2014**, *372* (2011). https://doi.org/10.1098/rsta.2013.0059.

(103) Fábri, C.; Halász, G. J.; Cederbaum, L. S.; Vibók, Á. Born-Oppenheimer Approximation in Optical Cavities: From Success to Breakdown. *Chem Sci* **2021**, *12* (4), 1251–1258. https://doi.org/10.1039/d0sc05164k.

(104) Tan, B. T.; Wu, P.; Anariba, F. Modeling Stress-Strain Nonlinear Mechanics via Entropy Changes on Surface Wetting Using the Born-Oppenheimer Approximation. *Results in Engineering* **2022**, *13*. https://doi.org/10.1016/j.rineng.2022.100349.

(105) Manzhos, S.; Carrington, T. Using Rectangular Collocation with Finite Difference Derivatives to Solve Electronic Schrödinger Equation. *Journal of Chemical Physics* **2018**, *149* (20). https://doi.org/10.1063/1.5052196.

(106) Pisana, S.; Lazzeri, M.; Casiraghi, C.; Novoselov, K. S.; Geim, A. K.; Ferrari, A. C.; Mauri, F. Breakdown of the Adiabatic Born-Oppenheimer Approximation in Graphene. *Nat Mater* **2007**, *6* (3), 198–201. https://doi.org/10.1038/nmat1846.

(107) Bunker, P. R.; Moss, R. E. The Breakdown of the Born-Oppenheimer Approximation: The Effective Vibration-Rotation Hamiltonian for a Diatomic Molecule. *Mol Phys* **1977**, *33* (2), 417–424. https://doi.org/10.1080/00268977700100351.

(108) He, Q.; Yu, B.; Li, Z.; Zhao, Y. Density Functional Theory for Battery Materials. *Energy and Environmental Materials*. John Wiley and Sons Inc December 1, 2019, pp 264–279. https://doi.org/10.1002/eem2.12056.

(109) Liao, X.; Lu, R.; Xia, L.; Liu, Q.; Wang, H.; Zhao, K.; Wang, Z.; Zhao, Y. Density Functional Theory for Electrocatalysis. *Energy and Environmental Materials*. John Wiley and Sons Inc January 1, 2022, pp 157–185. https://doi.org/10.1002/eem2.12204.

(110) Parr, R. C.; Yang, W. *DENSITY-FUNCTIONAL THEORY OF THE ELECTRONIC STRUCTURE OF MOLECULES' Further ANNUAL REVIEWS*; 1995; Vol. 46. www.annualreviews.org.

(111) Morgan, W. S.; Jorgensen, J. J.; Hess, B. C.; Hart, G. L. W. Efficiency of Generalized Regular K-Point Grids. *Comput Mater Sci* **2018**, *153*, 424–430. https://doi.org/10.1016/j.commatsci.2018.06.031.

(112) Hjorth Larsen, A.; JØrgen Mortensen, J.; Blomqvist, J.; Castelli, I. E.; Christensen, R.; Dułak, M.; Friis, J.; Groves, M. N.; Hammer, B.; Hargus, C.; Hermes, E. D.; Jennings, P. C.; Bjerre Jensen, P.; Kermode, J.; Kitchin, J. R.; Leonhard Kolsbjerg, E.; Kubal, J.; Kaasbjerg, K.; Lysgaard, S.; Bergmann Maronsson, J.; Maxson, T.; Olsen, T.; Pastewka, L.; Peterson, A.; Rostgaard, C.; SchiØtz, J.; Schütt, O.; Strange, M.; Thygesen, K. S.; Vegge, T.; Vilhelmsen, L.; Walter, M.; Zeng, Z.; Jacobsen, K. W. The Atomic Simulation Environment - A Python Library for Working with Atoms. *Journal of Physics Condensed Matter*. Institute of Physics Publishing June 7, 2017. https://doi.org/10.1088/1361-648X/aa680e.

(113) Chilukuri, B.; Mazur, U.; Hipps, K. W. Structure, Properties, and Reactivity of Porphyrins on Surfaces and Nanostructures with Periodic DFT Calculations. *Applied Sciences (Switzerland)* **2020**, *10* (3). https://doi.org/10.3390/app10030740.

(114) Mazurek, A. H.; Szeleszczuk, Ł.; Pisklak, D. M. Periodic DFT Calculations—Review of Applications in the Pharmaceutical Sciences. *Pharmaceutics*. MDPI AG May 1, 2020. https://doi.org/10.3390/pharmaceutics12050415.

(115) Gauthier, J. A.; Dickens, C. F.; Chen, L. D.; Doyle, A. D.; Nørskov, J. K. Solvation Effects for Oxygen Evolution Reaction Catalysis on IrO2(110). *Journal of Physical Chemistry C* **2017**, *121* (21), 11455–11463. https://doi.org/10.1021/acs.jpcc.7b02383.

(116) Ma, Z.; Wang, J. X. *Reaction Mechanism for Oxygen Evolution on RuO_2, IrO_2, and RuO_2@IrO_2 Core-Shell Nanocatalysts*; 2017.

(117) Yeh, K. Y.; Janik, M. J. Density Functional Theory-Based Electrochemical Models for the Oxygen Reduction Reaction: Comparison of Modeling Approaches for Electric Field and Solvent Effects. *J Comput Chem* **2011**, *32* (16), 3399–3408. https://doi.org/10.1002/jcc.21919.

(118) Zhang, Q.; Asthagiri, A. Solvation Effects on DFT Predictions of ORR Activity on Metal Surfaces. *Catal Today* **2019**, 35–43. https://doi.org/10.1016/j.cattod.2018.07.036.

(119) Chen, Y.; Banaszak Holl, M. M.; Orr, B. G. The Bonding Geometry of Alkylsilanes on Gold: Relation to Surface Pattern Development and STM Image Contrast. *Surf Sci* **2007**, *601* (9), 1937–1943. https://doi.org/10.1016/j.susc.2007.02.027.

(120) Christopher, P. Surface-Mediated Processes for Energy Production and Conversion: Critical Considerations in Model System Design for DFT Calculations. *ACS Energy Letters*. American Chemical Society December 14, 2018, pp 3015–3016. https://doi.org/10.1021/acsenergylett.8b02213.

(121) Yeh, K. Y.; Janik, M. J. Density Functional Theory-Based Electrochemical Models for the Oxygen Reduction Reaction: Comparison of Modeling Approaches for Electric Field and Solvent Effects. *J Comput Chem* **2011**, *32* (16), 3399–3408. https://doi.org/10.1002/jcc.21919.

(122) Luo, X.; Tan, X.; Ji, P.; Chen, L.; Yu, J.; Mu, S. Surface Reconstruction-Derived Heterostructures for Electrochemical Water Splitting. *EnergyChem*. Elsevier B.V. March 1, 2022. https://doi.org/10.1016/j.enchem.2022.100091.

(123) Zeng, Y.; Zhao, M.; Huang, Z.; Zhu, W.; Zheng, J.; Jiang, Q.; Wang, Z.; Liang, H. Surface Reconstruction of Water Splitting Electrocatalysts. *Advanced Energy Materials*. John Wiley and Sons Inc September 1, 2022. https://doi.org/10.1002/aenm.202201713.

(124) Massaro, A.; Pecoraro, A.; Hernández, S.; Talarico, G.; Muñoz-García, A. B.; Pavone, M. Oxygen Evolution Reaction at the Mo/W-Doped Bismuth Vanadate Surface: Assessing the Dopant Role by DFT Calculations. *Molecular Catalysis* **2022**, *517*. https://doi.org/10.1016/j.mcat.2021.112036.

(125) Nørskov, J. K.; Rossmeisl, J.; Logadottir, A.; Lindqvist, L.; Kitchin, J. R.; Bligaard, T.; Jónsson, H. Origin of the Overpotential for Oxygen Reduction at a Fuel-Cell Cathode. *Journal of Physical Chemistry B* **2004**, *108* (46), 17886–17892. https://doi.org/10.1021/jp047349j.

(126) Rossmeisl, J.; Qu, Z. W.; Zhu, H.; Kroes, G. J.; Nørskov, J. K. Electrolysis of Water on Oxide Surfaces. *Journal of Electroanalytical Chemistry* **2007**, *607* (1–2), 83–89. https://doi.org/10.1016/j.jelechem.2006.11.008.

(127) Skúlason, E.; Tripkovic, V.; Björketun, M. E.; Gudmundsdóttir, S.; Karlberg, G.; Rossmeisl, J.; Bligaard, T.; Jónsson, H.; Nørskov, J. K. Modeling the Electrochemical Hydrogen Oxidation and Evolution Reactions on the Basis of Density Functional Theory Calculations. *Journal of Physical Chemistry C* **2010**, *114* (42), 18182–18197. https://doi.org/10.1021/jp1048887.

(128) Kresse, G.; Furthmiiller B ', J. *Efficiency of Ab-Initio Total Energy Calculations for Metals and Semiconductors Using a Plane-Wave Basis Set*; 1996; Vol. 6.

(129) Hjorth Larsen, A.; JØrgen Mortensen, J.; Blomqvist, J.; Castelli, I. E.; Christensen, R.; Dułak, M.; Friis, J.; Groves, M. N.; Hammer, B.; Hargus, C.; Hermes, E. D.; Jennings, P. C.; Bjerre Jensen, P.; Kermode, J.; Kitchin, J. R.; Leonhard Kolsbjerg, E.; Kubal, J.; Kaasbjerg, K.; Lysgaard, S.; Bergmann Maronsson, J.; Maxson, T.; Olsen, T.; Pastewka, L.; Peterson, A.; Rostgaard, C.; SchiØtz, J.; Schütt, O.; Strange, M.; Thygesen, K. S.; Vegge, T.; Vilhelmsen, L.; Walter, M.; Zeng, Z.; Jacobsen, K. W. The Atomic Simulation Environment - A Python Library for Working with Atoms. *Journal of Physics Condensed Matter*. Institute of Physics Publishing June 7, 2017. https://doi.org/10.1088/1361-648X/aa680e.

(130) Perdew, J. P.; Burke, K.; Ernzerhof, M. *Generalized Gradient Approximation Made Simple*; 1996.

(131) Medford, A. J.; Moses, P. G.; Jacobsen, K. W.; Peterson, A. A. A Career in Catalysis: Jens Kehlet Nørskov. *ACS Catalysis*. American Chemical Society August 5, 2022, pp 9679–9689. https://doi.org/10.1021/acscatal.2c02217.

(132) Kulkarni, A.; Siahrostami, S.; Patel, A.; Nørskov, J. K. Understanding Catalytic Activity Trends in the Oxygen Reduction Reaction. *Chemical Reviews*. American Chemical Society March 14, 2018, pp 2302–2312. https://doi.org/10.1021/acs.chemrev.7b00488.

(133) Togo, A.; Tanaka, I. First Principles Phonon Calculations in Materials Science. *Scr Mater* **2015**, *108*, 1–5. https://doi.org/10.1016/j.scriptamat.2015.07.021.

(134) Bard, A.; Faulkner, L. *Electrochemical Methods: Fundamentals and Applications (2nd Ed.).*; Wiley., 2000.

(135) Atkins, P.; Keeler, J.; de Paula, J. *Atkins' Physical Chemistry (11th Ed.).*; Oxford University Press, 2017.

(136) Dickens, C. F.; Kirk, C.; Nørskov, J. K. Insights into the Electrochemical Oxygen Evolution Reaction with Ab Initio Calculations and Microkinetic Modeling: Beyond the Limiting Potential Volcano. *Journal of Physical Chemistry C* **2019**, *123* (31), 18960–18977. https://doi.org/10.1021/acs.jpcc.9b03830.

(137) Chang, Q.; Zhang, P.; Mostaghimi, A. H. B.; Zhao, X.; Denny, S. R.; Lee, J. H.; Gao, H.; Zhang, Y.; Xin, H. L.; Siahrostami, S.; Chen, J. G.; Chen, Z. Promoting H_2O_2 Production via 2-Electron Oxygen Reduction by Coordinating Partially Oxidized Pd with Defect Carbon. *Nat Commun* **2020**, *11* (1). https://doi.org/10.1038/s41467-020-15843-3.

(138) Verga, L. G.; Aarons, J.; Sarwar, M.; Thompsett, D.; Russell, A. E.; Skylaris, C. K. DFT Calculation of Oxygen Adsorption on Platinum Nanoparticles: Coverage and Size Effects. *Faraday Discussions*. Royal Society of Chemistry 2018, pp 497–522. https://doi.org/10.1039/c7fd00218a.

(139) Pillay, D.; Johannes, M. D.; Garsany, Y.; Swider-Lyons, K. E. Poisoning of Pt_3Co Electrodes: A Combined Experimental and DFT Study. *Journal of Physical Chemistry C* **2010**, *114* (17), 7822–7830. https://doi.org/10.1021/jp906778k.

(140) Dou, X.; Veksha, A.; Chan, W. P.; Oh, W. Da; Liang, Y. N.; Teoh, F.; Mohamed, D. K. B.; Giannis, A.; Lisak, G.; Lim, T. T. Poisoning Effects of H_2S and HCl on the Naphthalene Steam Reforming and Water-Gas Shift Activities of Ni and Fe Catalysts. *Fuel* **2019**, *241*, 1008–1018. https://doi.org/10.1016/j.fuel.2018.12.119.

(141) Schuch, N.; Verstraete, F. Computational Complexity of Interacting Electrons and Fundamental Limitations of Density Functionaltheory. *Nat Phys* **2009**, *5* (10), 732–735. https://doi.org/10.1038/nphys1370.

(142) Cohen, A. J.; Mori-Sánchez, P.; Yang, W. Insights into Current Limitations of Density Functional Theory. *Science*. August 8, 2008, pp 792–794. https://doi.org/10.1126/science.1158722.

(143) Pan, Y.; Chen, M.; Su, Z.; Wu, K.; Zhang, Y.; Long, D. Two-Dimensional CaO/Carbon Heterostructures with Unprecedented Catalytic Performance in Room-Temperature H2S Oxidization. *Appl Catal B* **2021**, *280*. https://doi.org/10.1016/j.apcatb.2020.119444.

(144) Mbah, J.; Srinivasan, S.; Krakow, B.; Wolan, J.; Goswami, Y.; Stefanakos, E.; Appathurai, N. Effect of RuO2-CoS2 Anode Nanostructured on Performance of H2S Electrolytic Splitting System. *Int J Hydrogen Energy* **2010**, *35* (19), 10094–10101. https://doi.org/10.1016/j.ijhydene.2010.08.023.

(145) Man, I. C.; Su, H. Y.; Calle-Vallejo, F.; Hansen, H. A.; Martínez, J. I.; Inoglu, N. G.; Kitchin, J.; Jaramillo, T. F.; Nørskov, J. K.; Rossmeisl, J. Universality in Oxygen Evolution Electrocatalysis on Oxide Surfaces. *ChemCatChem* **2011**, *3* (7), 1159–1165. https://doi.org/10.1002/cctc.201000397.

(146) Rossmeisl, J.; Logadottir, A.; Nørskov, J. K. Electrolysis of Water on (Oxidized) Metal Surfaces. *Chem Phys* **2005**, *319* (1–3), 178–184. https://doi.org/10.1016/j.chemphys.2005.05.038.

(147) Karamad, M.; Hansen, H. A.; Rossmeisl, J.; Nørskov, J. K. Mechanistic Pathway in the Electrochemical Reduction of CO2 on RuO2. *ACS Catal* **2015**, *5* (7), 4075–4081. https://doi.org/10.1021/cs501542n.

(148) Schweiger, H.; Raybaud, P.; Kresse, G.; Toulhoat, H. Shape and Edge Sites Modifications of MoS2 Catalytic Nanoparticles Induced by Working Conditions: A Theoretical Study. *J Catal* **2002**, *207* (1), 76–87. https://doi.org/10.1006/jcat.2002.3508.

(149) Yang, S. Z.; Gong, Y.; Manchanda, P.; Zhang, Y. Y.; Ye, G.; Chen, S.; Song, L.; Pantelides, S. T.; Ajayan, P. M.; Chisholm, M. F.; Zhou, W. Rhenium-Doped and Stabilized MoS_2 Atomic Layers with Basal-Plane Catalytic Activity. *Advanced Materials* **2018**, *30* (51). https://doi.org/10.1002/adma.201803477.

(150) Singh, V. K.; Nakate, U. T.; Bhuyan, P.; Chen, J.; Tran, D. T.; Park, S. Mo/Co Doped 1T-VS_2 Nanostructures as a Superior Bifunctional Electrocatalyst for Overall Water Splitting in Alkaline Media. *J Mater Chem A Mater* **2022**. https://doi.org/10.1039/d2ta00488g.

(151) Zaman, J.; Chakma, A. *Production of Hydrogen and Sulfur from Hydrogen Sulfide*; 1995; Vol. 41.

Appendices

ELSEVIER LICENSE
TERMS AND CONDITIONS

Sep 11, 2023

This Agreement between Mr. Sam Baratifar ("You") and Elsevier ("Elsevier") consists of your license details and the terms and conditions provided by Elsevier and Copyright Clearance Center.

License Number	5626071081810
License date	Sep 11, 2023
Licensed Content Publisher	Elsevier
Licensed Content Publication	Energy
Licensed Content Title	Hydrogen production through sorption-enhanced steam methane reforming and membrane technology: A review
Licensed Content Author	L. Barelli,G. Bidini,F. Gallorini,S. Servili
Licensed Content Date	Apr 1, 2008
Licensed Content Volume	33
Licensed Content Issue	4
Licensed Content Pages	17
Start Page	554
End Page	570

Type of Use	reuse in a thesis/dissertation
Portion	figures/tables/illustrations
Number of figures/tables/illustrations	1
Format	electronic
Are you the author of this Elsevier article?	No
Will you be translating?	No
Title	An involuntary gas to an asset; H2S to H2:A DFT study
Institution name	University of calgary
Expected presentation date	Sep 2023
Portions	Figure 1
Requestor Location	Mr. Sam Baratifar 404-4510 Valiant Dr NW Calgary, AB T3A 0X9 Canada Attn: Mr. Sam Baratifar
Publisher Tax ID	GB 494 6272 12
Total	0.00 CAD
Terms and Conditions	

INTRODUCTION

1. The publisher for this copyrighted material is Elsevier. By clicking "accept" in connection with completing this licensing transaction, you agree that the following terms and conditions apply to this transaction (along with the Billing and Payment terms and conditions established by Copyright Clearance Center, Inc. ("CCC"), at the time that you opened your RightsLink account and that are available at any time at https://myaccount.copyright.com).

GENERAL TERMS

2. Elsevier hereby grants you permission to reproduce the aforementioned material subject to the terms and conditions indicated.

3. Acknowledgement: If any part of the material to be used (for example, figures) has appeared in our publication with credit or acknowledgement to another source, permission must also be sought from that source. If such permission is not obtained then that material may not be included in your publication/copies. Suitable acknowledgement to the source must be made, either as a footnote or in a reference list at the end of your publication, as follows:

"Reprinted from Publication title, Vol /edition number, Author(s), Title of article / title of chapter, Pages No., Copyright (Year), with permission from Elsevier [OR APPLICABLE SOCIETY COPYRIGHT OWNER]." Also Lancet special credit - "Reprinted from The Lancet, Vol. number, Author(s), Title of article, Pages No., Copyright (Year), with permission from Elsevier."

4. Reproduction of this material is confined to the purpose and/or media for which permission is hereby given. The material may not be reproduced or used in any other way, including use in combination with an artificial intelligence tool (including to train an algorithm, test, process, analyse, generate output and/or develop any form of artificial intelligence tool), or to create any derivative work and/or service (including resulting from the use of artificial intelligence tools).

5. Altering/Modifying Material: Not Permitted. However figures and illustrations may be altered/adapted minimally to serve your work. Any other abbreviations, additions, deletions and/or any other alterations shall be made only with prior written authorization of Elsevier Ltd. (Please contact Elsevier's permissions helpdesk here). No modifications can be made to any Lancet figures/tables and they must be reproduced in full.

6. If the permission fee for the requested use of our material is waived in this instance, please be advised that your future requests for Elsevier materials may attract a fee.

7. Reservation of Rights: Publisher reserves all rights not specifically granted in the combination of (i) the license details provided by you and accepted in the course of this licensing transaction, (ii) these terms and conditions and (iii) CCC's Billing and Payment terms and conditions.

8. License Contingent Upon Payment: While you may exercise the rights licensed immediately upon issuance of the license at the end of the licensing process for the transaction, provided that you have disclosed complete and accurate details of your proposed use, no license is finally effective unless and until full payment is received from you (either by publisher or by CCC) as provided in CCC's Billing and Payment terms and conditions. If full payment is not received on a timely basis, then any license preliminarily granted shall be deemed automatically revoked and shall be void as if never granted. Further, in the event that you breach any of these terms and conditions or any of CCC's Billing and Payment terms and conditions, the license is automatically revoked and shall be void as if never granted. Use of materials as described in a revoked license, as well as any use of the

materials beyond the scope of an unrevoked license, may constitute copyright infringement and publisher reserves the right to take any and all action to protect its copyright in the materials.

9. Warranties: Publisher makes no representations or warranties with respect to the licensed material.

10. Indemnity: You hereby indemnify and agree to hold harmless publisher and CCC, and their respective officers, directors, employees and agents, from and against any and all claims arising out of your use of the licensed material other than as specifically authorized pursuant to this license.

11. No Transfer of License: This license is personal to you and may not be sublicensed, assigned, or transferred by you to any other person without publisher's written permission.

12. No Amendment Except in Writing: This license may not be amended except in a writing signed by both parties (or, in the case of publisher, by CCC on publisher's behalf).

13. Objection to Contrary Terms: Publisher hereby objects to any terms contained in any purchase order, acknowledgment, check endorsement or other writing prepared by you, which terms are inconsistent with these terms and conditions or CCC's Billing and Payment terms and conditions. These terms and conditions, together with CCC's Billing and Payment terms and conditions (which are incorporated herein), comprise the entire agreement between you and publisher (and CCC) concerning this licensing transaction. In the event of any conflict between your obligations established by these terms and conditions and those established by CCC's Billing and Payment terms and conditions, these terms and conditions shall control.

14. Revocation: Elsevier or Copyright Clearance Center may deny the permissions described in this License at their sole discretion, for any reason or no reason, with a full refund payable to you. Notice of such denial will be made using the contact information provided by you. Failure to receive such notice will not alter or invalidate the denial. In no event will Elsevier or Copyright Clearance Center be responsible or liable for any costs, expenses or damage incurred by you as a result of a denial of your permission request, other than a refund of the amount(s) paid by you to Elsevier and/or Copyright Clearance Center for denied permissions.

LIMITED LICENSE

The following terms and conditions apply only to specific license types:

15. **Translation**: This permission is granted for non-exclusive world **English** rights only unless your license was granted for translation rights. If you licensed translation rights you may only translate this content into the languages you requested. A professional translator must perform all translations and reproduce the content word for word preserving the integrity of the article.

16. **Posting licensed content on any Website**: The following terms and conditions apply as follows: Licensing material from an Elsevier journal: All content posted to the web site must maintain the copyright information line on the bottom of each image; A hyper-text must be included to the Homepage of the journal from which you are licensing at http://www.sciencedirect.com/science/journal/xxxxx or the Elsevier homepage for books at http://www.elsevier.com; Central Storage: This license does not include permission for a scanned version of the material to be stored in a central repository such as that provided by Heron/XanEdu.

Licensing material from an Elsevier book: A hyper-text link must be included to the Elsevier homepage at http://www.elsevier.com . All content posted to the web site must maintain the copyright information line on the bottom of each image.

Posting licensed content on Electronic reserve: In addition to the above the following clauses are applicable: The web site must be password-protected and made available only to bona fide students registered on a relevant course. This permission is granted for 1 year only. You may obtain a new license for future website posting.

17. **For journal authors:** the following clauses are applicable in addition to the above:

Preprints:

A preprint is an author's own write-up of research results and analysis, it has not been peer-reviewed, nor has it had any other value added to it by a publisher (such as formatting, copyright, technical enhancement etc.).

Authors can share their preprints anywhere at any time. Preprints should not be added to or enhanced in any way in order to appear more like, or to substitute for, the final versions of articles however authors can update their preprints on arXiv or RePEc with their Accepted Author Manuscript (see below).

If accepted for publication, we encourage authors to link from the preprint to their formal publication via its DOI. Millions of researchers have access to the formal publications on ScienceDirect, and so links will help users to find, access, cite and use the best available version. Please note that Cell Press, The Lancet and some society-owned have different preprint policies. Information on these policies is available on the journal homepage.

Accepted Author Manuscripts: An accepted author manuscript is the manuscript of an article that has been accepted for publication and which typically includes author-incorporated changes suggested during submission, peer review and editor-author communications.

Authors can share their accepted author manuscript:

- immediately
  - via their non-commercial person homepage or blog
  - by updating a preprint in arXiv or RePEc with the accepted manuscript
  - via their research institute or institutional repository for internal institutional uses or as part of an invitation-only research collaboration work-group
  - directly by providing copies to their students or to research collaborators for their personal use
  - for private scholarly sharing as part of an invitation-only work group on commercial sites with which Elsevier has an agreement
- After the embargo period
  - via non-commercial hosting platforms such as their institutional repository
  - via commercial sites with which Elsevier has an agreement

In all cases accepted manuscripts should:

- link to the formal publication via its DOI
- bear a CC-BY-NC-ND license - this is easy to do
- if aggregated with other manuscripts, for example in a repository or other site, be shared in alignment with our hosting policy not be added to or enhanced in any way to

appear more like, or to substitute for, the published journal article.

Published journal article (JPA): A published journal article (PJA) is the definitive final record of published research that appears or will appear in the journal and embodies all value-adding publishing activities including peer review co-ordination, copy-editing, formatting, (if relevant) pagination and online enrichment.

Policies for sharing publishing journal articles differ for subscription and gold open access articles:

Subscription Articles: If you are an author, please share a link to your article rather than the full-text. Millions of researchers have access to the formal publications on ScienceDirect, and so links will help your users to find, access, cite, and use the best available version.

Theses and dissertations which contain embedded PJAs as part of the formal submission can be posted publicly by the awarding institution with DOI links back to the formal publications on ScienceDirect.

If you are affiliated with a library that subscribes to ScienceDirect you have additional private sharing rights for others' research accessed under that agreement. This includes use for classroom teaching and internal training at the institution (including use in course packs and courseware programs), and inclusion of the article for grant funding purposes.

Gold Open Access Articles: May be shared according to the author-selected end-user license and should contain a CrossMark logo, the end user license, and a DOI link to the formal publication on ScienceDirect.

Please refer to Elsevier's posting policy for further information.

18. **For book authors** the following clauses are applicable in addition to the above: Authors are permitted to place a brief summary of their work online only. You are not allowed to download and post the published electronic version of your chapter, nor may you scan the printed edition to create an electronic version. **Posting to a repository:** Authors are permitted to post a summary of their chapter only in their institution's repository.

19. **Thesis/Dissertation**: If your license is for use in a thesis/dissertation your thesis may be submitted to your institution in either print or electronic form. Should your thesis be published commercially, please reapply for permission. These requirements include permission for the Library and Archives of Canada to supply single copies, on demand, of the complete thesis and include permission for Proquest/UMI to supply single copies, on demand, of the complete thesis. Should your thesis be published commercially, please reapply for permission. Theses and dissertations which contain embedded PJAs as part of the formal submission can be posted publicly by the awarding institution with DOI links back to the formal publications on ScienceDirect.

Elsevier Open Access Terms and Conditions

You can publish open access with Elsevier in hundreds of open access journals or in nearly 2000 established subscription journals that support open access publishing. Permitted third party re-use of these open access articles is defined by the author's choice of Creative Commons user license. See our open access license policy for more information.

Terms & Conditions applicable to all Open Access articles published with Elsevier:

Any reuse of the article must not represent the author as endorsing the adaptation of the article nor should the article be modified in such a way as to damage the author's honour or reputation. If any changes have been made, such changes must be clearly indicated.

The author(s) must be appropriately credited and we ask that you include the end user license and a DOI link to the formal publication on ScienceDirect.

If any part of the material to be used (for example, figures) has appeared in our publication with credit or acknowledgement to another source it is the responsibility of the user to ensure their reuse complies with the terms and conditions determined by the rights holder.

Additional Terms & Conditions applicable to each Creative Commons user license:

CC BY: The CC-BY license allows users to copy, to create extracts, abstracts and new works from the Article, to alter and revise the Article and to make commercial use of the Article (including reuse and/or resale of the Article by commercial entities), provided the user gives appropriate credit (with a link to the formal publication through the relevant DOI), provides a link to the license, indicates if changes were made and the licensor is not represented as endorsing the use made of the work. The full details of the license are available at http://creativecommons.org/licenses/by/4.0.

CC BY NC SA: The CC BY-NC-SA license allows users to copy, to create extracts, abstracts and new works from the Article, to alter and revise the Article, provided this is not done for commercial purposes, and that the user gives appropriate credit (with a link to the formal publication through the relevant DOI), provides a link to the license, indicates if changes were made and the licensor is not represented as endorsing the use made of the work. Further, any new works must be made available on the same conditions. The full details of the license are available at http://creativecommons.org/licenses/by-nc-sa/4.0.

CC BY NC ND: The CC BY-NC-ND license allows users to copy and distribute the Article, provided this is not done for commercial purposes and further does not permit distribution of the Article if it is changed or edited in any way, and provided the user gives appropriate credit (with a link to the formal publication through the relevant DOI), provides a link to the license, and that the licensor is not represented as endorsing the use made of the work. The full details of the license are available at http://creativecommons.org/licenses/by-nc-nd/4.0. Any commercial reuse of Open Access articles published with a CC BY NC SA or CC BY NC ND license requires permission from Elsevier and will be subject to a fee.

Commercial reuse includes:

- Associating advertising with the full text of the Article
- Charging fees for document delivery or access
- Article aggregation
- Systematic distribution via e-mail lists or share buttons

Posting or linking by commercial companies for use by customers of those companies.

20. **Other Conditions**:

v1.10

ELSEVIER LICENSE
TERMS AND CONDITIONS

Sep 11, 2023

This Agreement between Mr. Sam Baratifar ("You") and Elsevier ("Elsevier") consists of your license details and the terms and conditions provided by Elsevier and Copyright Clearance Center.

License Number	5626071422660
License date	Sep 11, 2023
Licensed Content Publisher	Elsevier
Licensed Content Publication	Carbon
Licensed Content Title	Alkaline carbon nanotubes as effective catalysts for H2S oxidation
Licensed Content Author	Qingjun Chen,Jitong Wang,Xiaojun Liu,Xin Zhao,Wenming Qiao,Donghui Long,Licheng Ling
Licensed Content Date	Oct 1, 2011
Licensed Content Volume	49
Licensed Content Issue	12
Licensed Content Pages	8
Start Page	3773
End Page	3780

Type of Use	reuse in a thesis/dissertation
Portion	figures/tables/illustrations
Number of figures/tables/illustrations	1
Format	electronic
Are you the author of this Elsevier article?	No
Will you be translating?	No
Title	An involuntary gas to an asset; H2S to H2:A DFT study
Institution name	University of calgary
Expected presentation date	Sep 2023
Portions	Figure 9
Requestor Location	Mr. Sam Baratifar 404-4510 Valiant Dr NW Calgary, AB T3A 0X9 Canada Attn: Mr. Sam Baratifar
Publisher Tax ID	GB 494 6272 12
Total	0.00 CAD
Terms and Conditions	

INTRODUCTION

ELSEVIER LICENSE
TERMS AND CONDITIONS

Sep 11, 2023

This Agreement between Mr. Sam Baratifar ("You") and Elsevier ("Elsevier") consists of your license details and the terms and conditions provided by Elsevier and Copyright Clearance Center.

License Number	5626080090529
License date	Sep 11, 2023
Licensed Content Publisher	Elsevier
Licensed Content Publication	Applied Catalysis B: Environmental
Licensed Content Title	Insight into the effect of morphology on catalytic performance of porous CeO2 nanocrystals for H2S selective oxidation
Licensed Content Author	Xiaohai Zheng,Yanli Li,Linyan Zhang,Lijuan Shen,Yihong Xiao,Yongfan Zhang,Chaktong Au,Lilong Jiang
Licensed Content Date	Sep 5, 2019
Licensed Content Volume	252
Licensed Content Issue	n/a
Licensed Content Pages	13
Start Page	98

End Page	110
Type of Use	reuse in a thesis/dissertation
Portion	figures/tables/illustrations
Number of figures/tables/illustrations	1
Format	electronic
Are you the author of this Elsevier article?	No
Will you be translating?	No
Title	An involuntary gas to an asset; H2S to H2:A DFT study
Institution name	University of calgary
Expected presentation date	Sep 2023
Portions	Fig 13
Requestor Location	Mr. Sam Baratifar 404-4510 Valiant Dr NW Calgary, AB T3A 0X9 Canada Attn: Mr. Sam Baratifar
Publisher Tax ID	GB 494 6272 12
Total	0.00 CAD
Terms and Conditions	

ELSEVIER LICENSE
TERMS AND CONDITIONS

Sep 11, 2023

This Agreement between Mr. Sam Baratifar ("You") and Elsevier ("Elsevier") consists of your license details and the terms and conditions provided by Elsevier and Copyright Clearance Center.

License Number	5626080250841
License date	Sep 11, 2023
Licensed Content Publisher	Elsevier
Licensed Content Publication	Chemical Engineering Journal
Licensed Content Title	Rational designed Co@N-doped carbon catalyst for high-efficient H2S selective oxidation by regulating electronic structures
Licensed Content Author	Yi Liu,Chengye Song,Yuchao Wang,Wenhong Cao,Yongpeng Lei,Qingguo Feng,Zhuo Chen,Shijing Liang,Liang Xu,Lilong Jiang
Licensed Content Date	Dec 1, 2020
Licensed Content Volume	401
Licensed Content Issue	n/a
Licensed Content Pages	1
Start Page	126038

End Page	0
Type of Use	reuse in a thesis/dissertation
Portion	figures/tables/illustrations
Number of figures/tables/illustrations	1
Format	electronic
Are you the author of this Elsevier article?	No
Will you be translating?	No
Title	An involuntary gas to an asset; H2S to H2:A DFT study
Institution name	University of calgary
Expected presentation date	Sep 2023
Portions	abstract
Requestor Location	Mr. Sam Baratifar 404-4510 Valiant Dr NW Calgary, AB T3A 0X9 Canada Attn: Mr. Sam Baratifar
Publisher Tax ID	GB 494 6272 12
Total	0.00 CAD
Terms and Conditions	

JOHN WILEY AND SONS LICENSE
TERMS AND CONDITIONS

Sep 11, 2023

This Agreement between Mr. Sam Baratifar ("You") and John Wiley and Sons ("John Wiley and Sons") consists of your license details and the terms and conditions provided by John Wiley and Sons and Copyright Clearance Center.

License Number	5626080983951
License date	Sep 11, 2023
Licensed Content Publisher	John Wiley and Sons
Licensed Content Publication	Journal of Computational Chemistry
Licensed Content Title	Density functional theory-based electrochemical models for the oxygen reduction reaction: Comparison of modeling approaches for electric field and solvent effects
Licensed Content Author	Kuan-Yu Yeh, Michael J. Janik
Licensed Content Date	Sep 7, 2011
Licensed Content Volume	32
Licensed Content Issue	16
Licensed Content Pages	10

Type of use	Dissertation/Thesis
Requestor type	University/Academic
Format	Electronic
Portion	Figure/table
Number of figures/tables	1
Will you be translating?	No
Title	An involuntary gas to an asset; H2S to H2:A DFT study
Institution name	University of calgary
Expected presentation date	Sep 2023
Portions	fig 6
Requestor Location	Mr. Sam Baratifar 404-4510 Valiant Dr NW Calgary, AB T3A 0X9 Canada Attn: Mr. Sam Baratifar
Publisher Tax ID	EU826007151
Total	0.00 CAD

Terms and Conditions

TERMS AND CONDITIONS

JOHN WILEY AND SONS LICENSE
TERMS AND CONDITIONS

Sep 11, 2023

This Agreement between Mr. Sam Baratifar ("You") and John Wiley and Sons ("John Wiley and Sons") consists of your license details and the terms and conditions provided by John Wiley and Sons and Copyright Clearance Center.

License Number	5626081181860
License date	Sep 11, 2023
Licensed Content Publisher	John Wiley and Sons
Licensed Content Publication	Advanced Energy Materials
Licensed Content Title	Surface Reconstruction of Water Splitting Electrocatalysts
Licensed Content Author	Hanfeng Liang, Zhoucheng Wang, Qiu Jiang, et al
Licensed Content Date	Jul 8, 2022
Licensed Content Volume	12
Licensed Content Issue	33
Licensed Content Pages	29
Type of use	Dissertation/Thesis
Requestor type	University/Academic
Format	Electronic

Portion	Figure/table
Number of figures/tables	1
Will you be translating?	No
Title	An involuntary gas to an asset; H2S to H2:A DFT study
Institution name	University of calgary
Expected presentation date	Sep 2023
Portions	table 1
Requestor Location	Mr. Sam Baratifar 404-4510 Valiant Dr NW Calgary, AB T3A 0X9 Canada Attn: Mr. Sam Baratifar
Publisher Tax ID	EU826007151
Total	0.00 CAD

Terms and Conditions

TERMS AND CONDITIONS

This copyrighted material is owned by or exclusively licensed to John Wiley & Sons, Inc. or one of its group companies (each a"Wiley Company") or handled on behalf of a society with which a Wiley Company has exclusive publishing rights in relation to a particular work (collectively "WILEY"). By clicking "accept" in connection with completing this licensing transaction, you agree that the following terms and conditions apply to this transaction (along with the billing and payment terms and conditions established by the Copyright Clearance Center Inc., ("CCC's Billing and Payment terms and conditions"), at the time that you opened your RightsLink account (these are available at any time at http://myaccount.copyright.com).

Terms and Conditions

ELSEVIER LICENSE
TERMS AND CONDITIONS

Sep 11, 2023

This Agreement between Mr. Sam Baratifar ("You") and Elsevier ("Elsevier") consists of your license details and the terms and conditions provided by Elsevier and Copyright Clearance Center.

License Number	5626081390756
License date	Sep 11, 2023
Licensed Content Publisher	Elsevier
Licensed Content Publication	Molecular Catalysis
Licensed Content Title	Oxygen evolution reaction at the Mo/W-doped bismuth vanadate surface: Assessing the dopant role by DFT calculations
Licensed Content Author	Arianna Massaro,Adriana Pecoraro,Simelys Hernández,Giovanni Talarico,Ana B. Muñoz-García,Michele Pavone
Licensed Content Date	Jan 1, 2022
Licensed Content Volume	517
Licensed Content Issue	n/a
Licensed Content Pages	1
Start Page	112036

End Page	0
Type of Use	reuse in a thesis/dissertation
Portion	figures/tables/illustrations
Number of figures/tables/illustrations	1
Format	electronic
Are you the author of this Elsevier article?	No
Will you be translating?	No
Title	An involuntary gas to an asset; H2S to H2:A DFT study
Institution name	University of calgary
Expected presentation date	Sep 2023
Portions	fig 3
Requestor Location	Mr. Sam Baratifar 404-4510 Valiant Dr NW Calgary, AB T3A 0X9 Canada Attn: Mr. Sam Baratifar
Publisher Tax ID	GB 494 6272 12
Total	0.00 CAD
Terms and Conditions	